Volume 93 • Number 1 • March 2022
Established in 1923 • ISSN 1945-0702

The Chemist

Journal of the American Institute of Chemists

In this Issue

Image courtesy of iGroup Global

Official journal of
The American Institute of Chemists, Inc.

 http://www.theaic.org/pub_thechemist_journals/

The Chemist

Established in 1923, The Chemist is the official publication of The American Institute of Chemists, Inc. (AIC). The Chemist was published quarterly in magazine format up until 2006. The Chemist is currently being set up and formatted as an online journal.

Subscription: $35 per year to members, $100 per year to non-members. Single copy: $50.
The Chemist (ISSN-0009-3025) is published online by The American Institute of Chemists, Inc.

Volume 93 | Issue 1 | 2022

The Chemist

Journal of the American Institute of Chemists

The Chemist (Established in 1923)

Editorial

Alexander G. Zestos
American University

In this issue of The Chemist, we shine a light on recent advances from our Chemical Pioneer award winners and other contributions. Highlighting the theme of diversity, equity, and inclusion (DEI), we include contributions from all over the world and four different continents (Africa, Asia, the Middle East, and North America). We deem it especially important to emphasize great scientific advances from regions of the world that have been underrepresented in the fields of science.

Despite the ongoing COVID-19 pandemic, the field of Chemistry has made many strong advances. One major change that the pandemic has brought is that the 2021 American Institute of Chemists (AIC) Chemical Pioneers Symposium was held as a virtual event on May 6, 2021 from 12:00 – 2:30 PM. Among the honorees was Prof. Jonathan L. Sessler, the Doherty-Welch Chair in Chemistry and Professor of Chemistry from the University of Texas at Austin. Prof. Sessler was also recently inducted and named as a member of the National Academy of Sciences.

Jonathan L. Sessler's work, "OxaliTEX-Pt(IV): A case study in medical inorganic chemical lead development", details the development of a drug in advanced stage preclinical development. This drug conjugate was invented and developed by Dr. Sessler and colleagues at the University of Texas at Austin and MD Anderson Cancer Center. The article provides a broad overview of the texaphyrin drug conjugate program licensing to the IQ Global group.

This issue also includes work by Amayreh et al. on low-cost, small-scale, and environmentally friendly galvanic cells. This work shows that simple electrochemical tools can be constructed on an affordable budget with everyday materials outside of the laboratory. Abdulrahim et al. characterized a seed oil of Luffa aegyptiaca with FT-IR and several other antioxidant analyses to show that biosurfactants can protect against oxidative degradation in allied products.

A review on multi-ferrocenyl systems by Ghosh et al. focuses primarily on the synthesis, properties, and application of multi-ferrocenyl systems, which have many potential applications in multielectron redox catalysis, electron storage devices, and as redox switchable molecules such as miniaturized molecular switches and sensor devices. Chen and Pretty discuss the selection of influential factors on fume hood evaluation. Several important surveys were conducted that showed that thermal challenge and inside clutter are influential factors, which are vital to reducing greenhouse gas emissions during field tests and for computational simulations of hood evaluation performance as well.

Tawari and colleagues detail hollow-fine-fibre membranes used for collapse pressure and pressure drop analysis. They showed that cellulose acetate (CA) hollow fine fibre membranes were used for water flux performance in brackish water desalination. Lastly, the Kulkarni group depict a novel synthesis method of α-methylene cinnamic acid using sodium hydroxide as a catalyst under microwave irradiation, which could have vast implications for organic synthesis.

As the pandemic continues, we are all seeing the ways in which chemistry has impacted everyday life and offers hope for the future. At this time, we would like to let you know that we are accepting submissions for our next issue and do hope that you consider submitting an article for consideration. We wish you a safe and happy year.

Sincerely,

Alexander G. Zestos
Editor, The Chemist

The Chemist
Journal of the American Institute of Chemists

OxaliTEX-Pt(IV): A case study in medicinal inorganic chemical lead development

Jonathan L. Sessler

Department of Chemistry, The University of Texas at Austin
105 E. 24th Street-A5300
Austin, TX 78712-1224. USA

Abstract: OxaliTEX-Pt(IV) was invented by Grégory Thiabaud, Jonathan F. Arambula, and Jonathan L. Sessler of The University of Texas at Austin and Zahid H. Siddik of the MD Anderson Cancer Center. It is the subject of US Patent No. 10,406,167 and corresponding foreign filings. OxaliTEX-Pt(IV) and related technologies were licensed to the IQ Global Group in September of 2019 and became the basis for OncoTEX, Inc. Currently, OxaliTEX-Pt(IV) is in an advanced stage of preclinical development. While its ultimate fate as a potential drug product awaits ongoing preclinical and planned clinical testing, OxaliTEX-Pt(IV) provides a textbook study in lead development in the porphyrin analogue-based medicinal inorganic space. This review article is designed to trace from a personal perspective the sequence of events that led to the selection of OxaliTEX-Pt(IV) as the putative first product of OncoTEX, Inc. A large number of coworkers and collaborators has allowed the present level of progress to be achieved. These individuals are explicitly thanked in the acknowledgment section of this paper and are recognized as authors on the cited publications reviewed in this report.

Key Words: OxaliTEX-Pt(IV), texaphyrins, drug discovery, cancer, OncoTEX, Inc.

1. Introduction

Texaphyrins are a class of pentaaza expanded porphyrins that were invented by members of the Sessler research group in the late 1980s [1-4]. They were seminal in their time in that they were the first analogues of porphyrins with an expanded central core that were documented as forming stable, non-labile 1:1 metal complexes with larger cations (i.e., those with ionic radii greater than accommodated within the core of porphyrins and related tetraaza macrocycles). Texaphyrins also garnered interest

early on because they were aromatic systems, possessing a 22 π-electron periphery. As such, they led to a reassessment of the canonical thinking that aromaticity effects began to wane within systems containing more than 18 π-electrons.

Both the coordination chemistry of texaphyrins and their electronic features were viewed as attractive in terms of potential technological development. In particular, they were found to form stable complexes with Lu(III) and Gd(III), both of which were characterized by lowest energy bands >700 nm in their respective UV-visible absorption spectra. The Lu(III) complex proved diamagnetic and a good singlet oxygen photosensitizer. In contrast, the Gd(III) complex was found to enhance so-called T_1 relaxation effects. Perhaps not surprisingly, therefore, these two complexes attracted early interest as photodynamic therapy (PDT) [5,6] and magnetic resonance imaging (MRI) agents, respectively [7,8]. The further finding that the texaphyrins were 1) relatively easy to reduce and then 2) readily re-oxidized by oxygen to 3) produce reactive oxygen species made them of interest as potential radiation sensitizers [9-13].

Efforts to test the above promise led to the founding of Pharmacyclics, Inc. by Richard A. Miller, MD and the author in 1991 and the creation of water solubilized texaphyrin lutetium and gadolinium complexes referred to as motexafin lutetium (**MLu**) and motexafin gadolinium (**MGd**), respectively (Figure 1). Both complexes entered clinical trials under the aegis of Pharmacyclics, Inc. with the greatest development effort focused on **MGd** [14].

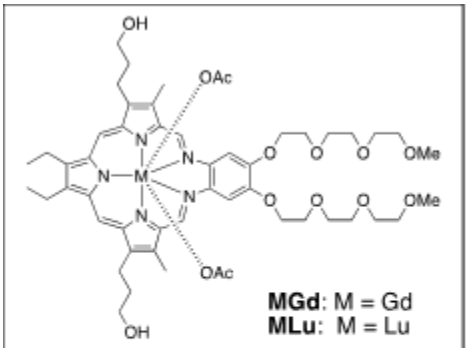

Figure 1. Water solubilized texaphyrins known as **MGd** and **MLu** that were the subject of early clinical trials under the aegis of Pharmacyclics, Inc.

Unfortunately, in spite of progressing through a Phase III trial in the mid-2000s as a possible radiation sensitizer for metastatic lung cancer, **MGd** did not receive FDA approval due to the trial not reaching statistical significance in its endpoint. On the other hand, the agent was found to be well tolerated by patients at the administrated dosage levels [15,16]. In addition, based on both MRI studies and limited patient biopsies, it was found that **MGd** localized well to solid tumors [17-19]. This led to the consideration that **MGd** could be strategically utilized as a carrier for

active anticancer agents that lack appreciable cancer targeting ability. The basic strategy that then began to evolve, shown in Figure 2, is that **MGd** would be functionalized in such a way that it could be linked to a specific chemotherapeutic so as to produce a conjugate that embodied the combined benefits of 1) targeting (due to the texaphyrin core) and 2) potency (due to the anticancer effect of the chemotherapeutic).

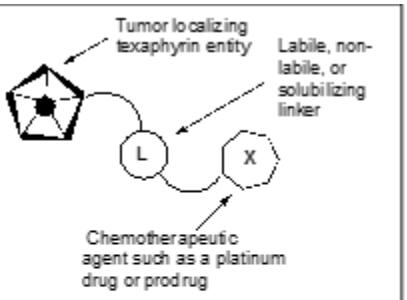

Figure 2. Texaphyrin conjugate concept. To date, much (but not all) effort has focused on conjugates based on **MGd** where the active payload is a platinum species.

While early on a number of possible therapeutic payloads were considered [20-24], most of the effort within our texaphyrin conjugate program has focused on using functionalized **MGd** as a carrier for an active platinum agent. It is the evolution of the latter program that is the subject of this retrospective report.

Currently, three Pt(II) complexes have been approved as cancer chemotherapeutics by the US FDA, namely cisplatin, carboplatin, and oxaliplatin (Figure 3). Together, these three agents remain part of the treatment regimen for roughly 50% of patients receiving cancer chemotherapy worldwide. Sadly, however, in many cases the administered platinum drugs are not curative. The FDA platinum drugs are noted for their lack of cancer targeting (thought responsible in part for systemic toxicity effects), as well as poor uptake/retention into cancer cells. These problems are exacerbated in the case of platinum resistance.

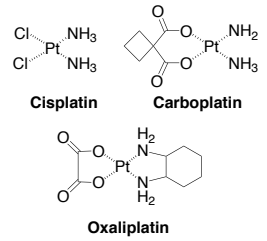

Figure 3. FDA-approved platinum drugs: Cisplatin, carboplatin, and oxaliplatin.

The determinants of platinum resistance are multifactorial. However, as the result of an incipient collaboration with Dr. Zahid Siddik of the MD Anderson Cancer Center we came to appreciate that resistance mechanisms include both pharmacological mechanisms (e.g., decreased drug uptake, increased GSH, and increased DNA adduct repair) and molecular mechanisms of resistance (e.g., a loss of the tumor suppressor protein 53 (p53) function, an increase in survivin, and an increase in B-cell lymphoma 2 (Bcl-2)) [25,26]. It was thought that developing texaphyrin-platinum conjugates could mitigate some of these clinical limitations.

In collaboration first with Dr. Darren Magda and other researchers then at Pharmacyclics, Inc., and subsequently with Dr. Siddik, a program was thus launched to create and test platinum-texaphyrin conjugates. This effort can be divided into three phases, namely early exploratory efforts, preparation of first generation systems, and development of second generation systems. As detailed below, this body of work has culminated in the selection of OxaliTEX-Pt(IV) as OncoTEX's initial drug lead.

2. Early Efforts to Create Texaphyrin-platinum Drug Conjugates

The first texaphyrin-platinum conjugates were reported in U.S. Patent no. 6,207,660 that issued in March of 2001 [27]. The first summary of our texaphyrin-conjugate program in the chemical literature was published in 2004 [20]. Included in the latter report was the synthesis of two texaphyrin-platinum(II) conjugates, **1** and **2**, based on the **MGd** core (Figure 4).

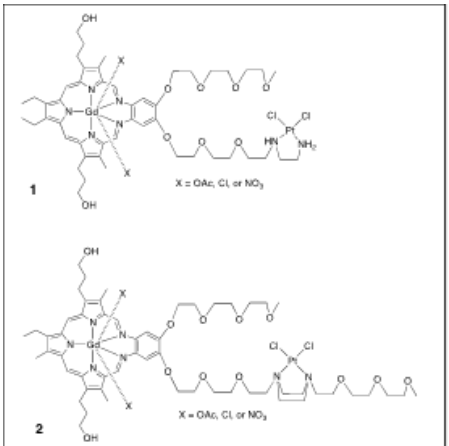

Figure 4. Early texaphyrin-platinum conjugates.

Unfortunately, neither conjugate proved appreciably soluble, either in aqueous media or organic solvents. This precluded a detailed study of these systems. An effort was thus made to redesign the synthetic approach.

3. First Generation Texaphyrin-platinum Drug Conjugates

Inspired by carboplatin, a malonate-based Pt(II) conjugate **3** was prepared (Figure 5).

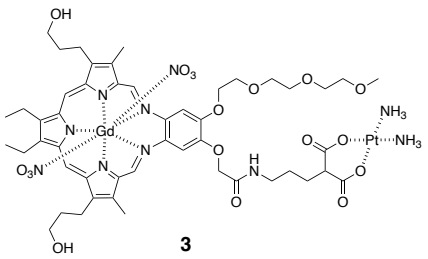

Figure 5. A carboplatin-inspired texaphyrin-platinum(II) conjugate that relies on a modified diaminocatechol subunit to provide for malonate-based Pt(II) coordination.

This synthetic effort, reported in 2009 by Arambula, *et al.*, provided the first generation of texaphyrin-platinum system suitable for biological testing [28]. As true for **1** and **2**, compound **3** was prepared by modifying the diaminocatechol portion of the gadolinium(III) texaphyrin core. The combined presence of both carboxylate chelators and free hydroxypropyl "arms" of the texaphyrin core was found to impart

aqueous solubility sufficient to allow for initial testing. First, the hydrolysis-based Pt(II) release, presumably as the active diamino diaquo complex, $Pt(NH_2)_2(H_2O)_2$, from the malonate chelator, was studied. A half-life for this release in phosphate-buffered saline was found to be ca. 72 h, a value that is commensurate with the rate of carboplatin hydrolysis [29]. Conjugate **3** was then tested *in vitro* using a standard tetrazolium dye (tetrazolium dye = 3-(4,5-dimethylthiazol-2-yl)-2,5-diphenyltetrazolium bromide; MTT) reduction assay on several cell lines. In a wild type ovarian cancer cell line, A2780, antiproliferative potency analogous to carboplatin was observed (IC_{50} = 1.4 mM for **3** vs 1.6 mM for carboplatin). On the other hand, in an isogenic platinum resistant cell line, 2780CP, conjugate **3** proved ca. 2x more potent than carboplatin (IC_{50} = 14.4 mM for **3** vs 26.3 mM for carboplatin). However, **MGd** itself proved relatively effective (IC_{50} = 13.7 mM) in treating the 2780CP cell line, as did the combination of **MGd** and carboplatin (IC_{50} = 11.6 mM). It was noted that conjugate **3** provided for the formation of a greater number of DNA-platinum adducts as compared to various controls [30]. As such, conjugate **3** was deemed effective at overcoming mechanisms of resistance involving the effective delivery or retention of platinum to cancer cells. However, this conjugate was not found capable of overcoming the DNA damage tolerance that is endemic to carboplatin treatments of platinum resistant cancers. An effort was thus made to create a texaphyrin-platinum conjugate capable of overcoming these latter resistance mechanisms.

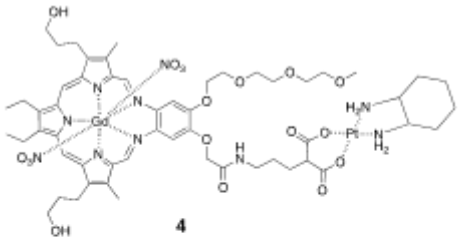

4

Figure 6. A oxaliplatin-inspired texaphyrin-platinum(II) conjugate that relies on a modified diaminocatechol subunit to provide for malonate-based Pt(II) coordination while incorporating a diaminocyclohexyl ligand characteristic of oxaliplatin.

Oxaliplatin, in contrast to cisplatin and carboplatin, is known to reactivate dormant p53 [31]. It was thus considered likely that replacing the nitrogenous ligands about the Pt(II) center in conjugate **3** with the diaminocyclohexyl (DACH) subunit present in oxaliplatin might serve to increase the ability to overcome platinum resistance. This led to the preparation of conjugate **4** (Figure 6) as reported by Arambula, *et al.* in 2012 [32]. As true for **3**, conjugate **4** proved capable of effectively delivering platinum to both wild type (A2780) and platinum resistance (2780CP) ovarian cancer cells, as determined by flameless atomic absorption spectroscopy (FAAS) analyses of the intracellular platinum concentrations. For conjugate **4**, no difference between the cell

lines was seen within error. Relative to oxaliplatin, conjugate **4** demonstrated a ≥2- and ≥4-fold increase in platinum uptake for the A2780 and 2780CP cell lines, respectively. However, despite the high potency **4** for both cell lines, only a modest level of DNA-Pt adduct formation was observed. For example, it was found that the intracellular Pt content in A2780 cells was equal for treatments involving **4** and cisplatin; however, the DNA-Pt adducts from cisplatin was found to be ~4-fold higher relative to **4**. This led us to infer that **4** might be participating in anticancer mechanisms similar to that of oxaliplatin that are independent of DNA damage [34].

In accord with our design expectations, conjugate **4** was found to induce expression of p53 and its functional activation in both the A2780 and 2780CP cell lines, as evidenced by Western blotting and monitoring of the transcriptional activation of p21 as a downstream target of p53. Conjugate **4** was thus found to mirror the behavior seen for oxaliplatin, but not cisplatin, a platinum drug that is unable to induce p53 induction in the case of the resistant 2780CP cell line (Figure 7).

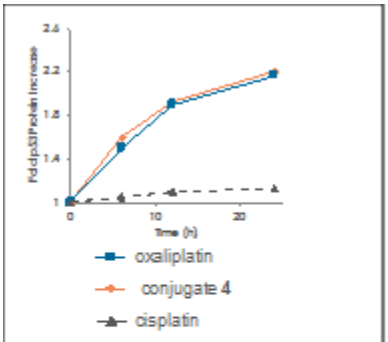

Figure 7. Activation of dormant p53 in 2780CP Pt resistant cells. The data for oxaliplatin and conjugate **4** were taken from ref. 32. Those for cisplatin were taken from ref. 33.

Unfortunately, efforts to translate the promise seen in the *in vitro* studies into xenograft murine tumor models proved challenging. Although in one preliminary study, evidence of tumor localization was seen through MR imaging (Figure 8), difficulties were encountered in finding a formulation adequate to allow for multiple tail vein injections.

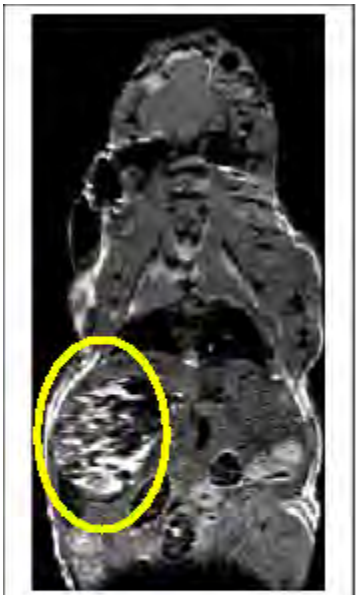

Figure 8. Results of a preliminary study showing a MR image recorded after treating a tumor-bearing mouse with conjugate **4**.

As a consequence, initial seemingly promising tumor uptake and growth inhibition results proved difficult to reproduce. A decision was thus made at this juncture to redesign our approach and 1) rely on Pt(IV) prodrug forms of FDA-approved platinum anticancer agents and 2) tether the Pt(IV) payload through the tripyrrane substituents, rather than the *ortho*-phenylenediamine subunit, as in the case of **3** and **4**. This led to the production of second generation texaphyrin-platinum prodrug conjugates as detailed below.

4. Second Generation Texaphyrin-platinum Prodrug Conjugates

As yet, no Pt(IV) agent has received FDA approval as an anticancer drug. However, such species have been extensively explored as potential prodrugs [35]. The canonical thinking underlying these efforts is that the inherently reducing environment of solids tumors, a reflection of the Warburg effect, would lead to reduction of the Pt(IV) form to produce the corresponding Pt(II) form. Pt(IV) complexes typically favor an hexacoordinate octahedral coordination environment, while Pt(II) complexes are characterized by square planar tetracoordination. A consequence of this difference is that, with appropriate design, metal-centered reduction can be used to effect release of an active Pt(II) drug via loss of the axial ligands present in the Pt(IV) prodrug form. Pt(IV) species are generally exchange inert; they are further attractive in that reduced off-target toxicity would be expected compared to the active Pt(II)

species. This expected reduction in toxicity provided an incentive to prepare Pt(IV) texaphyrin conjugates [36]. Further motivation came from an appreciation that, relative to the corresponding Pt(II) species, Pt(IV) complexes are generally more water soluble, which was expected to aid in formulation.

Given the above, we postulated that it would be possible to attach a gadolinium texaphyrin localizing core to a Pt(IV) prodrug form via a single axial carboxylate ligand. This ligation motif, in turn, would serve as a cleavable linker in the reduction was expected to sever the resulting texaphyrin-platinum(II) connection. As a first test of this hypothesis, the Pt(IV) texaphyrin conjugate **5** (Figure 9) was prepared as reported by Thiabaud, *et al.* in 2014 [37].

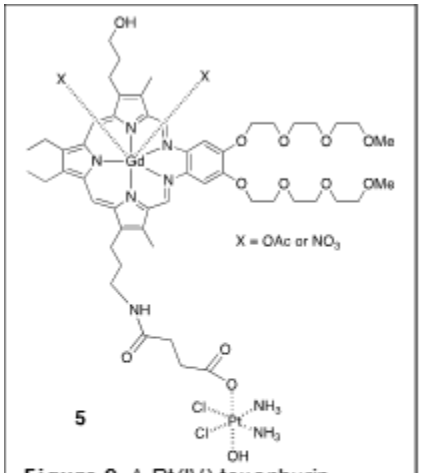

Figure 9. A Pt(IV) texaphyrin conjugate, **5**, that relies on reduction to effect cleavage of the texaphyrin and release the active Pt(II) form of cisplatin.

In this conjugate, the Pt(IV) center was designed to serve as a prodrug form of cisplatin. The critical design element is the axial carboxylate anion that serves to link the Pt(IV) center to the texaphyrin core. The requisite carboxylate species was put in place synthetically by coupling the succinyl functionalized Pt(IV) derivative, **6** (Figure 10), with the amine functionalized texaphryn **7**.

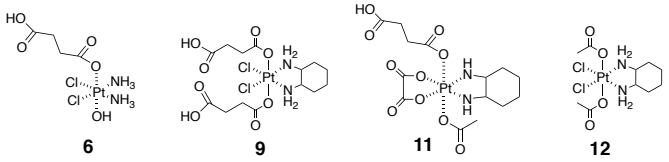

Figure 10. Key platinum(IV) synthetic intermediates and control compounds.

This key texaphyrin monoamine was prepared by subjecting **MGd** to mono-protection (to give **8**), followed by Mitsunobu amination, as originally detailed by Magda and collaborators in 2004 (cf. Scheme 1) [20].

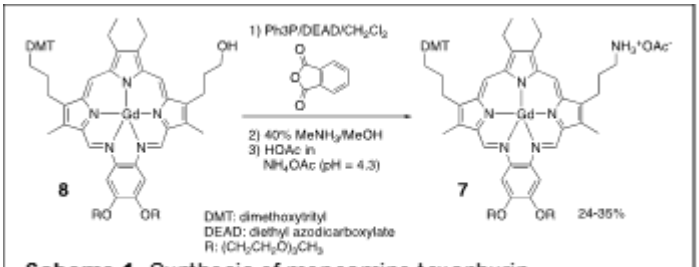

Scheme 1. Synthesis of monoamine texaphyrin.

The synthesis of this key precursor remains the subject of ongoing optimization efforts in the author's laboratory.

Conjugate **5** was found to be stable in the dark, but to undergo photo-induced reduction to release cisplatin under conditions of normal laboratory illumination. The increased hydrolytic stability relative to the earlier Pt(II) conjugates in the absence of light was considered to be an advantage, as was the apparent greater water solubility of **5** relative to, for example, conjugate **3**.

Next, *in vitro* studies, involving comparisons between the wild type and platinum resistant A2789 and 2780CP ovarian cancer cell lines in analogy to what was done for conjugates **3** and **4**, were carried out. These studies revealed that conjugate **5** was somewhat more potent than **3** on a per platinum basis (IC_{50} = 1.3 mM vs 1.6 mM in the A2780 cell line). Unfortunately, and as expected for a cis-platinum prodrug, the resistance factor (defined as IC_{50}(2780CP)/IC_{50}(A2780)) was less than that seen for oxaliplatin; it was ca. 8 in the case of conjugate **5** (vs. ca. 2 in the case of oxaliplatin). Thus, a decision was made to create analogues of **5** that incorporated a Pt(IV) center that upon reductive cleavage would release oxaliplatin as the active drug form.

A finding made subsequent to the publication of conjugates **5** and **6** provided a further incentive to prepare Pt(IV) prodrug forms of oxaliplatin. Specifically, on the basis of early studies showing that **MGd** would catalyze the reduction of dioxygen (to produce reactive oxygen species) in the presence of reducing metabolites that texaphyrins are not redox innocent [38], we came to appreciate that the gadolinium texaphyrin core might act as a redox cycler to facilitate the electron transfer-based conversion of Pt(IV) species to the corresponding Pt(II) forms. A study by Thiabaud, *et al.*, reported in 2016, provided experimental support for this proposition. It was found, for instance, that an equimolar mixture of the bis-succinyl Pt(IV) analogue of oxaliplatin (compound **9**; Figure 10) and **MGd** was more cytotoxic (by ca. 6x) than either species on its own [39].

Given the above findings, an effort was made to prepare texaphyrin conjugates containing a Pt(IV) analogue of oxaliplatin. As detailed in a recent (2020) report by Thiabaud, *et al.*, three mono-Pt(IV) deriv-atives (represented by generic structure **10**;

Figure 11) were thus prepared [40]. These systems differ only in the choice of the second axial ligand present on the Pt(IV) center. As in the case of conjugate **5**, these complexes were generated by coupling the corresponding succinyl substituted precursor (e.g., **11** in the case of the acetate form of **10**; Figure 10) with the monoamino texaphyrin derivative **7**.

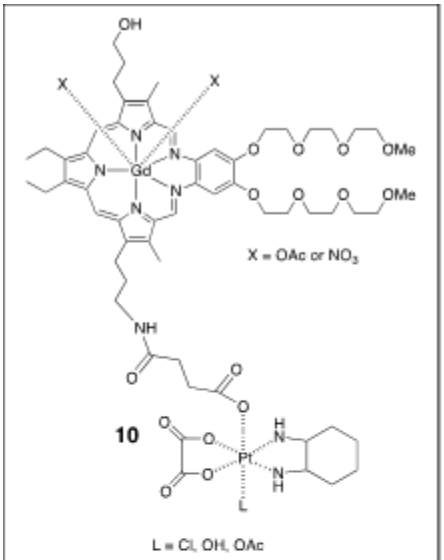

Figure 11. A set of Pt(IV) texaphyrin conjugates, **10**, designed to release the active Pt(II) form of oxaliplatin following reductive cleavage of the axial ligands (L). The three sets of complexes embodied by structure **10** were prepared; they differ in the nature of the axial ligand on the Pt(IV) trans to the succinyl linker. As detailed in the text, the properties of the acetate form were found to be the most optimal. Now referred to OxaliTEX-Pt(IV), this species has emerged as the current lead compound for OncoTEX, Inc.

Since all three versions of conjugate **10** contain a Pt(IV) center, none was expected to be active on its own; all would require reductive cleavage to give oxaliplatin to exert an anticancer effect. They thus provided a test bed for exploring the effect of the non-conjugating axial ligand on the Pt(IV) center. In accord with the literature [41], the effect was found to be substantial. In the presence of glutathione, an endogenous reductant, the chloride ligated version was found to be 90% reduced (and thus cleaved) within 10 minutes upon incubation at 37 ºC. In contrast, both the acetate and hydroxyl ligated versions were relatively stable, remaining ca. 75% intact under these same incubation conditions for roughly 1 and 2 hours, respectively. This

difference in relative stability was found to track with the redox potentials, with the chloride ligated species proving to be substantially easier to reduce than the other two forms. On the other hand, cell proliferation assays revealed that the acetate form of **10** was more potent by a factor of ca. 2 than the corresponding hydroxyl species. It was thus speculated that it represented a Goldilocks version of the complex wherein the inherent stability was high enough to allow for its use, while reduction remained sufficiently facile to allow for release of the active Pt(II) oxaliplatin form [40].

A doubly functionalized version of the acetate form of **10** (i.e., with both hydroxypropyl moieties of the tripyrrane replaced by the Pt(IV) oxaliplatin prodrug) was also prepared. However, its solubility features were less attractive than those of **10**. In fact, the acetate version of conjugate **10**, now referred to as OxaliTEX-Pt(IV), proved soluble in aqueous media. This feature made it very attractive in terms of formulation efforts. It was thus selected for in depth study [40].

Initial *in vitro* tests confirmed that, per our design expectations, there was no difference in the potency of OxaliTEX-Pt(IV) for the wild type and platinum resistance A2780 and 2780CP cell lines within error (resistance factor ≤1.2). OxaliTEX-Pt(IV) also proved more effective than a combination of **MGd** and the control Pt(IV) oxaliplatin analogue **12** (structure shown in Figure 10). OxaliTEX-Pt(IV) was further tested in a number of other cell lines, with potency being observed in all cases as inferred from MTT assays. In A549 human lung cancer cells, for instance, an IC_{50} of ca. 2.1 mM was recorded in an *in vitro* study involving a 5-day incubation period. Further, and as expected for an oxaliplatin prodrug, activation of p53 by OxaliTEX-Pt(IV) was seen in the platinum resistant 2780CP cells, as assessed by monitoring the transcriptional activation of p21 as a downstream target of p53. Finally, *in vitro* studies with the A549 cell line also revealed 1.7x more Pt being taken up into the cells as compared to oxaliplatin. This latter finding was taken as support for the hypothesis underlying the texaphyrin conjugate program, namely that the use of an **MGd** core aids in uptake into cancer cells.

Based on the above, OxaliTEX-Pt(IV) was selected for study *in vivo* [40]. A number of animal studies were thus carried out using various mouse models. As a predicate to tests of efficacy, tolerability was tested using athymic nude mice. Repeat dose studies revealed that OxaliTEX-Pt(IV) was well tolerated with no significant body weight loss being observed over a 30-day period when mice were dosed via intravenous (*i.v.*) tail vein injection (60 mg/kg per dose) on days 1, 5, 9, and 13 (referred to as 2qwx2) with concurrent and subsequent monitoring. Confirmatory analyses revealed that up to 70 mg/kg could be tolerated. This is ca. 4x the limit found for oxaliplatin on an equivalent per-platinum (i.e., per mole) basis.

Initial evidence of antitumor efficacy was seen in athymic nude mice bearing established subcutaneous (s.c.) A549 human lung cancer xenografts (n = 9 mice per group). At the study end point, day 28, mice treated with oxaliplatin exhibited statistically insignificant growth inhibition relative to the vehicle group. In contrast, statistically significant (relative to the oxaliplatin group) tumor growth inhibition was seen in xenograft-bearing mice treated *i.v.* with OxaliTEX-Pt(IV) (values of 51, 58, and 61%, respectively, for the 50, 60, and 70 mg/kg per dose cohorts).

Efficacy studies involving OxaliTEX-Pt(IV) were also conducted in mice bearing cell-derived (A2780 ovarian and HCT116 colon) and syngeneic tumors (CT26 colon and EMT6 breast) s.c. xenografts. Statistically significant anticancer activity against all four tumor types was seen relative to both the vehicle and oxaliplatin-treated mice. In these studies, OxaliTex-Pt(IV) and oxaliplatin were studied near their respective maximum tolerated doses (MTDs) of 70 mg/kg and 4 mg/kg, with administration being effected via tail vein injection on days 1, 5, 9, and 13 in both cases (Figure 12).

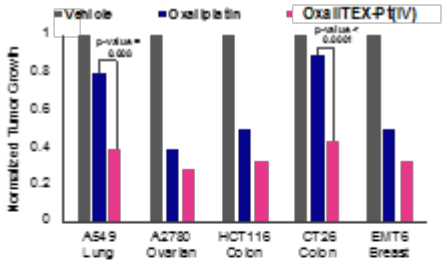

Figure 12. In vivo efficacy of OxaliTEX-PT(IV) (70 mg/kg per dose administered 2qwx2, i.e., on days 1, 5, 9, 13 vs. oxaliplatin (4 mg/kg per dose also administered on days 1, 5, 9, 13) in various s.c. xenograft tumor (A549, A2780, HCT116) and syngeneic tumor (CT26, EMT6) models. The study end point for the A549 model was day 30. The study end point for all other models was the day at which the vehicle-treated mice reached maximum tumor burden. The final data associated with this study were published in ref. 40.

To assess whether OxaliTEX-Pt(IV) might have a role to play in treating tumors that are characterized by poor responses to traditional platinum agents, further efficacy studies in patient-derived xenografts (PDXs), including the 0253 ovarian cancer xenograft (provided by Champions Oncology), were carried out. Mice bearing 0253 ovarian PDX tumors did not respond to treatment with carboplatin (the current standard of care platinum drug for this disease) when administered at a dose level near its MTD. In contrast, treatment with OxaliTEX-Pt(IV), again at a dose close to the MTD, resulted in 95% tumor growth inhibition at the end of the study (Figure 13, left). This delay also translated to a statistically significant increase in survival (Figure 13, right).

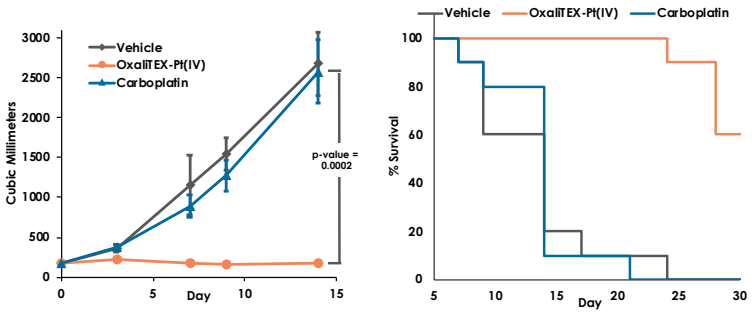

Figure 13. Tumor growth delay (left) and (right) Kaplan–Meier curves of mice bearing 0253 ovarian patient-derived xenograft (PDX) tumors (n = 10 per group). In treatment arm of this study, mice were administered 70 mg/kg per dose of OxaliTEX-Pt(IV) *i.v.* via tail vein injection on days 0, 4, 8, and 12 (2qwx2). The carboplatin group received 30 mg/kg per dose of carboplatin on days 0, 4, 8, 12, 16, and 20 (2qwx3). Error bars represent the standard deviation. P value between OxaliTex-Pt(IV) and carboplatin on day 14 was 0.0002. These data were originally published in ref. 40.

Promising results were also found in related studies involving the 0069 colorectal PDX model. In neither case was appreciable weight loss seen during the course of the studies (cf., e.g., Figure 14). This latter finding was taken as evidence that, at the near-MTD doses administered, OxaliTEX-Pt(IV) was well tolerated.

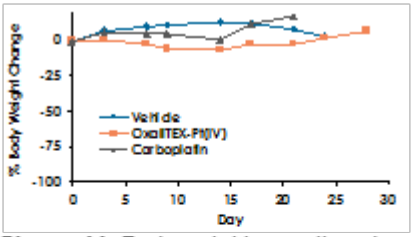

Figure 14. Body weights monitored as a function of time for the study shown in Figure 12. Mice were administered vehicle, OxaliTEX-(IV) and carboplatin via tail vein injection. The regimens are as follows: Vehicle and OxaliTEX (70 mg/kg/dose on days 1,5,9,13. Carboplatin (30 mg/kg/dose for 2qwx3).

As a complement to the efficacy studies, initial biodistribution studies were carried out. It was found that the conjugation of the Pt(IV) prodrug that makes up OxaliTEX-Pt(IV) to the amphiphilic gadolinium texaphyrin core, serves to alter the biodistribution away from the kidney and more toward the liver relative to what is normally seen for platinum drugs. This redistribution and presumed change in dominant clearance pathways may prove beneficial in a clinical setting given the renal

toxicity issues that have long plagued cisplatin.

In a separate experiment involving mice bearing HCT116 colon xenografts, a statistically significant increased level of tumor tissue localization was seen for OxaliTEX-Pt(IV) relative to oxaliplatin (based on analyses of excised tumors) after normalization to the amount of agent administered. Localization of OxaliTEX-Pt(IV) in cancerous lesions in preference to healthy tissues was further corroborated with pharmacokinetic studies in mice. It was found that that the low-level exposure to "free" Pt contributes to drug tolerance in the case of normal tissues, whereas tumor-targeting as provided by OxaliTEX, contributes to greater tumor uptake that enhances antitumor effects [42]. This was taken as further support for the notion that conjugation of an active drug or prodrug to a texaphyrin core can lead to enhancements in tumor localization. Thus, this result serves not just to underscore the promise inherent in OxaliTEX-Pt(IV) as a drug lead, it also validates ongoing efforts to develop texaphyrins as tumor-targeting carriers for a range of active therapeutics beyond platinum.

5. Conclusion

In September of 2019 the intellectual property rights [43,44] underpinning the texaphyrin drug conjugate program were licensed to the IQ Global Group by The University of Texas at Austin and MD Anderson Cancer Center [45]. Active efforts are now ongoing to streamline and scaleup the synthesis of OxaliTEX-Pt(IV), including so-called GMP manufacturing, and carry out IND-enabling preclinical studies involving a variety of additional animal models. In parallel, work is being devoted to the creation of new texaphyrin conjugates wherein both the central texaphyrin core and the nature of the appended active agent are varied. It is expected that the results of these efforts will be communicated in due course.

Acknowledgments

The author expresses his gratitude to the many team members who have helped develop the texaphyrin-platinum conjugate project, including Darren J. Magda, Richard A. Miller, Tarak Mody, Pavel Anzenbacher, Jr., Joan Carvalho, Mark Fountain, Wen-hao Wei, Jonathan F. Arambula, Grégory Thiabaud, Kwan Soo Hong, Greg Lyness, Alan B. Watts, Zahid Siddik, Guangan He, Rick Finch, Sajal Sen, Calvin Chao, and Adam Sedgwick. Over the course of the project lifetime, funding for the work in Austin has been provided by the National Institutes of Health (grant CA68682), Pharmacyclics, Inc., The University of Texas at Austin TI-3D (supported by the Robert A. Welch Foundation, grant H-F-0032), the American Cancer Society (grant PF-11-015-01-CDD to J. F. Arambula) the Cancer Prevention and Research Institute of Texas (grants RP120393 and RP140108). Current project funding is provided by OncoTEX, and the Robert A. Welch Found-ation (F-1018).

References

1. Sessler JL, Murai T, Lynch V, Cyr M. *J. Am. Chem. Soc.*, 1988, 110, 5586-5588.
2. Sessler JL, Murai T, Hemmi G. *Inorg. Chem.*, 1989, 28, 3390-3393.
3. Sessler JL, Mody TD, Hemmi GW, Lynch V. *Inorg. Chem.*, 1993, 32, 3175-3187.
4. Sessler JL, Murai T, Hemmi G. U.S. Patent no. 4,935,498.
5. Sessler JL, Hemmi G, Maiya BG, Harriman A, Judy ML, Boriak R, Matthews JL, Ehrenberg B, Malik Z, Nitzan Y, Rück A. *Proc. SPIE Int. Opt. Eng.*, 1991, 1426, 318-329.
6. Young SW, Woodburn KW, Wright M, Mody TD, Fan Q, Sessler, JL, Dow WC, Miller RA. *Photochem. Photobiol.*, 1996, 63, 892-897.
7. Sessler JL, Mody TD, Hemmi GW, Lynch V, Young SW, Miller RA. *J. Am. Chem. Soc.*, 1993, 115, 10368-10369.
8. Young SW, Sidhu MK, Qing F, Muller HH, Neuder M, Zanassi G, Mody TD, Hemmi G, Dow W, Mutch JD, Sessler JL, Miller RA. *Invest. Radiol.*, 1994, 29, 330-338.
9. Young SW, Quing F, Harriman A, Sessler JL, Dow WC, Mody TD, Hemmi G, Hao Y, Miller RA. *Proc. Natl. Acad. Sci. USA*, 1996, 93, 6610-6615. Correction: *Proc. Natl. Acad. Sci. USA*, 1999, 96, 2569.
10. Miller RA, Woodburn K, Fan Q, Renschler M, Sessler JL, Koutcher JA. *Int. J. Biol. Radiat Oncol.*, 1999, 45, 981-989.
11. Sessler JL, Tvermoes NA, Davis J, Anzenbacher P, Jursíková K, Sato W, Seidel D, Lynch V, Black CB, Try A, Andrioletti B, Hemmi G, Mody TD, Magda DJ, Král V. *Pure Appl. Chem.*, 1999, 71, 2009-2018.
12. Sessler JL, Miller RA. *Biochem. Pharmacol.,* 2000, 59, 733-739.
13. Magda D, Lepp C, Gerasimchuk N, Lee I, Sessler JL, Lin A, Biaglow J, Miller RA. *Int. J. Radiat. Biol. Oncol. Phys.*, 2001, 51 1025-1036.
14. Magda DJ, Sessler JL, Gerasimchuk N, Miller RA in Medicinal Inorganic Chemistry, eds. Sessler JL, Doctrow S, McMurry T, Lippard SJ, American Chemical Society Symposium Series 903, Oxford University Press, 2005, ch. 8, pp 110-136.
15. Mehta MP, Shapiro WR, Phan SC, Gervais R, Carrie C, Chabot P, Patchell RA. Glantz MJ, Recht L, Langer C, Sur RK, Roa WH, Mahe MA, Forti A, Nieder C, Meyers CA Smith JA, Miller R.A., Renschler MF. *Int. J. Radiat. Oncol. Biol. Phys.*, 2009, 73, 1069-1076.
16. Mehta MP, Rodrigus P, Terhaard CHJ, Rao A, Suh J, Roa W, Souhami L, Bezjak A, Leibenhaut M, Komaki R, Schultz C, Timmerman R, Curran W, Smith J, Phan SC, Miller RA, Renschler MF. *J. Clin. Oncol.*, 2003, 21, 2529-2536.
17. Miller RA, Woodburn K, Fan Q, Renschler MF, Sessler JL, Koutcher JA. *Int. J. Radiat. Oncol. Biol. Phys.*, 1999, 45, 981-989.
18. Mehta MP, Khuntia D. *Neurosurgery*, 2005, 57, S33-S44.
19. Mehta MP, Shapiro WR, Glantz MJ, Patchell RA, Weitzner MA, Meyers CA, Schultz CJ, Roa WH, Leibenhaut M, Ford J, Curran W, Phan S, Smith JA, Miller RA, Renschler MF. *J. Clin. Oncol.*, 2002, 20, 3445-3453.
20. Magda DJ, Wang Z, Gerasimchuk N, Wei WH, Anzenbacher P, Sessler JL. *Pure Appl. Chem.*, 2004, 76, 365-374.
21. Wei WH, Fountain ME, Sessler JL,

Magda DJ, Wang Z, Miller RA in Macrocyclic Chemistry, ed. Gloe K, Springer, Dordrecht, 2005, ch 25, pp 407-425.
22. Wei WH, Fountain M, Magda D, Wang Z, Lecane P, Mesfin M, Miles D, Sessler JL. *Org. Biomol. Chem.*, 2005, 3, 3290-3296.
23. Lee MH, Kim EJ, Lee H, Kim HM, Chang MJ, Park SY, Hong KS, Kim JS, Sessler JL. *J. Am. Chem. Soc.*, 2016, 138, 16380-16387.
24. Arambula JF, Sessler JL. *Chem.*, 2020, 6, 1634-1651.
25. Siddik ZH. *Oncogene*, 2003, 22, 7265-7279.
26. Siddik ZH in Drug Resistance in Cancer Cells, eds. Mehta K, Siddik ZH, Springer Science: New York, 2009, ch. 9, pp. 209-231.
27. Sessler JL, Magda D, Mody TD, Anzenbacher P, Carvalho J. U.S. Patent no. 6,207,660.
28. Arambula JF, Sessler JL, Fountain ME, Wei WH, Magda D, Siddik ZH. *Dalton Trans.*, 2009, 48, 10834-10840.
29. Gust R, Schnurr B. *Monatsh. Chem.*, 1999, 130, 637-644.
30. Arambula JF, Siddik Z, Sessler JL. *Bioorg. Med. Chem. Lett.,* 2011, 21, 1701-1705.
31. Martinez-Rivera M, Siddik ZH. *Biochem. Pharmacol.*, 2012, 83, 1049-1062.
32. Arambula J, Sessler JL, Siddik ZH. *Med. Chem. Commun.*, 2012, 3, 1275-1281.
33. Xie X, He G, Siddik ZH. *Mol. Cancer Res.*, 2017, 15, 328-339.
34. Bruno P, Liu Y, Park G, Murai J, Koch CE, Eisen TJ, Pritchjard, JR, Pommier Y, Lippard SJ, Hemann, MT. *Nat Med.*, 2017, 23**,** 461-471.
35. Johnstone TC, Suntharalingam K, Lippard SJ. *Chem. Rev.*, 2016 116, 3436-3486.
36. Preihs C, Arambula J, Magda D, Jeong H, Yoo D, Cheon J, Siddik Z, Sessler JL., *Inorg. Chem.*, 2013, 52*,* 12184-12192.
37. Thiabaud G, Arambula JF, Siddik ZH, Sessler JL. *Chem. Eur. J.*, 2014, 20, 8942-8947.
38. Magda D, Lepp C, Gerasimchuk N, Lecane P, Miller RA, Biaglow JE, Sessler JL. *Chem. Commun.,* 2002, 2730-2731.
39. Thiabaud G, McCall R, He G, Arambula JF, Siddik ZH, Sessler JL. *Angew. Chem., Int. Ed. Engl.*, 2016, 55, 12626-12631.
40. Thiabaud G, He G, Sen S, Shelton KA, Baze WB, Segura L, Alaniz J, Macias RM, Lyness G, Watts AB, Kim HM, Lee H, Cho MY, Hong KS, Finch R, Siddik ZH, Arambula JF, Sessler JL. *Proc. Natl. Acad. Sci. USA*, 2020 117, 7021-7029.
41. Wexselblatt D, Gibson DJ. *Inorg. Biochem.*, 2012, 117, 220-229.
42. He G, Thiabaud G, Shelton KA, Segura LJ, Sessler JL, Finch RA, Siddik ZH, Arambula JF. *Cancer Res.*, 2021 (81) (13 Supplement) 1073.
43. Sessler JL, Arambula J, Siddik Z, Thiabaud G. U.S. Patent No. 10,406,167.
44. Sessler JL, Lee MH. U.S. Patent Application no. 20190231888.
45. The iQ Group Global acquires new anticancer drug platform from University of Texas [last accessed: August 15, 2001] https://www.prnewswire.com/news-releases/the-iq-group-global-acquires-new-anticancer-drug-platform-from-university-of-texas-300918642.html

The Chemist
Journal of the American Institute of Chemists

Hollow-fine-fibre Membranes: Collapse Pressure and Pressure Drop Analysis

Akram Tawari [a,*], Bashir Brika [b]

[a] *Department of Process Engineering, Faculty of Engineering, Stellenbosch University Stellenbosch, South Africa*
(E-mail: tawari@live.com)
[b] *Libyan Advanced Center of Chemical Analysis, Libyan Authority for Scientific Research Tripoli, Libya*
(E-mail: bashirforlibya@gmail.com)

Abstract: The aim of this work is to produce cellulose acetate (CA) hollow-fine-fibre membranes with good water flux performance in the 95 – 96% salt retention range for brackish water desalination from first principles. First, the acceptable range of fibre dimensions was determined by means of a collapse pressure calculation using the elastic buckling pressure equation (thin shell assumption). Second, the pressure drop across the fibre wall in the hollow-fine fibre was determined by using the Hagen-Poiseuille equation to determine how this would affect the chosen fibre dimensions. It was determined that the acceptable range of fibre dimensions was 222 – 247 µm, and the wall thickness was 50 µm. Fibres with these dimensions exhibited a high resistance to brackish water operating pressure of 20 – 25 bar, without collapse. The pressure drop calculations of these dimensions showed a sufficiently low pressure drop across the fibres.

Key Words: hollow-fine-fibre membrane, cellulose acetate, collapse pressure, pressure drop

*Corresponding author

1. Introduction

Hollow-fibre membranes are of high commercial importance. Their fabrication by spinning dopes or mixtures containing membrane forming materials (polymers) has been described in a series of patents by Mahon (1966), assigned to the Dow Chemical Company [1,2].

Hollow-fibre membranes were developed to be used for a wide range of applications, such as water purification (e.g., potable water production from saline or non-saline resources, bioseparation, wastewater treatment), gas separation and membrane contactors [3-5].

The diameters of hollow fibres vary over a broad range, from 50 to 3000 μm. Hollow fibres can either made as a homogenous dense structure or, more preferably, an asymmetric microporous structure. Hollow-fine-fibre RO membranes operate at high pressures and this is accomplished by engineering the membrane material into special modules. Essentially, a hollow-fine-fibre membranes module consists of thousands or millions of individual fine fibres, depending on fibre dimensions, which are then are looped into a bundle around a perforated central feed tube. Both ends of the fibre bundle are sealed off by a potting resin creating a tube-sheet, open on one end and closed on the other end (Figure 1).

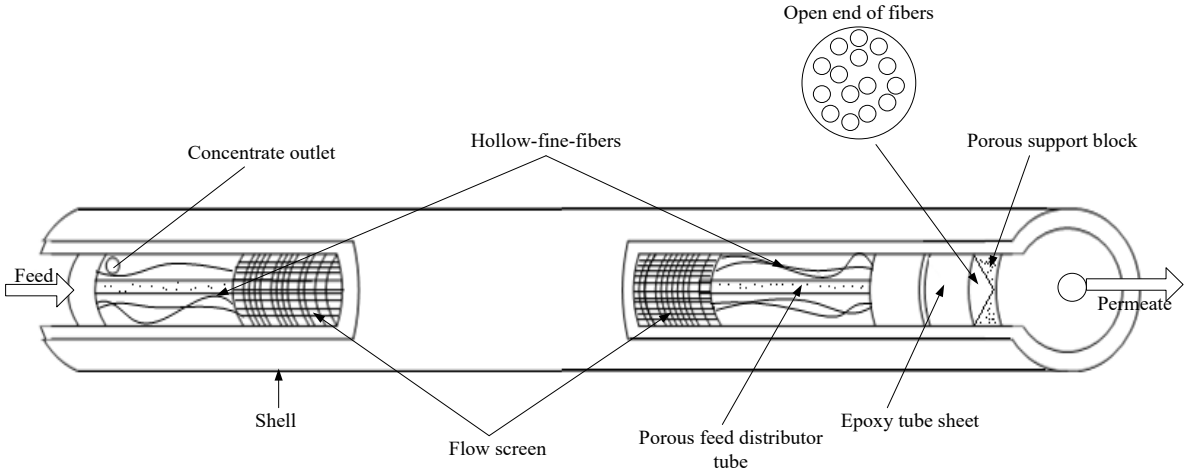

Figure 1. Schematic Presentation of a Hollow-fine-fibre Module (Du Pont B9 Permeator)

Hollow fibres have key advantages over other membrane configurations, such as flat-sheets. Hollow fibres have extremely high membrane surface area to pressure-vessel volume, which gives high productivity per unit volume. It is for this reason that hollow fibres are commonly used in industry [6]. The other advantage of the hollow fibres is that they are self-supporting, unlike the flat-sheet membranes that need a supporting material. In addition, concentration polarization usually is smaller under most practical conditions in hollow fibres than in flat-sheet membrane systems [7].

It is well known that it is very difficult to develop a hollow-fibre spinning process by adopting the process conditions developed for asymmetric flat-sheet membranes. This is because there are two coagulation processes occurring during the spinning of hollow fibre (the interior and exterior surfaces), while there is only one coagulation process on the surface for an asymmetric flat-sheet membrane.

The spinning of asymmetric hollow-fibre membranes requires special handling procedures in order to achieve and maintain optimum permeation properties [8],

particularly in the following steps in the fabrication process:

- spinning of plasticized fibres;
- processing the fibres in a wet swollen state;
- replasticizing the fibres after the spinning operation; and
- physical modification of the fibres after the spinning operation.

The objectives of this study are the following:

- ✓ To determine the acceptable range of fibre diameters for brackish water desalination by means of collapse pressure analysis, using the elastic buckling pressure equation for a thin shell under external pressure (thin shell assumption).
- ✓ To determine the pressure drop (DP) along the fibre bore in the hollow-fine-fibre by using the Hagen-Poiseuille equation in order to determine how DP affects the chosen fibre dimensions.

To perform collapse pressure tests on produced fibres to validate the calculated fibre dimensions data.

2. Collapse and Pressure Drop Calculations

In order for hollow-fine-fibre membrane to be useful in RO pressure applications, it must be able to withstand a considerable trans-membrane pressure difference. The ability of brackish water hollow-fine-fibre membranes to withstand its operating pressures without collapse, will be taken into account as an issue; firstly, to produce highly resistant hollow-fine-fibre diameters by using a suitable spinneret, and secondly, to provide a membrane module with high packing density (the smaller fibre dimensions, the higher resistance to brackish water operating pressures and subsequently the higher packing density). To determine the acceptable fibre dimension for RO, it was necessary to adopt the buckling pressure equation of cylindrical shells under external pressures to equate fibre dimensions to collapse pressure. Note that the smaller the fibre dimensions are, the higher pressure drop across the membrane, thus calculating the pressure drop across the fibre bore must also be taken into account to determine the acceptable fibre dimensions [9].

Elastic Collapse Pressure on Cylindrical Shells Subjected to External Pressure

Elastic collapsing pressure is the maximum pressure that can be applied to hollow cylindrical tubes for wall deformation to remain reversible. At higher pressures, the tubes collapse. When the external pressure applied on a cylindrical shell or tube exceeds certain values, the tube collapses, with longitudinal corrugations, according to the pressure increase [10]. This problem of finding the pressure required to bring about this collapse depends for its solution upon what is known in mathematical elasticity as the general theory of cylindrical shells under external pressure. For this reason, more rigid mathematical theory, which has been adopted by Southwell [10], showed a good agreement with the theory of collapse pressure of bore tubes. This theory of elastic

collapsing pressure will be used in this study and its formula is expressed by the following equation (1):

$$P = 2\frac{E}{1-V^2}\,(t/OD)^3 \quad (1)$$

where P is the collapse pressure, E is Young's modulus (GPa), v is the Poisson's ratio (dimensionless), OD is the outside diameter (μm), and t is thickness of the hollow fibre (μm) (outside radius - inside radius).

The equation suggests that collapse pressure of hollow fibre is very high because OD is very small.

Pressure Drop Across the Wall of a Hollow-fine-fibre Membranes

There is ample evidence in the literature suggesting that the pressure drop along the fibre bore varies considerably with the fibre diameter, the smaller the diameter, the higher the pressure drop [11]. It is therefore necessary to calculate the effect of pressure drop in the fibre bore and how much of this variation in the pressure drop will affect the chosen fibre dimensions determined by collapse pressure calculations. In this study, the steady laminar flow of incompressible fluid through the hollow-fine-fibre with a semi-permeable wall and length will be expressed by the Hagen-Poiseuille equation for laminar flow [12], in order to calculate the pressure drop across the fibre bore.

Pressure Drop Across the Fibre Wall of the Hollow-fine-fibre Membranes

Hermans [13,14] studied the effect of hydraulic flow characteristics of Berman's analysis in a permeable wall of a tubes on the flow mechanism of a hollow fibre and suggested that a Poiseulle's equation can be applied to the flow pattern inside the fibres. He therefore combined that equation with a membrane transport equation of pure water and proposed an initial model for complete water retention by hollow-fibre RO membranes. This model was taken as a basis by Orofino [15] in the development of the hollow filament technology for a RO desalination system.

The axial flow on the inside of a single hollow fibre was studied by Chen and Petty [16]. They studied the volumetric flow of an incompressible fluid undergoing RO in a hollow fibre with a semipermeable wall by applying Darcy's law for membrane transport. The fibre was sealed at one end with epoxy and open at the other end to atmospheric pressure. They used a diffusion model to describe the passage of salt through the membrane. However, Evanglista and Jonsson [17] proposed a model were the pressure drop inside a hollow fibre was considered with the concentration polarization on the shell side.

Sekino [18] used the Kimura-Sourirajan model to propose a friction-concentration-polarization model by employing the solution diffusion model and concentration polarization, and calculating the pressure drop in the hollow fibre bore using the Poiseuille equation and the pressure drop on the shell side by the Ergun equation.

Ohya et al. [19] studied the RO characteristics of a B-9 hollow-fibre membrane by neglecting the pressure drop on both the shell side and in the fibre bore. They took into account the effect of concentration polarization on the bulk side. Other assumptions, including neglecting the osmotic pressure and the concentration

polarization on the bulk side of the membranes, where made by Starov et al. [20] and Smart et al. [21], who optimized the performance of various hollow fibre geometries with their mathematical model.

Collapse Pressure Calculations

The purpose of this calculation is to determine an acceptable range of CA hollow-fine-fibre dimensions for brackish water membranes, with sufficient strength to withstand high operating pressures without collapse. This acceptable range of the fibre dimensions will also be used in addition to the pressure drop calculations, for selecting an appropriate spinneret orifice dimensions to prepare the required hollow-fine fibres in this study. Acceptable fibre dimension was obtained by using the elastic buckling (collapse) pressure equation for a cylindrical shell or tube under external pressures [22]. The collapse pressure of hollow-fibre membrane is given by equation 1. Therefore, to determine the acceptable fibre dimension from equation 1, the following parameters should be obtained.

1- Fibre wall thickness can be obtained by assuming the geometry of hollow-fine-fibre membrane as a thick-walled cylinder of nominal circular shape that has a ratio of outside to inside diameter of 2:1. This ratio was chosen arbitrarily. Based on the above geometry and the object of producing hollow-fine-fibre in this study, the wall thickness t is assumed to be 50 μm, which is the mean from the fibre's outside to its inside diameter (equation 2).

$$t = (OD - ID)/2 \tag{2}$$

2- The overall osmotic pressure of sea water is considered to be 25 bar.

3- The Poisson ratio (v), which is the ratio of transverse contraction strain to longitudinal extension strain in the direction of stretching force.

Poisson's ratio (v) can be expressed as (equation3):

$$\nu = \varepsilon_t / \varepsilon_l \tag{3}$$

where (v) is the Poisson's ratio, ε_t is the transverse strain and ε_l is the longitudinal or axial strain of the hollow fibre.

4- Young's modulus, which is (E), is a measure of the stiffness of an isotropic elastic material to elastic deformation. It is defined as the ratio of the tensile stress to the tensile strain.

Young's modulus (E) can be expressed as (equation4):

$$E = \sigma / \varepsilon \tag{4}$$

Stress and strain for Poisson's ratio and Young's modulus can be expressed as (equations 5-6):

$$\sigma = F\,A \tag{5}$$

$$\varepsilon = dl\,/\,L \tag{6}$$

where F is the force applied, A is the cross-sectional area through which the force is applied, dl is change in length, and L is initial length of the hollow fibre.

For isotropic materials the bulk and shear modulus are linked to Young's modulus (E) and Poisson's ratio (v) [23] by (equation 7):

$$E = 2\,G\,(1 + v) \qquad E = 6\,K\,(0.5 - v) \tag{7}$$

where (G) is shear modulus, which is the ratio of shear stress to the shear strain, (K) is the bulk modulus, which is the substance's resistance to uniform compression.

The Poisson's ratio of a stable, isotropic, elastic material cannot be less than -1.0 nor greater than 0.5 due to the requirement that the elastic modulus; the shear modulus and bulk modulus have positive values [24]. Most materials have Poisson's ratio values ranging between 0.0 and 0.5. Rubber has a Poisson ratio of nearly 0.5. Cork's Poisson ratio is close to 0. CA Poisson ratio is 0.4 [25]. Typical Young's modulus (modulus of elasticity) values found in the literature for CA hollow fibres was as high as 0.114 GPa and as low as 0.094 GPa.127 The first value was for a CA hollow fibre prepared by the wet spinning process for microfiltration from a dope solution containing 27% CA and 73% formic acid. The second value was also for CA prepared by wet spinning from a dope solution containing 26.5% CA, 0.5% chitosan and 73% formic acid [26]. These values of Young's modulus were typically an order of magnitude less than the value of the Young's modulus of CA as raw material (1 – 4 GPa, mechanical properties of CA powder from Eastman Company). This is likely because the values of 1 – 4 GPa are general characteristics of the polymer material and not specifically for hollow fibre geometries which have an asymmetric porous structure. The acceptable fibre dimension can then be obtained by deriving the outside diameter from equation 1, giving equation 8. The parameters used in equation 8 were chosen from polymer characteristics taken from literature, allowing the outside diameter to be predicted. Therefore equation 8 becomes:

$$O\Delta = \sqrt[3]{\frac{2\,Et^3}{P(1-v^2)}} \tag{8}$$

$OD \cong 237\mu m$

Determining the effect of changing fibre dimensions on the collapse pressure can also be calculated using equation 1 with changing the fibre dimensions of the obtained fibre diameter (237 μm), while maintaining a constant wall thickness. These calculations are presented in Tables 1 and 2, respectively. Figure 2 shows the effect on the collapse pressure of a hollow-fine-fibre, calculated using both values of Young's

modulus (0.114 and 0.094 GPa). Tables 1 and 2 show the influence of varying the outside fibre diameter of 237 μm on the collapse pressure values at two different Young's modulus values. The variation of outside fibre diameter was done by keeping a constant wall thickness, while increasing and decreasing the inside and outside fibre diameter, respectively, at constant value of 5 μm. The inside diameter was calculated by substituting the value of 237 μm and wall thickness of 50 μm in equation 2.

Table 1. Hollow-fine-fibre Collapse Pressure (Young's modulus 0.114 GPa, wall thickness 50 μm)

Inside diameter ID (μm)	Outside diameter OD (μm)	Collapse pressure P (GPa)	Collapse pressure bar
62	162	0.00798	79.80
67	167	0.007285	72.84
72	172	0.006668	66.67
77	177	0.006119	61.18
82	182	0.005628	56.27
87	187	0.005188	51.88
92	192	0.004794	47.93
97	197	0.004438	44.37
102	202	0.004116	41.16
107	207	0.003825	38.25
112	212	0.003561	35.60
117	217	0.00332	33.20
122	222	0.003101	31.01
127	227	0.002901	29.00
132	232	0.002717	27.17
137	237	0.002549	25.48
142	242	0.002394	23.93
147	247	0.002252	22.51

Table 2. Hollow-fine-fibre Collapse Pressure (Young's modulus 0.094 GPa, wall thickness 50 µm)

Inside diameter ID (µm)	Outside diameter OD (µm)	Collapse pressure P (GPa)	Collapse pressure bar
62	162	0.00654	65.45
67	167	0.00597	59.74
72	172	0.00546	54.68
77	177	0.00501	50.18
82	182	0.00461	46.15
87	187	0.00425	42.55
92	192	0.00393	39.31
97	197	0.00363	36.39
102	202	0.00337	33.76
107	207	0.00313	31.37
112	212	0.00292	29.20
117	217	0.00272	27.23
122	222	0.00254	25.43
127	227	0.00237	23.79
132	232	0.00222	22.28
137	237	0.00209	20.90
142	242	0.00196	19.63
147	247	0.00184	18.46

The results show that the collapse pressure decreases gradually with increasing outside diameters and decreasing Young's modulus. Therefore, the collapse pressure is directly dependent on the Young's modulus and inversely to the outside diameter. From Figure 2, there is a clear indication that the Young's modulus and the fibre dimensions have a significant effect on the collapse pressure and subsequently give the hollow-fine-fibre enough mechanical strength to withstand high operating pressures encountered in RO without collapse.

It can be seen from Figure 2 that there is an acceptable range of fibre dimensions (222 – 247 µm) that showed an ability to withstand the operating pressure for brackish water applications. Typically, the operating pressure used for brackish water desalination would be in the range of 20 – 25 bar as the lower salt concentration creates a lower osmotic pressure and therefore the

lower RO pressure is possible. Therefore, a 50 µm wall thickness and outside fibre diameters within the range of 222 – 247 µm would be acceptable for brackish water RO applications.

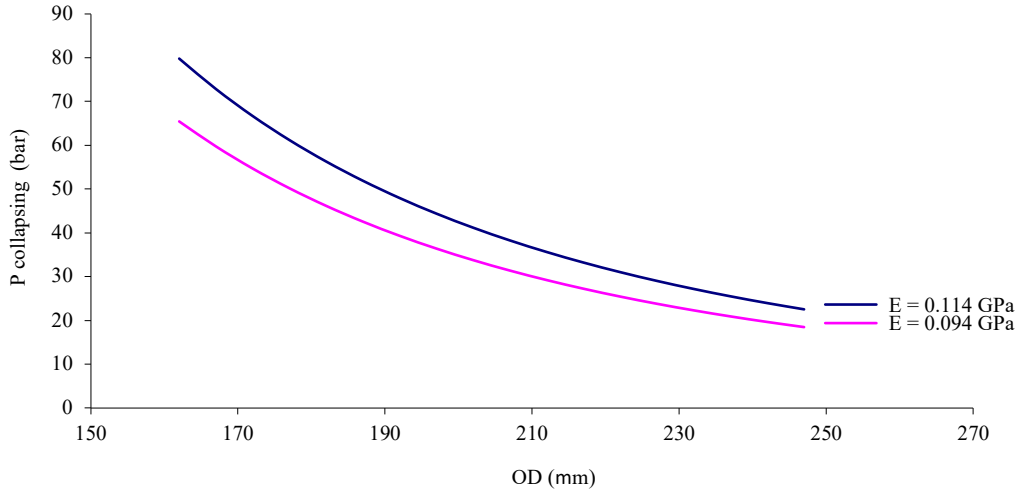

Figure 2. Collapse Pressure of Hollow Fibre, Calculated Using Both Values of Young's Modulus (0.114 and 0.094 GPa)

3. Pressure Drop Across the Wall of a Hollow-fine-fibre Membrane

Pressure drop along the fibre bore is greatly affected by the size of internal diameter [11]. Therefore, the pressure drop calculation is necessary for the specified range of the fibre dimensions determined above.

The pressure drop along the fibre bore is calculated by the Hagen-Poiseuille equation. Numerical analysis by a computer program (FORTRAN) is used to solve the equation and the software codes are shown in Appendix A. The governing equations in this calculation are fluid pressure drop, material balance and membrane transport equations.

The assumptions made in this calculation are as follows:

- The flux in the fibre bore is from the left to the right, where there is no pressure drop at the sealed end from the left, but there is a pressure drop along the length of the fibre towards the right. The fibre is assumed to be 1 m long. At one end, the fibre is sealed and other end, it is open to the atmospheric pressure (Figure 3).

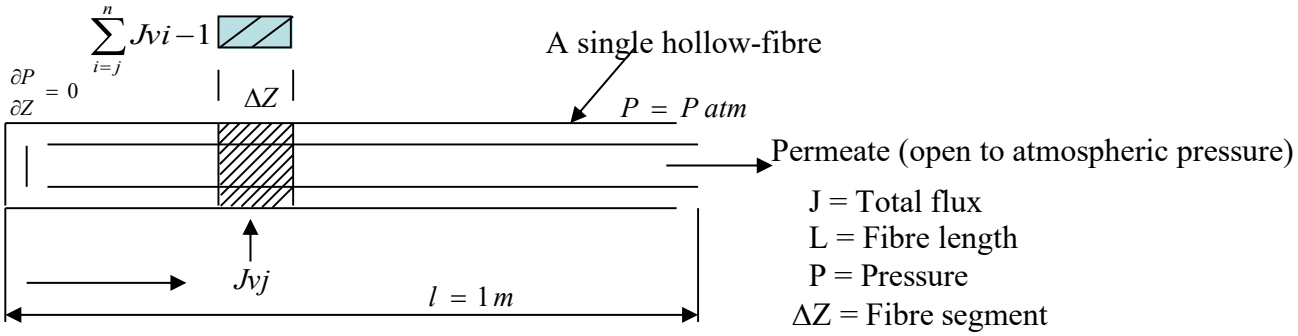

Figure 3. Schematic Diagram of Single Hollow-fine-fibre

- The pressure drop in the shell is small, and the pressure in the shell is nearly equal to the feed pressure.

Fluid Pressure Drop Equations

The axial pressure drop inside the fibres is expressed by the Hagen-Poiseuille equation (9):

$$\Delta P = \frac{128\,\mu\,Z\,Q_P}{\pi\,d_I^4} \tag{9}$$

Differentiating this equation with respect to the length of the fibre, we get (equation 10):

$$\frac{dP}{dZ} = \frac{128\,\mu\,Q_p}{\pi\,d^4{}_I} \tag{10}$$

where P is the pressure inside the fibre (Pa), Z is the axial direction of the fibre (m), d_I is the inside fibre radius (m), μ is the dynamic viscosity of water = 0.798×10^{-3} (Pa.s), and Q is the flow rate (m^3/sec).

$$\frac{dQ}{dZ} = \pi\,d_O\,J_v$$

Material Balance Equation

The material balance within the fibre bore is given by the following equation (11):

$$0 \le Z \le L \tag{11}$$

where d_O is the outside radius (m), J_v is the total flux or the solution flux across the membrane (m^3/m^2 sec) and L is the length of the fibre (m). Differentiation of equation 10 and substitution into equation 11 yields (equation 12):

$$\frac{d^2P}{d^2Z} = \frac{128\,\mu}{d_I^4}\,d_O\,J_v \tag{12}$$

Equation 12 has the following boundary conditions:

at $Z = 0$ $\quad p = p$ atm = 101 325 Pa

at $Z = L$ $\quad \frac{dP}{dz} = 0$

In order to determine the pressure drop along the fibre, the axial direction of the fibre (Z-coordinate) is divided into m = 100 segments each segment is 1 cm in length. Regarding the pressure drop in the fibre bore, however, the axial direction is defined as the length of the fibre. Integrating of equation 12 to obtain the permeate pressure (P_{PJ}) in the fibre segment ΔZ with respect to Z_1 and Z_2 yields (equation 13):

$$\int_{Z1}^{Z2} \frac{dP}{dZ} = \int_{Z1}^{Z2} \frac{128\,\mu}{d_I^4}\,d_O\,J_v\,Z \tag{13}$$

Discretisation of equation 13 by changing it to a linear equation yields equation 14.

$$P_{Pj} - P_{Pj-1} = \frac{128\,\mu\,\Delta Z^2\,d}{d_I^4}\sum_{i=j}^{n} Jvi \tag{14}$$

This equation will be solved numerically by FORTRAN where P_{pj} is the pressure inside the fibre (Pa), ΔZ is the distance between two segments (length of fibre divided by number of segments) (m), d_I is the inside fibre radius (m), μ is the dynamic viscosity of water (Pa.s) = 0.798×10^{-3}, J_v is the total flux or the solution flux across the membrane segment (m^3/m^2 sec), and j subscript at axial coordinates.

Membrane Transport Equations

The solution-diffusion model is a practical model for explaining membrane permeation, and is described as follows:

Water flux $J_w = A\ (\Delta P - \Delta\pi)$ kg/m^2.s

$$J_w = A\ (P_B - P_p) - (\pi_M - \pi_P)$$

$$\pi = \alpha C$$

where π is the osmotic pressure, C is the solute concentration, α is osmotic pressure proportionary constant

then: $J_w = A\ (P_B - P_p) - \alpha\ (C_M - C_P)$

Solute flux $J_s = B\ \Delta C$ kg/m^2.s

$$J_s = B\ (C_M - C_P)$$

where J_w is the water flux through the membrane, J_s is the solute flux through the membrane, A is the water permeability constant, B is the solute permeability constant, P_B is bulk pressure P_P is the permeate pressure, π_M is osmotic pressure on membrane surface, π_P is osmotic pressure on the bore side, and C_p is permeate concentration.

The effect of concentration polarization is usually very small in hollow-fibre RO systems because of relatively low product flux, which is sufficient to reduce the effect of concentration polarization [27]. Where high membrane flux leads to a rapid build-up of retained solutes on the membrane surface and results in concentration polarization [28]. The interface concentration C_M at the membrane surface can be replaced by the local brine concentration C_B.

then:

$$J_w = A\ [\Delta P - \alpha\ (C_B - C_p)]$$

$$J_s = B\ (C_B - C_p)$$

With a tight membrane structure, such as those used for RO desalination processes, a further assumption can be made. The product concentration C_p can be neglected because the flux is so low in these membranes. High-flux membranes have high C_p.

$$J_w = A\ (\Delta P - \alpha C_B)$$

$$J_s = BC_B$$

The total flux or solution flux (J_v) in the equations above is given by the sum of the water flux and the solute flux, (J_s). With highly selective membranes the solute flux can be also neglected.

$$J_v = J_w + J_s/\rho \approx J_w/\rho$$

$$J_v = J_w/\rho$$

In addition, our assumptions will include the use of pure water as feed solution. Thus, the local brine concentration (feed concentration) C_B can be neglected, and the solution flux equation becomes (equation 15):

$$J_v = J_w = A\,(\Delta P) = A\,(P_B - P_p)/\rho \quad (15)$$

Numerical Analysis to Determine the Pressure Drop

The solution flux is calculated according to equation 15, which assumes that permeate pressure (Pp) is equal to atmospheric pressure 101 325 Pa. The bulk pressure P_B is assumed to be equal to the feed pressure. For brackish water desalination at lower salt concentration, lower feed pressure, as low as 20 bar, are used. With slightly higher concentration, the high feed pressure of around 25 bar can be used. Equation 15 requires a water permeability constant for CA. This was found in the literature as 4.294 × 10^{-10} Kg/m^2.s.Pa [29]. This water permeability constant is used in the solution-diffusion model and when using pure water is equal to

$$A_w = D_w\ c_w\ v_w/RTl$$

where D is the diffusion coefficient m^2/s, c is the molar concentration kg-mol/m^3, v is the molar volume m^3/mol, R is the gas constant 8.314 J/mol.K, T is the absolute temperature K, l is the membrane thickness (mm), and the subscript w indicating the solvent (water).

According to the Kimura and Sourirajan approach of transport phenomena across RO membranes, the solvent and solute fluxes through the membrane are mainly characterized by two phenomena: solvent transport in terms of the pure water permeability constant A, and solute transport in terms of the solute permeability constant B [30]. The solute permeability constant was neglected in this calculation as the feed concentration was assumed to be pure water flux. Therefore, the solution flux for a single hollow-fine-fibre will be calculated as follows:

$$(J_v) = 4.294\times10^{-10}(25\times10^5 - 101325)/1000 = 1.03\times10^{-6}\ \text{m}^3/\text{m}^2.\text{sec}.$$

The pressure drop can be obtained using equation 14, and the finite difference method is applied to numerically solve it. Figure 4 shows the pressure drop across the fibre wall of assumed diameter above for hollow-fine-fibre membranes at wall thickness of 50 μm.

Figure 4 shows that the pressure drop along the fibre length decreases significantly as the diameter of the hollow fibre increases. Pressure drop in the fibre bore plays an important role in the productivity of the fibre. The smaller the fibre dimensions, the higher the pressure drop and subsequently lower water flux (less product). Therefore, the workable fibre dimensions should have a smaller pressure drop and also a high collapse pressure resistance within the operating conditions for a brackish water membrane. It can be seen from Figure 4 that, as the fibre diameter increases while maintaining a constant wall thickness, the pressure drop in the fibre bore decreases.

The number of fibres that can be accommodated in the module of a given size also decreases. It can be seen from Figure 4 that the range of fibre dimensions of 222 – 247 μm obtained by the collapse pressure calculations have reasonable values of pressure drops compared to smaller fibre dimensions where the pressure drop is high. Hence, the pressure drop calculations will also limit the selection of fibre diameters for brackish water desalination. Therefore, the range of 222 – 247 μm would be acceptable for making CA hollow-fine-fibre membrane for brackish water desalination in terms of collapse pressure and pressure drop.

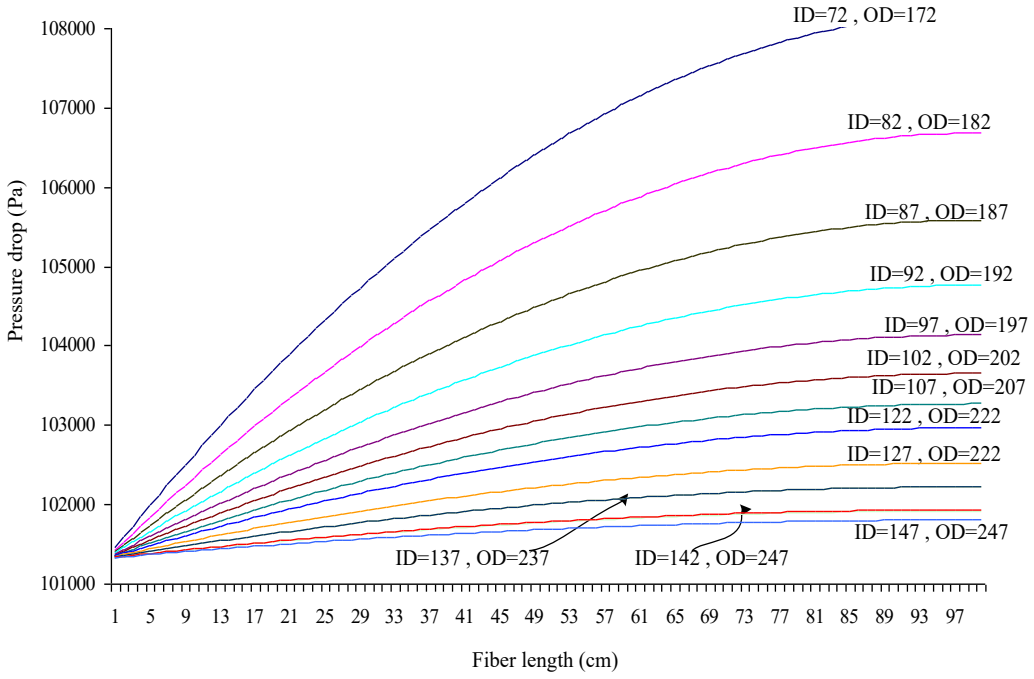

Figure 4. Pressure Drop Across the Fibre Wall of Hollow-fine-fibre Membranes

4. Conclusion

The relationships between the collapse pressure and pressure drop calculations were considered in order to determine an acceptable range of fibre dimensions capable to withstand brackish water operating conditions of 20 – 25 bar with smaller pressure drop. The collapse pressure calculations showed that outside diameters and membrane wall thickness play an important role in determining the membrane operating pressures. A fibre dimensions in the range of 222 – 247 μm showed good resistance against collapse of brackish water operating conditions. The hollow-fine-fibres with range obtained above (222 – 247 μm) also showed a lower pressure drop within the brackish water operating conditions during the calculations. Thus, the hollow-fine-fibre membranes in the range of (222 – 247 μm) showed high resistance to withstand the brackish water operating conditions at relatively low ratio of wall thickness 50 μm to outside diameter and thereby provide an advantageously large bore diameter to minimize the pressure drop to permeate passing within the bore.

References

1. Mahon HI, Permeability separatory apparatus, permeability separatory membrane element, method of making the same and process utilizing the same, U.S. Patent Number 3 228 876, 1966.
2. Mahon HI, Permeability separator and process using hollow fibre, U.S. Patent Number 3 228 877, 1966.
3. Ho WSW. Recent developments and applications for hollow fibre membranes. *J. Chin. Inst. Chem. Eng.*, 2003, 34, 75.
4. Gabelman A, Hwang ST. Hollow fibre membrane contactors. *J. Membr. Sci.*, 1999, 159, 61.
5. Dance EL, Davis TE, Mahon HI, McLain EA, Skiens WE, "Development of Cellulose Triacetate Hollow Fibre Reverse Osmosis Modules for Brackish Water Desalination", Research and Development Report for Contract DI-14-01-0001-2248 to Dow Chemical Co, 1971.
6. Ziabiciki A in Fundamentals of Fibre Formation, John Wiley & Sons, New York, 1976.
7. Mohamed S, William NG. An experimental study of the complete-mixing model for radial flow hollow fibre reverse osmosis systems. *Desalination*, 1984, 49, 57.
8. Mahon HI, Lipps BJ in Hollow Fibre Membranes, Encyclopedia of Polymer Science and Engineering, John Wiley & Sons, New York, 1971, 258.
9. Doshi MR, Gill WN, Kabadi VN. Optimal design of hollow fibre modules. *Am. Inst. Chem. Eng. J.*, 1977, 765.
10. Case J in The Strength of Materials: A Treatise on the Theory of Stress Calculations for Engineers, Edward Arnold, London, 1983.
11. Hanbury WT, Yuceer A. Constriction of B10 hollow fibre diameters under

operating conditions. *Desalination*, 1985, 54, 27-44.
12. De Nevers N in Fluid Mechanics for Chemical Engineers, 3rd ed., McGraw-Hill, New York, 2005.
13. Hermans JJ. Hydrodynamics of hollow fibre reverse osmosis modules. *Membr. Dig.*, 1978, 1, 45.
14. Hermans JJ. Physical aspects governing the design of hollow fibre modules. *Desalination*, 1972, 26, 45.
15. Orofino TA, "Development of Hollow Filament Technology for Reverse Osmosis Desalination Systems", Office of Saline Water and Development, Progress Report No. 549, USA, 1970.
16. Chen C, Petty CA. Flow characteristics of semipermeable hollow fibres undergoing reverse osmosis. *Desalination*, 1973, 12, 281.
17. Evanglista F, Jonsson G, "Explicit Design of Hollow Fibre Reverse Osmosis Systems", Proceedings of the 1990 International Congress on Membranes and Membrane Processes, Chicago, USA, 1990, 2, 1081.
18. Sekino M. Precise analytical model of hollow fibre reverse osmosis modules. *J. Membr. Sci.*, 1993, 85, 241.
19. Ohya H, Nakajima H, Tagaki K, Kagawa S, Negishi Y. An analysis of reverse osmotic characteristics of B9 hollow fibre module. *Desalination*, 1977, 21, 257.
20. Starov VM, Smart J, Lloyd DR. Performance optimization of hollow fibre reverse osmosis membranes, Part I. Development of theory. *J. Membr. Sci.*, 1995, 103, 257.
21. Smart J, Starov VM, Lloyd DR. Performance optimization of hollow fibre reverse osmosis membranes, Part II. Comparative study of flow configurations. *J. Membr. Sci.*, 1996, 119, 117.
22. Jacobs EP, "Statistical and Numerical Techniques in the Optimization of Membrane Fabrication Variables", Ph.D. Thesis, University of Stellenbosch, South Africa, 1988.
23. Chanda M, Salil KR in Plastics Technology Handbook, 3rd ed., Marcel Dekker, New York, 1998.
24. Gercek H. Poisson's ratio values for rocks. *Int. J. Rock Mech. Min. Sci.*, 2007, 44, 1.
25. Fischer F, Rigacci A, Pirard R, Berthon-Fabry S, Achard P. Cellulose-based aerogels. *Polymer*, 2006, 47, 7636.
26. Chunxiu L, Renbi B. Preparation of chitosan/cellulose acetate blend hollow fibres for adsorptive performance. *J. Membr. Sci.*, 2005, 2005, 68.
27. William NG, Bansal B. Hollow fibre reverse osmosis systems analysis and design. *Am. Inst. Chem. Eng. J.*, 1973, 19, 823.
28. Porter MC. Concentration polarization with membrane ultrafiltration. *Ind. Eng. Chem. Prod. Res. Dev.*, 1972, 11, 234.
29. Nader MA, Abderrahim A. Modeling an industrial reverse osmosis unit. *Desalination*, 1999, 126, 33.
30. Kimura S, Sourirajan S. Analysis of data in reverse osmosis with porous cellulose acetate membranes used. *Am. Inst. Chem. Eng. J.*, 1976, 497.
31. Frith CF in Electronic-Grade Water Production Using Reverse Osmosis Technology, Reverse Osmosis Technology: Applications for High-Purity Water Production, ed. B. S. Parekh, Marcel Dekker, New York, 1988, 279.

Appendix A. FORTRAN Codes

```
pressure drop calculation

real Jv
Dimension Jv(100),Pp(100)


l=1
d1=0.00072
d0=0.000172
Dz=0.01
m=100

Pb=25e5
alfa=0.55
R=1000
u=0.000798
A=4.294e-10


S=3.14*d0*l


Pp(0)=101325

flux=1.03E-06

aJv1=flux/m

do j = 1, m
    Jv(j)=A*((Pb-Pp(j))-(alfa*A-B)*(Cb-Cp))/R
    F=0.0
    do i = 1, j
         F=F+Jv(i)
    end do
    F=aJv1*(m-j)
    Pp(j)=Pp(j-1)+128*u*Dz**2*d0*F/d1**4
    write(*,*) Pp(j)
end do


end
```


The Chemist
Journal of the American Institute of Chemists

Selection of Influential Factors on Fume Hood Containment Performance Based on Questionnaire Survey and Fuzzy Comprehensive Evaluation

Kang Chen [a,b,*], Jeremy Pretty [b]

[a] *Henkel AG & Co. KGaA, Shanghai, China 201203*
[b] *Capitol Technology University, Laurel, Maryland, USA 20708*
(E-mail: tjck6@163.com, kchen@captechu.edu)

Abstract: There are multiple influential factors affecting fume hood containment performance in real laboratory environments and it is of great importance to prioritize these factors for further analysis of their impacts. Without a systematic approach, it is a common practice for researchers to select target influential factors based on their experience or even randomly, consequently imposing heavy financial burdens on themselves and increasing the environmental footprint. This interdisciplinary research aimed to propose a systematic and optimized approach for selecting influential factors of fume hood containment performance evaluation through questionnaire survey and fuzzy comprehensive evaluation. The questionnaire survey collected basic information of influential factors on fume hood containment performance, and then fuzzy comprehensive evaluation (FCE) was conducted in order to prioritize and select critical factors. The results of this study suggest that thermal challenge and inside clutter have significant fuzzy membership (84.5% and 89%, respectively) among all the influential factors and might be considered for further analysis of their impacts on fume hood containment performance. Proper selection of influential factors is vital to reducing the volume of the greenhouse gas emission during field test as well as the computational efforts in numerical simulation for hood performance evaluation. Further, the approach adopted in this study can also be referred to by industrial hygienists and ventilation engineers to determine the optimal methodology for fume hood containment performance evaluation.

Key Words: fume hood, influential factors, containment performance, questionnaire survey, fuzzy comprehensive evaluation, laboratory environment

*Corresponding author

1. Introduction

The fume hood has been adopted as a primary exposure control device given its ubiquitous presence in research laboratories (See Figure 1 for its profile and key features [1]).

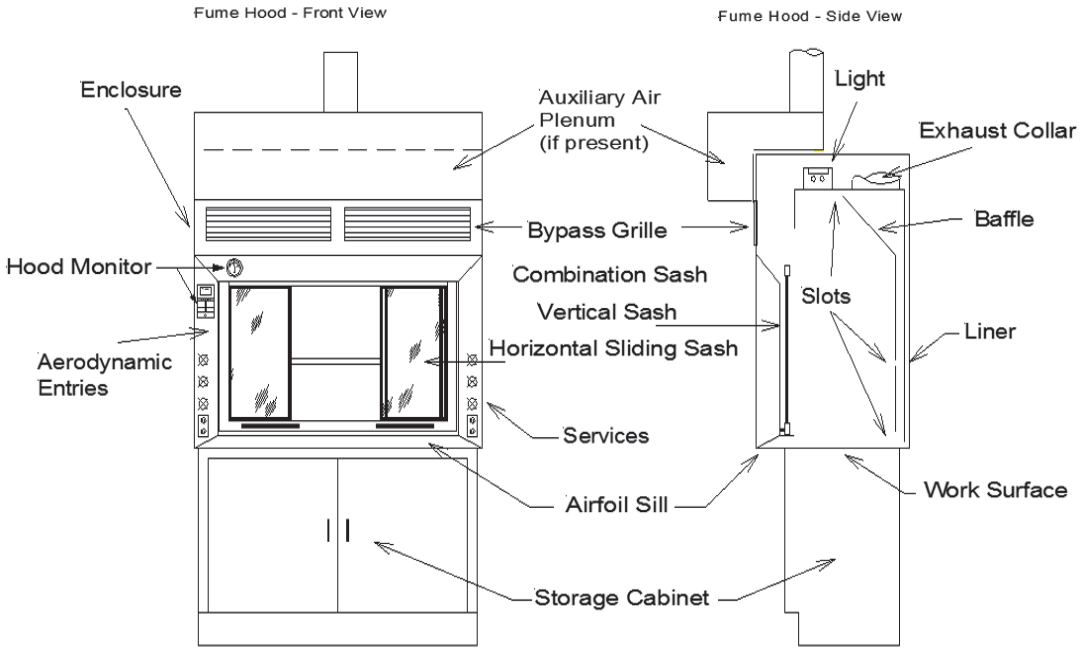

Figure 1. Key Components of a Typical Bench Top Laboratory Fume Hood

It provides the widest range of protection from hazardous emission scenarios that include small to very large quantities of low to extremely hazardous materials generated at rates from less than 0.1 lpm to as much as 10 lpm [2].

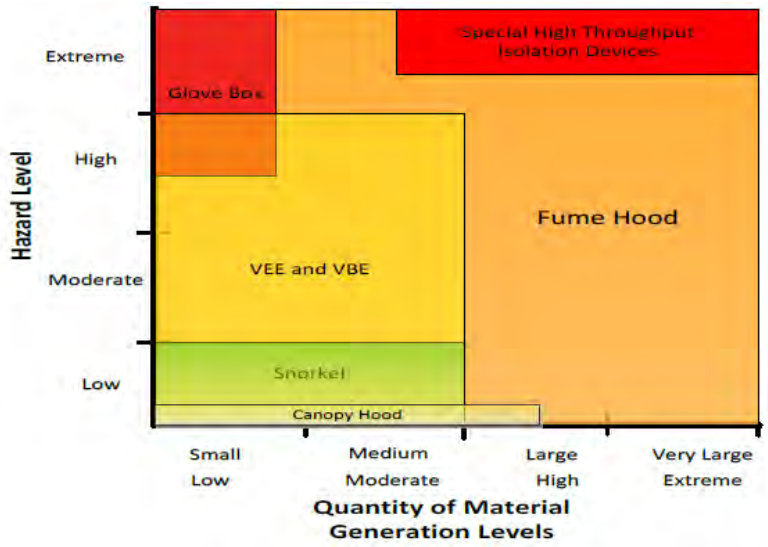

Figure 2. Application Matrix of Exposure Control Devices in Laboratory Environments

Figure 2 shows a diagram representing the increasing hazard level and generation potential (rate and quantity) on the axis Y and axis X, respectively [2]. Different types of exposure control devices (ECDs) shown on the diagram are utilized according to the matrix of hazard level and generation potential. Scientists and researchers working in laboratories mainly rely on robust fume hood performance to protect themselves from overexposure to hazardous airborne chemicals generated during experimental activities. This is critically important in case highly hazardous materials, e.g., ototoxicants or active pharmaceutical ingredients (APIs), are handled in the fume hood along with excessive noise exposure [3-5]. With the increasing complexity of laboratory experimental process, fume hood containment performance is affected by a wider variety of internal and external influential factors. According to ASHRAE standard 110 Methods of Testing Performance of Laboratory Fume Hoods, three alternate ratings can be determined depending on the purpose and condition of the test, namely "as manufactured" (AM) test, "as installed" (AI) test and "as used" (AU) test. While the AM test and AI test are aimed to evaluate the original hood design and installation integrity, respectively, the AU test investigates fume hood containment performance under the influence of real operational factors, which may include hood clutter, thermal challenge, contaminant emission character, maladjustment of the baffles, design and operation of the general ventilation systems, etc. [1]

2. Previous Research of Influential Factors on Fume Hood Containment Performance

The fume hood containment performance will be degraded by negative impacts from both internal and external influential factors, which leads to potential leakage of contaminants, and personal overexposure to

hazardous materials or indoor air pollution, consequently [6-9].

In a recent research, Chen et al. explored the relationship between fume hood containment failure and three common influential factors through comprehensive numerical simulation with verification of field test [10]. The authors concluded that the tracer gas emission character seems to be a more dominant factor that contributes to hood containment failure, compared with the thermal challenge and inside clutters. However, this up-to-date research does not consider selecting multiple influential

factors in a systematical way. In previous studies, Johnston et al. [11,12] linked thermal load generated by meeker burners and higher breathing zone concentrations of tracers in a positive linear relationship, while Ahn et al. [13] proposed a novel experimental method to explore the feasibility of using carbon dioxide (CO_2) as an alternative tracer gas to analyze the relationship between sash opening heights, thermal loads, hood clutters and leakage values. A systematic review of quantitative experimental studies on factors affecting fume hood performance was conducted by Ahn et al. [6] and the review summarized that the distance between the emission point and breathing zone, the presence of a mannequin or real human subject, and the height or space of sash opening are the strongest potentials among all the influential factors on the performance of laboratory fume hoods. The importance of studying the effect of all these factors in a systematic and comprehensive manner was emphasized by the authors. He and Steven [14] investigated the interactions between the hood face velocity and the indoor cross-draft airflow velocity and underlined that these factors have significant effects ($p < 0.05$) on hood containment performance, namely log-transformed breathing zone concentrations of the tracer gas. In their study, both the collar and bottom flange posed a negative impact on reducing manikin exposures, but such kind of impact can be mitigated through proper design of the hood sash.

Although the field investigation (e.g., face velocity measurement and flow visualization) seems to be practical and effective in hood performance evaluation, only several influential factors were considered in the research above because it will be cost-ineffective, time-consuming, or even impossible to evaluate all the potential factors in one single experimental study. On the other hand, computational fluid dynamics (CFD), as an emerging technology, has been widely adopted by research for quantitative evaluation of fume hood performance thanks to the increasingly improved computational capability. Michele and Alessio [15] proposed a CFD numerical procedure to analyze the effect of blockages in the sash area on hood containment performance. This novel research defined an equation to address viscous-induced effects, including boundary layer separation, lazy airflow and recirculation. This improved Dalla Valle Equation well describes the capturing velocity decay in front of the hood and shows a good fit with the results of numerical simulation, allowing a maximum deviation of 17.3 %. Another CFD study conducted by Hu et al. [16] highlighted that the location of the exhaust duct should not be located too close to the sash of the fume hood and the contaminant leakage is most likely to occur near either the bottom of the sash or the floor of the fume hood. Such conclusions are in line with the experimental findings by Fletcher and Johnson [17,18]. Other studies have also reported the promising use of CFD in assessing and quantifying the impact of influential factors

on laboratory fume hood containment performance. Sangrok et al. [19] performed an initial research that calculate the leakage rate of the fume hood in order to determine a factor for workplace exposure assessment. The leakage rate derived from the numerical simulation is 3% with face velocities between 0.1 and 1.0 m/s at the sash opening, which provides fundamental data for evaluating the personal exposure dose during the processes of dispensing, dilution, and preparation of the radioisotopes. Through CFD simulation, Hu et al. [20] found that the level of contaminant leakage was related to not only the volume of the recirculating airflow behind the hood sash, but also the blockage caused by the baffles. Wherever the tracer ejector was placed, the level of the tracer leakage close to the bottom of the sash was the highest along the working aperture. These findings derived from numerical simulation are in consistent with previous experimental observations [18], which makes CFD modelling a good alternative to performing costly field experiments. While still incomplete, the growing body of evidence indicates that numerical simulation could be considered in laboratory fume hood performance evaluation at least as a supplementary method to physical measurements [21-26].

The research mentioned above have revealed the relationship between various influential factors and fume hood containment performance, either qualitatively or quantitatively. Nevertheless, none of these studies adopt a systematic and optimized approach in selecting influential factors for hood containment performance evaluation. Currently, there are no pertinent methodologies and practices available in the literature. Therefore, the aim of this paper is

to develop a new method for prioritizing and selecting critical influential factors on fume hood containment performance using questionnaire survey and fuzzy comprehensive evaluation.

3. Design and Delivery of the Survey Instrument

Based on the literature review in the prior section, a combined (open-ended and close-ended) survey questionnaire was constructed and delivered to representative fume hood end-users in order to collect basic information of fume hoods used on site and potential improvement opportunities of safe application. An email-back questionnaire is utilized as the survey delivery mechanism in this research. This type of survey provides an opportunity to reach a much broader audience rapidly than many other survey methods, though the potential response rate might be lower. In addition, it is generally less expensive than a telephone survey, and participants can have a better understanding of the questions with adequate response time.

The questionnaire consists of four main sections: (1) background information regarding application of fume hoods; (2) multiple influential factors with three levels of weight for the participants to rank; (3) methodologies for fume hood containment performance evaluation; and (4) potential improvement opportunities for safe application of fume hoods. Detailed questions are exemplified in Table 1 and all of them are written in a neutral and non-

leading way for respondents in order to prevent their responses from being biased toward any predefined ideas [27,28]. Thus, the variety of perspectives can be maximized. Before formal delivery of the survey, the questionnaire was pilot tested to three environmental health & safety professionals, two fume hood application experts, and one laboratory ventilation engineer who has been working with fume hoods for more than ten years. The participants in this beta test were asked to provide comments in terms of contents, delivery methods, the feasibility and comprehensibility of the survey, etc. [29]. This panel of multidisciplinary experts reported that the survey questions were easy to understand for both professionals and practitioners. They also suggested that delivering the survey through email would enable the participants to respond in a clear and prompt way. After minor revisions, the survey questionnaire was then distributed to 52 research institutes, universities and industrial companies, individually, and administrated within two months for collection of their responses.

Table 1. Questionnaire Sample for Selection of Influential Factors on Fume Hood Containment Performance

Basic information of fume hood application in the laboratory	BU of end-user			Dept. of end-user	
	Time of commissioning			Status of operation	□ good □ acceptable
	Main purpose (Multiple choice) †		□ normal operation □ distillation □ perchloric acid operation □ radioactive operation □ ototoxics operation		
	Quantity of fume hoods				
	Main instruments used in the fume hood		Name:		
Influential factors on fume hood containment performance†	Hood design and geometry (e.g., baffle and location of the exhaust pipeline)		□ critical (90%♀)	□ important (50%♀)	□ minor (10%♀)
	Operational parameter	Face velocity	□ critical (90%)	□ important (50%)	□ minor (10%)
		VAV system	□ critical (90%)	□ important (50%)	□ minor (10%)
	Operational environment	Location of fume hoods	□ critical (90%)	□ important (50%)	□ minor (10%)
		Distance between fume hoods	□ critical (90%)	□ important (50%)	□ minor (10%)
	Operation process (e.g., sash/human subject movement)		□ critical (90%)	□ important (50%)	□ minor (10%)
	Experimental process	Inside clutter (e.g., multiple large instruments)	□ critical (90%)	□ important (50%)	□ minor (10%)
		contaminants emission character (e.g.,	□ critical (90%)	□ important (50%)	□ minor (10%)

		hazardous materials dispensing, solvent evaporation)			
		thermal challenge (i.e., thermal load inside of fume hoods)	□ critical（90%）	□ important（50%）	□ minor（10%）
	TPM of blowers and valves		□ critical（90%）	□ important（50%）	□ minor（10%）
Methodologies for hood containment performance evaluation	Face velocity measurement		□ critical（90%）	□ important（50%）	□ minor（10%）
	Smoke visualization		□ critical（90%）	□ important（50%）	□ minor（10%）
	Laser-assisted or ultraviolet-fluorescence based visualization		□ critical（90%）	□ important（50%）	□ minor（10%）
	Tracer gas testing		□ critical（90%）	□ important（50%）	□ minor（10%）
	CFD modelling		□ critical（90%）	□ important（50%）	□ minor（10%）
potential improvement opportunities of fume hood safe application	1. interlock between exhaust volume and contaminant generation rate or concentration（example）				
	2. aerodynamically-generated noise abatement（example）				
	3.				
	4.				

† Compulsory questions to be answered by the survey participants

♀ Percentage of weight (membership degree) in three categories for each influential factor

With the joint efforts, 39 questionnaires were sent back finally from the survey participants and the feedback rate is relatively high considering the limited time resource. The information collected from the questionnaire survey supports selecting critical fume hood performance influential factors in the following sections, and might guide methodologies for hood containment performance evaluation in future studies as well.

4. Fuzzy Comprehensive Evaluation of the Influential Factors

In this section, there are two major steps in the selection of critical influential factors on fume hood containment performance, namely preliminary statistical analysis and fuzzy comprehensive evaluation. The first step is a screening process which is aimed at prioritizing relatively important items among a great variety of influential factors as specified in the survey questionnaire. The selectivity (S) of each influential factor was determined by the following equation (1):

$$S_j = \mathrm{w}_1 \sum_{1}^{q_1} n_1 + \mathrm{w}_2 \sum_{1}^{q_2} n_2 + \mathrm{w}_3 \sum_{1}^{q_3} n_3, \quad j = 1, 2, ..., 10 \tag{1}$$

where: q_1, q_2, q_3, the number of questionnaires in three membership degrees, respectively; S_j, the selectivity of each influential factor in the questionnaire; w_1, w_2, w_3, the percentage of weight (membership degree) in three categories (90%, 50% and 10%, respectively) for each influential factor in Table 1; and n_1, n_2, n_3, the sum of influential factors selected by survey participants under three membership degrees for each influential factor.

For example, 29 participants considered hood design and geometry as a critical influential factor to be analyzed, 8 participants regarded it as an important factor, while 2 participants marked it as a minor factor only. Therefore, for this influential factor (hood design and geometry), its selectivity is calculated as: S_1= 0.9×29 + 0.5×8 + 0.1×2= 30.3. Similarly, the selectivity of all the other influential factors in the questionnaire can be obtained as below:

S_2= 0.9×25＋0.5×14＋0.1×0= 29.5;
S_3= 0.9×25＋0.5×8＋0.1×6= 27.1;
S_4= 0.9×20＋0.5×15＋0.1×4= 25.9;
S_5= 0.9×22＋0.5×9＋0.1×8= 25.1;
S_6= 0.9×30＋0.5×7＋0.1×2= 30.7;
S_7= 0.9×32＋0.5×5＋0.1×2= 31.5;
S_8= 0.9×36＋0.5×3＋0.1×0= 33.9;
S_9= 0.9×32＋0.5×6＋0.1×1= 31.9;
S_{10}= 0.9×29＋0.5×10＋0.1×0= 31.1

Followed by the calculation of the selectivity above, five relatively important influential factors have been screened out as contaminants emission character (S_8), thermal challenge (S_9), inside clutter (S_7), TPM of blowers and valves (S_{10}) and operation process (S_6).

Secondly, fuzzy comprehensive evaluation (FCE) of the influential factors screened out was implemented thereafter in order to improve cost-effectiveness of fume hood containment performance analysis. The FCE method was proposed initially by Zadeh in the 1960s [30-31] and has been widely applied in hierarchical cluster analysis (HCA) for interdisciplinary studies including but not limited to biological genetics, information science and control engineering [32-34]. It is extremely useful in evaluation of interactive factors or factors that cannot be quantified directly [35]. Through fuzzy transformation and comprehensive evaluation, the integrated selectivity of each factor was obtained and the whole process became less subjective as the evaluation system is more complicated and comprehensive. Finally, two influential factors were identified further as critical research objects in fume hood containment performance evaluation. Detailed evaluation and calculation process is illustrated in Figure 3 and explained in the following paragraphs.

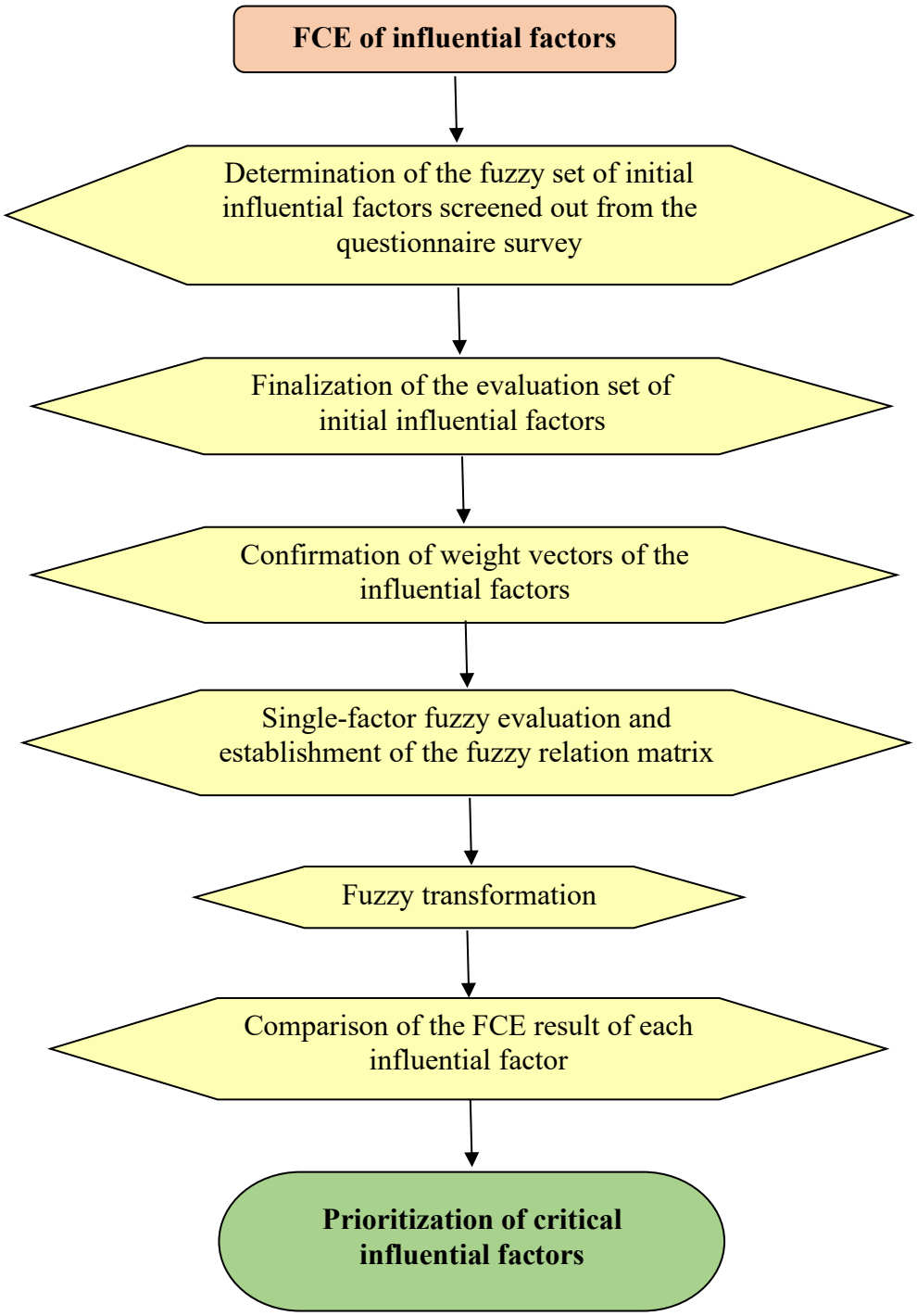

Figure 3. Flow Chart of Fuzzy Comprehensive Evaluation (FCE) of Influential Factors

Step 1, the fuzzy set of initial influential factors screened out from the questionnaire survey was determined as $X = \{x_1, x_2, x_3, x_4, x_5\}$ = {thermal challenge, inside clutter, contaminants emission character, operation process, TPM of blowers and valves}.

Step 2, the evaluation set of initial influential factors was proposed based on economic viability and technological feasibility. Meanwhile, excessive number of elements in the evaluation set should be avoided as this might lead to minimization of the weight coefficient, and consequently poor resolution of membership degrees and difficulty in prioritization of influential factors due to ultra-fuzzy phenomenon [36]. Thus, the evaluation set of initial influential factors was defined as $U = \{u_1, u_2, u_3, u_4, u_5\}$ = {experiment complexity, economic cost, environmental pollution, modelling complexity, factor quantifiability}.

Step 3, the weight vectors of each element in the evaluation set were derived from expert panel discussion as $A = \{a_1, a_2, a_3, a_4, a_5\} = \{0.25, 0.2, 0.2, 0.1, 0.25\}$.

Step 4, the integrated selectivity set could be determined in a relatively straightforward way as $V = \{v_1, v_2\}$ = {good, poor}. Based on the single factor fuzzy mathematics evaluation data in Table 2, the following fuzzy matrices of the integrated selectivity for each influential factor were established.

$$R_1 = \begin{pmatrix} 0.7 & 0.3 \\ 0.9 & 0.1 \\ 1 & 0 \\ 0.4 & 0.6 \\ 1 & 0 \end{pmatrix}, \quad R_2 = \begin{pmatrix} 0.8 & 0.2 \\ 1 & 0 \\ 1 & 0 \\ 0.4 & 0.6 \\ 1 & 0 \end{pmatrix}, \quad R_3 = \begin{pmatrix} 0.4 & 0.6 \\ 0 & 1 \\ 0.2 & 0.8 \\ 0.8 & 0.2 \\ 0.9 & 0.1 \end{pmatrix}, \quad R_4 = \begin{pmatrix} 0.1 & 0.9 \\ 0.2 & 0.8 \\ 1 & 0 \\ 0.1 & 0.9 \\ 0.1 & 0.9 \end{pmatrix}, \quad R_5 = \begin{pmatrix} 0.4 & 0.6 \\ 0.4 & 0.6 \\ 0.9 & 0.1 \\ 0.1 & 0.9 \\ 0.1 & 0.9 \end{pmatrix}$$

Table 2. Single Factor Fuzzy Mathematics Evaluation

Influential Factors / ***Set Elements***	thermal challenge		inside clutter		contaminants emission character		operation process		TPM of blowers and valves	
Selectivity	good	poor	good	poor	good	poor	good	poor	good	poor
experiment complexity	0.7	0.3	0.8	0.2	0.4	0.6	0.1	0.9	0.4	0.6
economic cost	0.9	0.1	1	0	0	1	0.2	0.8	0.4	0.6
environmental pollution	1	0	1	0	0.2	0.8	1	0	0.9	0.1
modelling complexity	0.4	0.6	0.4	0.6	0.8	0.2	0.1	0.9	0.1	0.9
factor quantifiability	1	0	1	0	0.9	0.1	0.1	0.9	0.1	0.9

Step 5, the weight averaged composite operator $M(\bullet, \oplus)$ was selected for fuzzy composition and transformation, and the whole process could be explained conceptually using the following equation (2):

$$b_j = \min\left(1, \sum_{\substack{i=1 \\ j=1,2}}^{5} a_i r_{ij}\right) \tag{2}$$

where: b_j, the calculated vector of fuzzy comprehensive evaluation; a_i, the weight vector of each element in the evaluation set in Step 3; and r_{ij}, the element in the fuzzy matrix of the integrated selectivity for each influential factor in Step 4.

The merit of this weight averaged composite operator lies in its combination of both weight coefficient and fuzzy relationship, which could express the interactive effect of multiple influential factors more accurately. The vector of fuzzy comprehensive evaluation for each influential factor was calculated specifically based on the equation (3) below:

$$B_n = A \bullet R_n = (a_1, a_2, a_3, a_4, a_5)\begin{pmatrix} r_{11} & r_{12} \\ r_{21} & r_{22} \\ r_{31} & r_{32} \\ r_{41} & r_{42} \\ r_{51} & r_{52} \end{pmatrix} = (b_{n1}, b_{n2}) \tag{3}$$

where n (1, 2, 3, 4, 5) represents for the five initial influential factors screened out from the questionnaire survey.

Thus, as for the thermal challenge,

$$B_1 = (0.25, 0.2, 0.2, 0.1, 0.25)\begin{pmatrix} 0.7 & 0.3 \\ 0.9 & 0.1 \\ 1 & 0 \\ 0.4 & 0.6 \\ 1 & 0 \end{pmatrix} = (0.845, 0.155);$$

likewise, the vectors of fuzzy comprehensive evaluation for inside clutter, contaminants emission character, operation process, and TPM of blowers and valves are listed below, respectively.

$$B_2 = (0.25, 0.2, 0.2, 0.1, 0.25)\begin{pmatrix} 0.8 & 0.2 \\ 1 & 0 \\ 1 & 0 \\ 0.4 & 0.6 \\ 1 & 0 \end{pmatrix} = (0.89, 0.11);$$

$$B_3 = (0.25, 0.2, 0.2, 0.1, 0.25)\begin{pmatrix} 0.4 & 0.6 \\ 0 & 1 \\ 0.2 & 0.8 \\ 0.8 & 0.2 \\ 0.9 & 0.1 \end{pmatrix} = (0.525, 0.555);$$

it is plausible to normalize this fuzzy vector according to equation 4 below because the sum of elements in the vector is not equal to one (0.525 + 0.555= 1.08).

$$B_i' = \frac{B_i}{\sum_1^n B_i} \tag{4}$$

Through normalization, $B_3 = (0.486, 0.514)$;

$$B_4 = (0.25, 0.2, 0.2, 0.1, 0.25)\begin{pmatrix} 0.1 & 0.9 \\ 0.2 & 0.8 \\ 1 & 0 \\ 0.1 & 0.9 \\ 0.1 & 0.9 \end{pmatrix} = (0.3, 0.7);$$

$$B_5 = (0.25, 0.2, 0.2, 0.1, 0.25)\begin{pmatrix} 0.4 & 0.6 \\ 0.4 & 0.6 \\ 0.9 & 0.1 \\ 0.1 & 0.9 \\ 0.1 & 0.9 \end{pmatrix} = (0.395, 0.605)$$

Lastly, thermal challenge and inside clutter demonstrate optimal fuzzy membership (84.5% and 89%, respectively), while the fuzzy membership of contaminants emission

character, operation process, TPM of blowers and valves are relatively low (48.6%, 30% and 39.5%, respectively). Based on the maximum membership principle, thermal challenge and inside clutter are prioritized as the target influential factors for further evaluation of fume hood containment performance. Nevertheless, it is noteworthy that the fuzzy membership of contaminants emission character is much higher than those of operation process and TPM of blowers and valves, which means that contaminants emission character might need to be considered if it interacts with another factor with high membership in real laboratory environments.

5. Discussion and Conclusion

In this study, previous research of influential factors on fume hood containment performance were reviewed systematically in terms of field test and numerical simulation, which facilitated a better overview of the most common influential factors. A comprehensive survey questionnaire was proposed afterwards in order to collect semi-quantitative data regarding influential factors on fume hood containment performance from the perspective of end-users and experts. With these supportive references, the authors explored the feasibility of selecting influential factors of fume hood containment performance through questionnaire survey and fuzzy comprehensive evaluation. There are numerous influential factors that lead to negative impacts on fume hood containment performance, which in turn add difficulties for indoor environmentalists or industrial hygienists to determine critical factors for further analysis. Although researchers could either select target influential factors based on their experience merely or choose some factors randomly, waste of study time and experimental resources is inevitable as factors are not prioritized properly. Particularly, this issue could be exacerbated when a substantial number of tracer gas testing or CFD modelling are conducted for fume hood containment performance evaluation because the former generates large volume of greenhouse gases (GHG) and the latter requires great computational efforts [37,38].

Thanks to the effective questionnaire survey as well as the comprehensive fuzzy evaluation, two influential factors with strong fuzzy membership were identified eventually for fume hood containment performance evaluation, namely thermal challenge (membership degree 84.5%) and inside clutter (membership degree 89%). While there is no applicable approach in selecting influential factors previously, this paper provides a novel quantitative method to prioritize all the factors and select critical ones among them, which makes further evaluation of fume hood containment performance more cost-effective and time efficient.

There are some recognized challenges in the present study, which can nevertheless be addressed in future work. In the fuzzy comprehensive evaluation, for instance, it is difficult to quantify the weight vectors of each element in the evaluation set accurately, albeit we believe the panel judgement renders valuable data for reference. Relatively small number of questionnaire samples due to time and

resource limitations might be another drawback for building up the soundness of the survey. Recommendations for future work include, firstly, expand the scope of the survey and try to acquire more questionnaire samples, which can enhance the overall quality of the survey to some extent and provide more useful data for fuzzy evaluation. Additionally, determination of methodologies for fume hood containment performance evaluation based on the survey questionnaire might be a promising extension of the current study because new technologies are emerging increasingly (e.g., laser-assisted or ultraviolet-fluorescence-based visualization, particle image velocimetry (PIV) measurements [39-45]), and it is not a simple process for selection of optimal methods. Last but not least, it is worthwhile to develop a quantitative algorithm in the future through which the weight vector of each element in the evaluation set can be define more accurately and less subjectively.

Acknowledgments

The authors thank experts from ESIS, Inc., ALS Global, East China University of Science and Technology, University of Saskatchewan, Tongji University, ShanghaiTech University and Shanghai Maritime University who actively participated in the questionnaire survey. Ada Cheng from MESCURE Safety and Technology Institute and Lou DiBerardinis from MIT are highly appreciated for their preliminary review and technical guidance on the design and delivery of the survey instrument.

References

1. American Society of Heating, Refrigerating and Air-Conditioning Engineers. Method of Testing Performance of Laboratory Fume Hoods, ASHRAE, Atlanta, GA, 2016. (ANSI/ASHRAE 110).
2. Scientific Equipment and Furniture Association. Guide to Selection and Management of Exposure Control Devices in Laboratories (Version 3), SEFA Publications, Garden City, NY, 2017.
3. Fuente A, Qiu W, Zhang M, Xie H, Kardous CA, Campo P, Morata TC. Use of the kurtosis statistic in an evaluation of the effects of noise and solvent exposures on the hearing thresholds of workers: An exploratory study. *J. Acoust. Soc. Am.*, 2018, 143(3), 1704. DOI: 10.1121/1.5028368.
4. Chen K, Yang JL, Zhang HB, Zhang WJ. Low level noise analysis in laboratory fume hood. *J. Chem. Health Saf.*, 2017, 24(1), 2–7. DOI: 10.1016/j.jchas.2016.03.002.
5. Chen K, Zhang HB, Zhang WJ. Measures to alleviate fume hood noise. *Am. Lab.*, 2018, 50(3), 10-13.
6. Ahn K, Susan W, Louis DB, Michael E. A Review of Published Quantitative Experimental Studies on

Factors Affecting Laboratory Fume Hood Performance. *J. Occup. Environ. Hyg.*, 2008, 5(11), 735-753. DOI: 10.1080/15459620802399989.
7. ACGIH. Industrial Ventilation: A Manual of Recommended Practice, ACGIH Publications, Cincinnati, OH, 2004.
8. Burgess WA, Ellenbecker MJ, Treitman RD in Ventilation for Control of the Work Environment, 2nd ed., John Wiley & Sons, Inc., Hoboken, NJ, 2004, pp 220–224.
9. Koenigsberg J. How does your fume hood rate? New assessment of current fume hood design and operations. *J. Chem. Educ.*, 1992, 69(5), 408-412. DOI: 10.1021/ed069p408.
10. Chen K, Wang WZ, Zhang WJ. Investigation of influential factors on laboratory fume hood containment performance. *Sci. Technol. Built Environ.*, 2020, 26(3), 387-399. DOI: 10.1080/23744731.2019.1637192.
11. Johnston JD, Chessin SJ, Chesnovar BW, Lillquist DR. The effect of thermal loading on laboratory fume hood performance. *Appl. Occup. Environ. Hyg.*, 2000, 15(11), 863–868. DOI: 10.1080/10473220050175751.
12. Chessin SJ, Johnston JD. Thermal loading as a causal factor in exceeding the 0.1 PPM laboratory fume hood control level. *Appl. Occup. Environ. Hyg.*, 2002, 17(7), 512–518. DOI: 10.1080/10473220290035769.
13. Ahn K, Ellenbecker MJ, Woskie SR, DiBerardinis LJ. A new quantitative method for testing performance of in-use laboratory chemical fume hoods. *J. Chem. Health Saf.*, 2016, 23(4), 32–37. DOI: 10.1016/j.jchas.2015.10.021.
14. He XJ, Steven EG. Quantitative Evaluation of the Performance of an Industrial Benchtop Enclosing Hood. *J. Occup. Environ. Hyg.*, 2013, 10(8), 409-418. DOI: 10.1080/15459624.2013.800466.
15. Michele P, Alessio S. A numerical method for the efficient design of free opening hoods in industrial and domestic applications. *Energy*, 2014, 74: 484–493. DOI: 10.1016/j.energy.2014.07.014.
16. Hu PX, Ingham DB, Wen X. Effect of the location the exhaust duct, an exterior obstruction and handle on the air flow inside and around a fume hood. *Ann. Occup. Hyg.*, 1996, 40(2), 127–144. DOI: 10.1016/0003-4878(95)00071-2.
17. Fletcher B, Johnson AE. Containment testing of fume cupboards- I methods. *Ann. Occup. Hyg.*, 1992, 36(3), 239-252. DOI: 10.1093/annhyg/36.3.239.
18. Fletcher B, Johnson AE. Containment testing of fume cupboards—II. Test room measurements. *Ann. Occup. Hyg.*, 1992., 36(4), 395-405. DOI: 10.1093/annhyg/36.4.395.
19. Kim S, Yang H. Estimation of leakage rate of air from a fume hood in a radioisotope laboratory using CFD simulations. *Appl. Radiat. Isot.*, 2018, 140, 300-304. DOI: 10.1016/j.apradiso.2018.07.021.
20. Hu PX, Ingham DB, Wen X. Effect of baffles and a louvered bypass on the airflow and the convective patterns of contaminant inside a fume hood. *Am. Ind. Hyg. Assoc. J.*, 1998, 59(5), 303–312. DOI: 10.1080/15428119891010550.
21. Sam KY, Lee SH, Ban ZH. Computational fluid dynamics (CFD) modelling on effect of fume extraction. *J. Chem. Health Saf.*, 2019, 26(6), 20-31. DOI: 10.1016/j.jchas.2019.04.004.
22. Sławomir P, Piotr K, Michał P. Experimental and numerical flow

analysis and design optimization of a fume hood using the CFD method. *Chem. Eng. Res. Des.*, 2018, 132, 627-643. DOI: 10.1016/j.cherd.2018.02.011.
23. Kolesnikov A, Ryan R, Walters DB. Use of CFD to design containment systems for work with hazardous materials. *Chem. Health Saf.*, 2003, 10(2), 17–20. DOI: 10.1016/S1074-9098(02)00456-2.
24. Flynn MR, Sills ED. On the use of computational fluid dynamics in the prediction and control of exposure to airborne contaminants—An illustration using spray painting. *Ann. Occup. Hyg.*, 2000, 44(3), 191–202. DOI: 10.1016/S0003-4878(99)00091-5.
25. Durst F, Pereira JCF. Experimental and numerical investigations of the performance of fume cupboards. *Build. Environ.*, 1991, 26(2), 153-164. DOI: 10.1016/0360-1323(91)90022-4.
26. Nichnolson GP, Clark RP, Calcina-Goff ML. Computational fluid dynamics as a method for assessing fume cupboard performance. *Ann. Occup. Hyg.*, 2000, 44(3), 203-217. DOI: 10.1016/S0003-4878(99)00086-1.
27. National Oceanic and Atmospheric Administration. Introduction to Survey Design and Delivery, NOAA Publications, Washington, DC, 2015.
28. Ogunsola OT, Wang JK, Li S. Survey of particle production rates from process activities in pharmaceutical and biological cleanrooms. *Sci. Technol. Built Environ.*, 2019, 25(6), 692-704. DOI: 10.1080/23744731.2019.1581501.
29. Timothy NS, Sang DC, Ahn K. Awareness and perceptions of ergonomic programs between workers and managers surveyed in the construction industry. *Work*, 2018, 61(1), 41-54. DOI: 10.3233/WOR-182778.
30. Zadeh LA. Fuzzy sets. *Inf. Control*, 1965, 8(3), 338-353. DOI: 10.1016/S0019-9958(65)90241-X.
31. Zadeh LA. Fuzzy sets as a basis for a theory of possibility. *Fuzzy Set Syst.*, 1978, 1(1), 3-28. DOI: 10.1016/0165-0114(78)90029-5.
32. Zheng GZ, Li K, Bu WT, Wang YJ. Fuzzy comprehensive evaluation of human physiological state in indoor high temperature environments. *Build. Environ.*, 2019, 150, 108-118. DOI: 10.1016/j.buildenv.2018.12.063.
33. Mohandes SR, Zhang XQ. Towards the development of a comprehensive hybrid fuzzy-based occupational risk assessment model for construction workers. *Saf. Sci.*, 2019, 115, 294-309. DOI: 10.1016/j.ssci.2019.02.018.
34. Muhammad T, Biswajit S. An interactive fuzzy programming approach for a sustainable supplier selection under textile supply chain management. *Comput. Ind. Eng.*, 2021, 155, 107164. DOI: 10.1016/j.cie.2021.107164.
35. Hui Z, He XQ, Hani M. Fuzzy comprehensive evaluation of virtual reality mine safety training system. *Saf. Sci.*, 2019, 120, 341-351. DOI: 10.1016/j.ssci.2019.07.009.
36. Chen LQ, Zhang P, Ma JL, Wang CL. Fuzzy integrative assessment of oil and gas pipeline risks. *Nat. Gas Ind.*, 2003, 23(2), 117-119.
37. California Code of Regulations, Title 8, Section 5154.1: Ventilation Requirements for Laboratory-Type Hood Operations, 2021. Accessed 2021 Jan 31. http://www.dir.ca.gov/title8/5154_1.html.
American Society of Heating,

38. Refrigerating and Air-Conditioning Engineers, “Determination of Suitable Replacement of SF6 When Used as a Tracer Gas in Accordance with ANSI/ASHRAE Standard 110 (Version 2)”, ASHRAE Report No.: 1573-RP, Atlanta, GA, 2020.
39. Biraj ST, Dahlhaug OG, Bhola T. Flow measurements around guide vanes of Francis turbine: A PIV approach. *Renewable Energy*, 2018, 126, 177-188. DOI: 10.1016/j.renene.2018.03.042.
40. Xie XM, Claude LM, Nicolas D, Philippe S, Luc F. Local hydrodynamic investigation by PIV and CFD within a Dynamic filtration unit under laminar flow. *Sep. Purif. Technol.*, 2018, 198, 38-51. DOI: 10.1016/j.seppur.2017.04.009.
41. Hans HM, Dragana A, Fredrik I, Andreas H. A validation of commonly used CFD methods applied to rotor stator mixers using PIV measurements of fluid velocity and turbulence. *Chem. Eng. Sci.*, 2018, 177, 340-353. DOI: 10.1016/j.ces.2017.11.037.
42. Poller B, Hall S, Bailey C, Gregory S, Clark R, Roberts P, Tunbridge A, Poran V, Crook B, Evans C. “VIOLET”: A fluorescence-based simulation exercise for training healthcare workers in the use of personal protective equipment. *J. Hosp. Infect.*, 2018, 99(2), 229-235. DOI: 10.1016/j.jhin.2018.01.021.
43. Hall S, Poller B, Bailey C, Gregory S, Clark R, Roberts P, Tunbridge A, Poran V, Evans C, Crook B. Use of ultraviolet-fluorescence-based simulation in evaluation of personal protective equipment worn for first assessment and care of a patient with suspected high-consequence infectious disease. *J. Hosp. Infect.*, 2018, 99(2), 218-228. DOI: 10.1016/j.jhin.2018.01.002.
44. Todd B, John S, Justin P, Roger S, Richard J. Ebola virus disease: The use of fluorescents as markers of contamination for personal protective equipment. *IDCases*, 2015, 2(1), 27-30. DOI: 10.1016/j.idcr.2014.12.003.
45. Chen JK, Huang RF, Hsin PY, Hsu CM, Chen CW. Flow and containment characteristics of an air-curtain fume hood operated at high temperatures. *Ind. Health*, 2012, 50(2), 103-114. DOI: 10.2486/indhealth.MS1326.

The Chemist
Journal of the American Institute of Chemists

A Review on Multi-ferrocenyl Systems

Ghosh A [a]*, Karan P[a], Chatterjee S [b]

[a] *Department of Pure and Applied Science, Midnapore City College Midnapore, West Bengal, India, 721129*

[b] *Department of Chemistry, National Institute of Technology Rourkela Odisha, India, 769008*

(Tel: +91 8280103667; E-mail: avishek.ghosh.mcc@gmail.com)

Abstract: Conjugated binuclear and poly-nuclear mixed-valence metal complexes have been of great importance because of their association with biologically inspired electron transfer processes. This kind of system with tunable electron transfer properties has a potential application in molecular electronics and optoelectronic materials. Multi-ferrocenyl compounds with strong metal-metal coupling are an important class of molecule with multi-redox, magnetic coupling, and unpaired electron density migration-like properties. These types of compounds are potentially useful in molecular electronics, quantum cellular automata, and optoelectronic materials to fabricate high-speed photonic or redox devices. This review paper focuses on the synthesis, properties study, and application of multi-ferrocenyl systems.

Key Words: multi-ferrocenyl, synthesis, application

Ethics Approval: Not applicable as no involvement of human participants or any other biological objects.

Conflicts of Interest: The authors declare no conflict of interest.

*Corresponding author

1. Introduction

The synthesis of multi-ferrocenyl molecular systems with specific redox, optoelectronic, magnetic, and conductive properties are important class compounds for several modern technologies [1]. Among the metallocene-based organometallic systems [2], multi-ferrocenyl systems are preferred as potential candidates for molecular electronics due to their intrinsic ferrocene based redox characteristics. Particularly the

conjugated and bridging multi-ferrocenyl system with multi-electron redox behavior has great importance because of the formation of mixed-valence species which triggers the migration of electrons within the molecular framework [3]. These switchable arrays have been significantly investigated on the conjugated chain with the ferrocenyl unit for their application in optoelectronic materials. Most of these multi-ferrocenyl systems belong to the mixed-valence system where at least two chemically equivalent ferrocenyl units are electronically coupled and give rise to species with extended electronic communication among the redox units [4]. In this review paper the synthesis, structural feature, properties, and application of multi-ferrocenyl systems will be discussed.

2. Di-ferrocenyl Linkages

A variety of di-ferrocenyl compounds have been synthesized in the last decade and their different properties were studied. In recent years, several di-ferrocenyl molecules with conjugated as well as non-conjugated bridging chains have been synthesized to understand their electronic coupling between the redox-active units. In addition to the linearly conjugated bridging ligands between the ferrocenyl moieties, cross-conjugated type bridging ligands are also explored [5-14]. The binuclear and poly-nuclear mixed-valence metal complexes with p conjugated bridging ligand have attracted continuous interest for decades, which led to the study of electron transfer processes. Yuan et al. have reported three dihydro pyrazole bridged ferrocenyl systems by the reaction of diferrocenyl chalcone with hydrazine hydrate followed by acylation with acyl chloride. The diferrocenyl pyrazole derivatives have been structurally characterized by single-crystal X-ray diffraction study which shows that the two ferrocenyl fragments are pointed at two different planes and connected to pyrazole ring carbon atoms. The bond distance between the Cp ring of ferrocene and the Pyrazole group is considerably shorter than the normal C-C bond which confirms distinct conjugation between the ferrocenyl and pyrazole ring (Figure 1) [15].

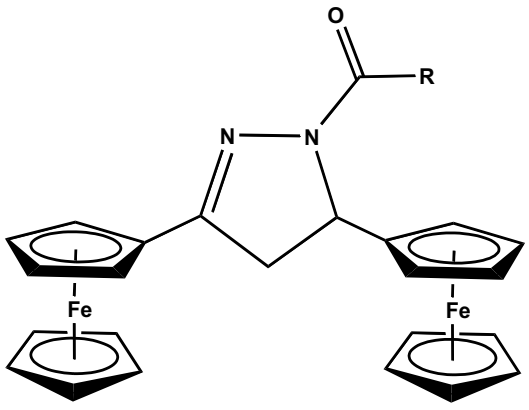

R= CH_2CH_2COOEt, C_6H_5, p-pyridyl

Figure 1. Dihydropyrazole Bridged Di-ferrocenyl Systems

Recently, a research group of Molina has designed a novel synthetic strategy for the preparation of 1,1'-ferrocenyl triazole compound from ferrocene by a series of reactions involving lithiation, click reaction, and Staudinger reaction with trimethyl phosphine to give an iminophosphorane derivative which further undergoes Aza-Witting type of coupling reaction with various aldehydes to give the diferrocenyl triazole derivatives, 1,1'-[Ar-CH=N(h^5-C_5H_4)Fe{(h^5-C_5H_4)(NN=NC=CH)(h^5-C_5H_4)Fe(h^5-C_5H_5)], {Ar= pyrene, quinoline, fluorene} (Figure 2) [16].

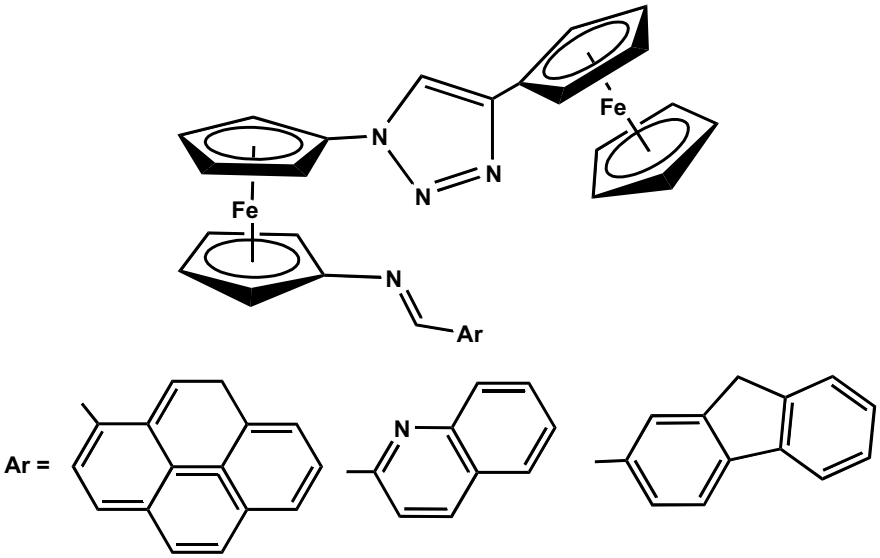

Figure 2. Diferrocenyl Triazole Derivatives

Structural characterization shows that the two cyclopentadienyl rings in the central ferrocenyl unit are arranged in an eclipsed position. One of the substituents on the central ferrocenyl moiety contains a quinoline ring which is coplanar with the imine group and the Cp ring, while the other substituent at the Cp ring is connected via a triazole ring to the terminal ferrocenyl moiety. Cyclic voltammetry study of the compound showed two ferrocene-based redox couples corresponding to the presence of two ferrocenyl units positioned in a different environment. The oxidation potential for the monosubstituted ferrocene has been observed at lower potential as compared to that of the di-substituted ferrocenyl fragment. The compound has been as a receptor molecule showing a distinct shift of the redox potentials due to the addition of Pb^{+2} and Zn^{+2} metal cations. The metal recognition properties of the ferrocenyl receptors with Ni^{2+}, Cd^{2+}, $Zn^{2+,}$ and Pb^{2+} cations have also been confirmed by the change in intensities of the energy bands in the UV-Visible spectroscopy. The binding interaction of the metal ion-receptor system occurs via the imine group of the receptor, the N atom of the quinoline ring, and weak interaction with the triazole unit.

Hu et al. has reported a series of 2,5-disubstituted five-membered pyrrole and thiophene bridged di-ferrocenyl compounds

and studied their electronic coupling between the redox-active centers. Pyrrole bridged di-ferrocenyl compounds have been synthesized by a one-pot reaction of 1,4-diferrocenyl butadiene with aniline derivative in presence of CuI as a catalyst. 2,5-Diferrocenyl thiophene was prepared by the thermal reaction of 1,4-diferrocenylbutadiene with sodium sulfide. Previously, Mathur et al. has reported the synthesis of the thiophene bridged compound using a photolytic reaction of chromium and molybdenum hexacarbonyl in presence of sulphur [17,18]. Recently, the Lang group has synthesized a series of substituted 1,1'-diferrocenyl thiophene compounds by Negishi C-C cross-coupling method to study the influence of electron-withdrawing substituents at the ferrocenyl moieties and electron-donating functionalities at the thiophene bridge on the electronic behavior of the molecular system [19]. Cyclic voltammetry study of all these thiophene and pyrrole bridged di-ferrocenyl compounds showed two well-resolved reversible redox wave for the two identical ferrocenyl moieties which confirms distinct electronic communication between the two electroactive groups via the heterocyclic bridge. Besides, the influence of the substituent on the extent of redox separation has also been observed and further revealed a class II type valence trap situation in the corresponding mixed valence species (Figure 3) [20].

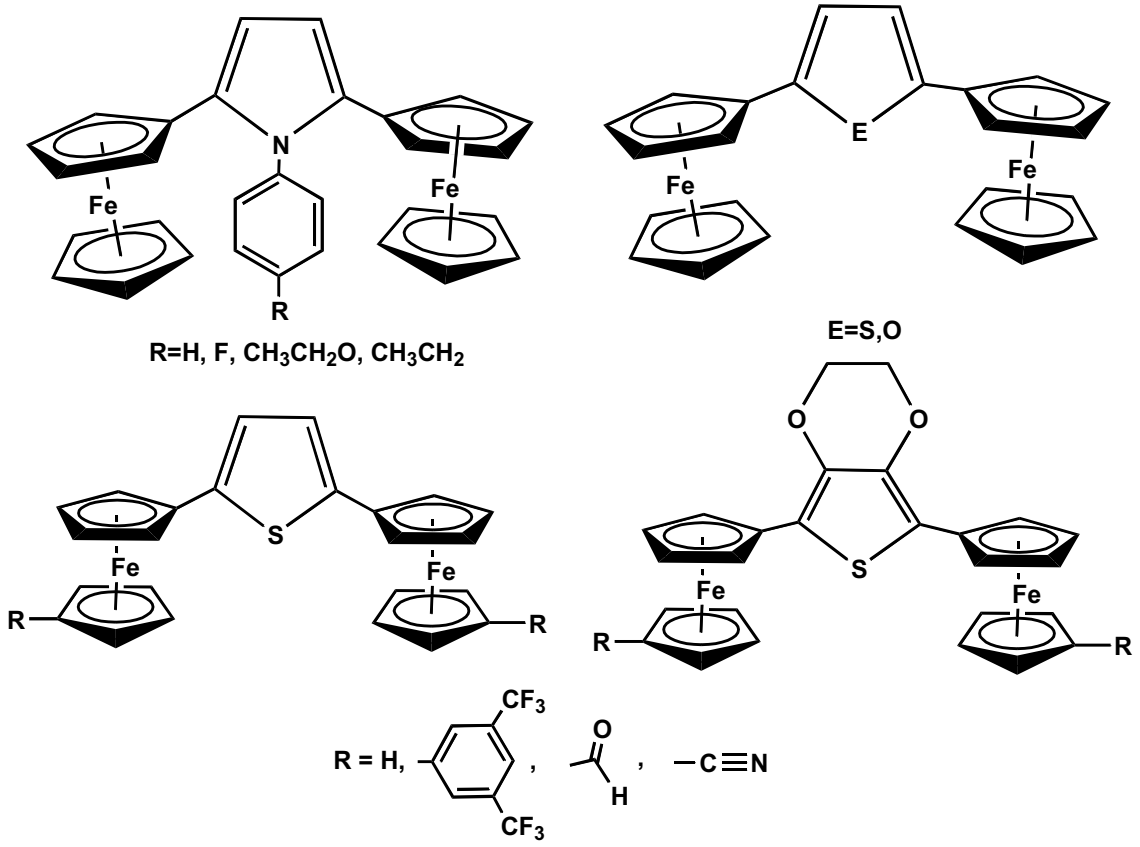

Figure 3. Heterocycle Bridged Di-ferrocenyl System

Three geminal-diethynylethene bridged di-ferrocenyl compounds have been recently reported using the Corey-Fuchs olefination process of a keto compound to give a dibromo olefin intermediate, which under Sonogashira condition gave the geminal-diethynylethene bridged di-ferrocenyl system. The structural characterization shows a typical planar Y-shaped geometry of the gem-diethynylethene backbone with the formation of a chair-like conformation of the cyclohexane or thiopyran pendant substituent. The non-bonded Fe...Fe distance between the two ferrocenyl units is in the range 6.76 -9.17 Å, depending upon the bridging substituent. Although two ferrocenyl units are equivalent, the cyclic voltammetric and IVCT study showed a pair of redox couples indicating strong electronic communication between the two redox centers and the presence of a class II mixed valence system within the molecular framework (Scheme 1) [21].

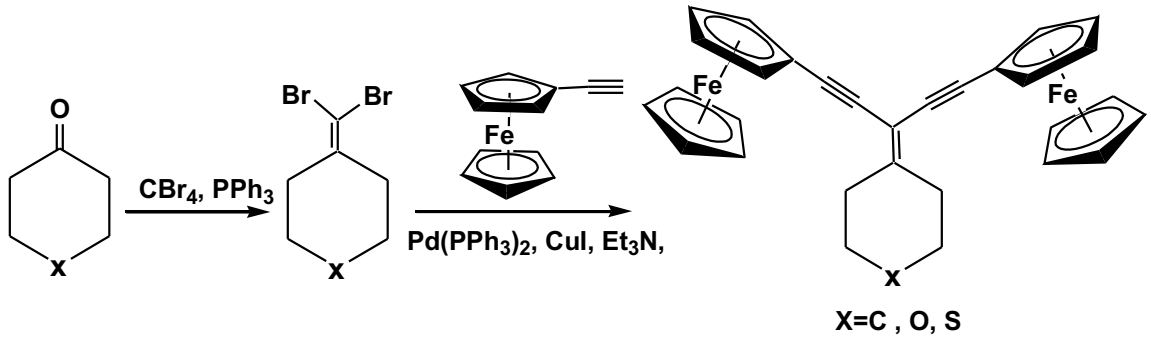

Scheme 1. Synthesis of Geminal-diethynylethene Bridged Di-ferrocenyl Compounds

Chatterjee et al. has reported some ferrocene and diferrocene based hydrazone derivatives that can selectively sense Pb^{2+}metal cation. A diferrocenyl based hydrazone–enone compound has shown effective sensing properties. The compound has been synthesized using a two-step reaction method; the first step being the reaction of 1,1'-diacetyl ferrocene with respective hydrazide to produces the corresponding ferrocenyl hydrazone derivative, which was used for the reaction with monoaldehyde ferrocene in a basic condition to give the diferrocenyl hydrazone-enone derivatives (Scheme 2).

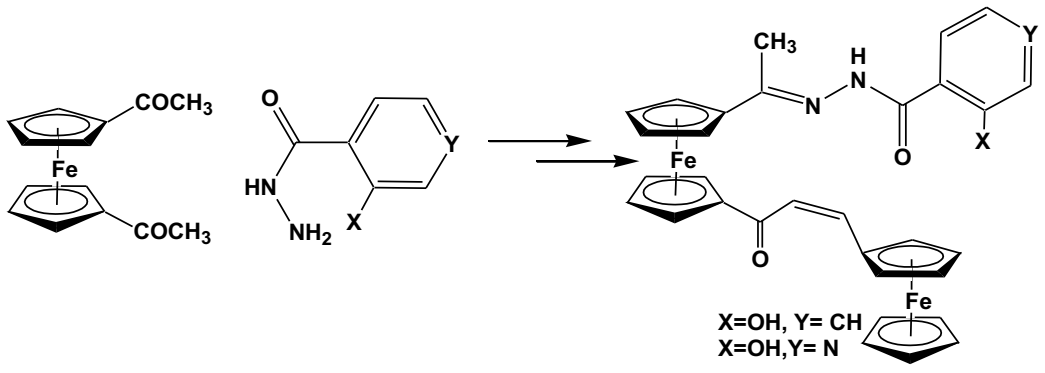

Scheme 2. Diferrocenyl Hydrazone-enone Derivatives

The structures have been confirmed using a single- crystal X-ray diffraction study which shows the presence of two non-equivalent ferrocenyl units oriented opposite to each other and connected to hydrazone and enone moieties. The hydrazone and enone chain in the molecule are oriented in eclipsed conformation. The cyclic voltammetry study shows two reversible one-electron redox waves confirming the presence of two chemically non-equivalent ferrocenyl units.

The UV-Visible binding study shows that the compound selectively interacts with the Pb^{2+} ion with a marked displacement of the spectral bands while other cations show no significant change in their spectral property. Theoretical calculation predicted the site of Pb^{2+} interaction mainly through the ketonic oxygen, imine nitrogen, and cyclopentadienyl ring of the molecular system as shown in Figure 4 [22].

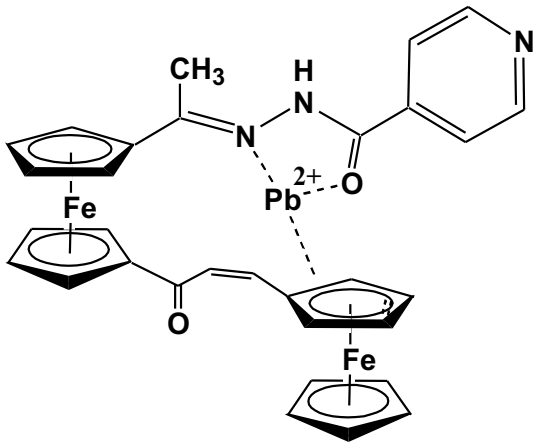

Figure 4. Pb^{2+} Interaction by Diferrocenyl Hydrazone-enone Derivatives

Nemykin et al. has reported di-ferrocenyl compounds (Figure 5) with two chemically equivalent ferrocenyl units.

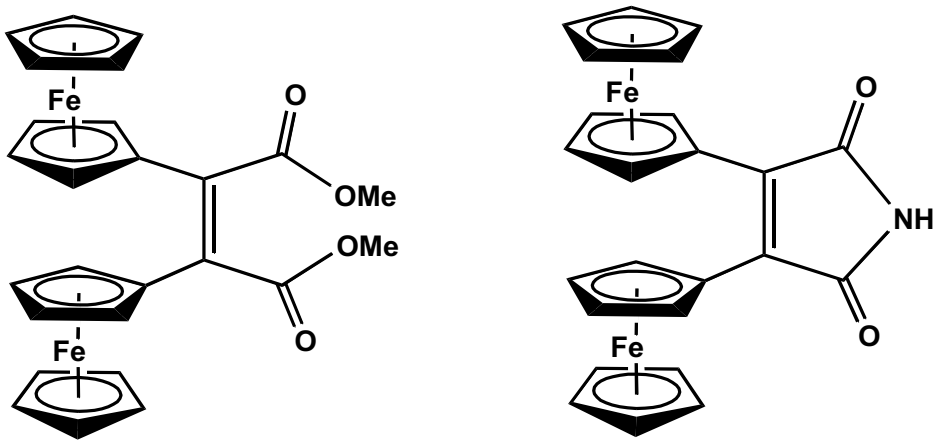

Figure 5. Electronically Coupled Di-ferrocenyl System

The single-crystal X-ray diffraction analysis shows that the two ferrocenyl units are locked in anti-conformation to each other while the ester and the imide groups are attached to the ferrocenyl unit. The cyclic voltammetric study shows two separate one-electron reversible redox processes indicating substantial electronic communication between the two redox centers. The occurrence of absorption bands in the near-infrared region for the oxidized species confirms inter-valence charge transfer and the electronic communication between the redox units [23].

3. Tri-ferrocenyl Architectures

Different types of tri-ferrocenyl systems have been prepared with "star-shaped", linear, cyclic architecture and their interactions were studied mainly to understand their mixed-valence capacity. The interaction among the ferrocenyl systems occurs through various bridging groups and depends upon the extent of conjugation, chain length, etc. The synthesis and characterization of homoleptic tri(ferrocenyl) "star-shaped" derivatives, with heteroatoms like B, N, P, S, Se, Sb, Bi, has been described by Togni and Hayashi which shows a range of multi-ferrocenyl derivatives with bridging main group atoms [24]. Some early report shows that a tri-ferrocenyl compound with a bridging E-C(O), (E = S, Se, Te) unit was synthesized from lithiated ferrocenyl chalcogenols with ferrocenyl acyl chloride (Figure 6).

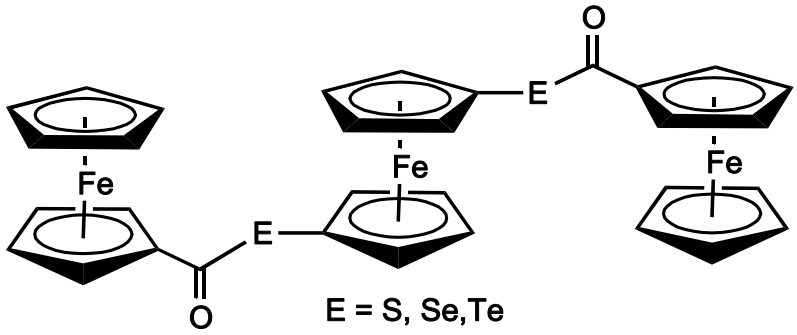

Figure 6. Tri-ferrocenyl Compound with a Bridging E-C(O)

The heteroatom bridged multi-ferrocenyl compounds have shown remarkable chelating properties with various metal fragments [25].

Pena and Cowan described the intervalence electron transfer property of a series of heteroatom-containing tri-ferrocenyl compounds, like triferrocenyl boranes, triferrocenyl phosphine, triferrocenyl phosphine oxide, and triferrocenyl methane, and studied their near IR absorption potential due to the formation of mixed-valence species [26]. Recently, a Si-bridged tri-ferrocenyl compound has been synthesized and their electronic communication among the three ferrocene units was established by cyclic voltammetric study [27]. Wrackmeyer

et al. have reported a tri(ferrocenyl)-aluminum-pyridine compound by the reaction of lithiated ferrocene with aluminium chloride and pyridine. The structure shows three ferrocenyl units at different orientations and attached to the Al center, while a pyridine group is also forming an adduct with the Al atom [28]. A tri-ferrocenyl substituted guanidine compound has been synthesized from ferrocenyl azide using a series of reaction steps involving the formation of ferrocenyl isocyanate, a diferrocenylcarbodiimide derivative that reacted with ferrocenyl methylamine. The compound has been found to act as a receptor molecule for the electrochemical sensing of a dihydrogen phosphate anion [29]. Very recently, Low et al. have synthetically designed a conjugated tri-ferrocenyl compound by $Pd(PPH_3)_4$/CuI catalyzed cross-coupling reaction of dibromo-ferrocenyl ethane with ferrocenyl acetylene. The compound was characterized by single-crystal X-ray diffraction and the electronic effect among the ferrocenyl moieties on potential electronic communication behavior was studied. Cyclic voltammetry using a strong ion-pair electrolyte n-$Bu_4N[PF_6]$ showed broad, overlapping waves arising from the sequential oxidation of the ferrocenyl moieties in electronically and chemically similar environments (Figure 7) [30].

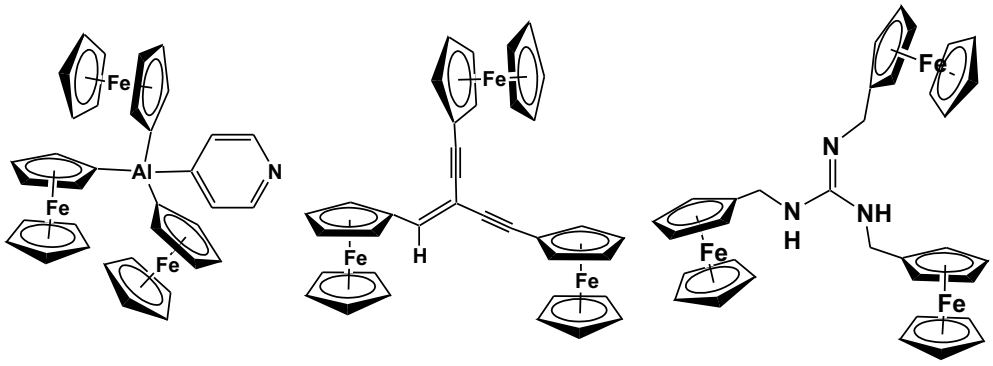

Figure 7. Star-shaped Tri-ferrocenyl Architectures

Lang et al. have reported the synthesis of "star-shaped" tri-ferrocenyl based six-membered aromatic ring including benzene, pyridine, and triazine (Scheme 3).

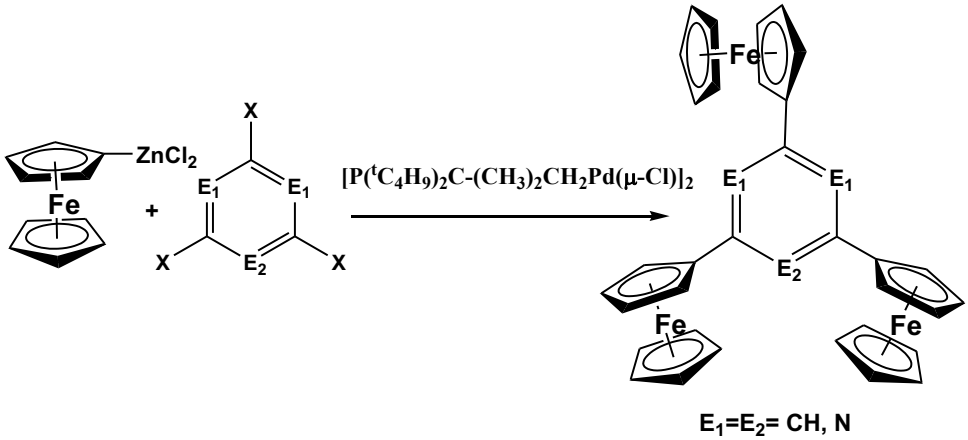

Scheme 3. Synthesis of the Tri-ferrocenyl Six-membered Aromatic Ring

The compounds have been prepared by Negishi coupling reaction between the halogenated aromatic or heteroaromatic ring and ferrocenyl zinc chloride in presence of $[P(^tC_4H_9)_2C\text{-}(CH_3)_2CH_2Pd(\mu\text{-}Cl)]_2$ catalysts. Spectral and structural analysis shows that all the three ferrocenes are chemically equivalent while the cyclopentadienyl ligands of three ferrocenyl units are present in eclipsed conformation. The cyclic voltammetry study shows three well-resolved one-electron redox peaks suggesting an electronic coupling across the electroactive groups. IVCT study with the partially oxidized mixed valent complex shows weak intervalence charge transfer absorption due to some electronic communication in the molecule [31].

Appel et al. [32] and Thilagar et al. [33] have separately synthesized redox-active boraxine compounds and established their electronic communication within the redox-active groups (Figure 8).

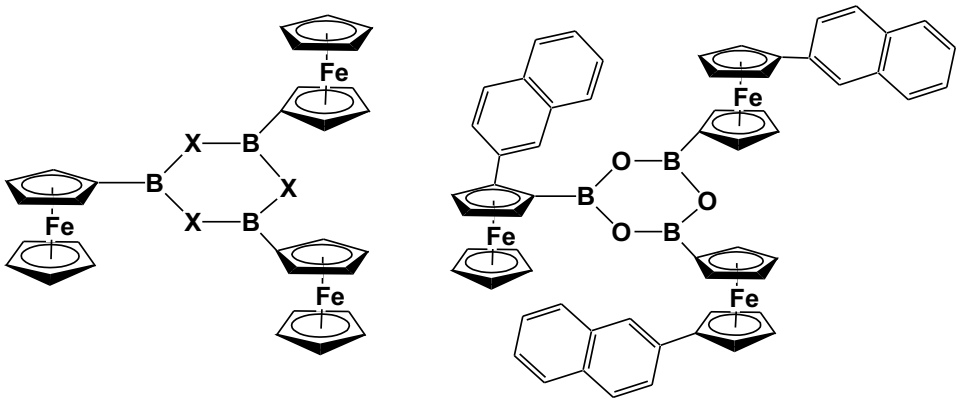

Figure 8. Tri-ferrocenyl Boraxine Compounds

Single-crystal structural analysis of the selenium analog shows the presence of three ferrocenyl fragments attached to a planar B_3X_3 ring (X= O, S, Se). The cyclic voltammetry study shows three well-resolved one-electron redox waves indicating sufficient electronic communications between the ferrocenyl centers. The addition of a Lewis base 4-dimethyl amino-pyridine (DMAP) shows the negative shift of redox signals which indicates the potential of these compounds for their use in Lewis acid-catalyzed processes.

Synthesis of a tri-ferrocenyl complex of dihydro-1H-trindene has been carried out by a two-step process involving the conversion of dihydro-1H-trindene to bromohydrins by the reaction with N-bromosuccinimide to give tribromo-1H-trindene, which gave the tri-ferrocenyl derivative by Negishi cross-coupling with ferrocenylzinc chloride in presence of $PdCl_2(PPh_3)_2$ catalyst (Scheme 4).

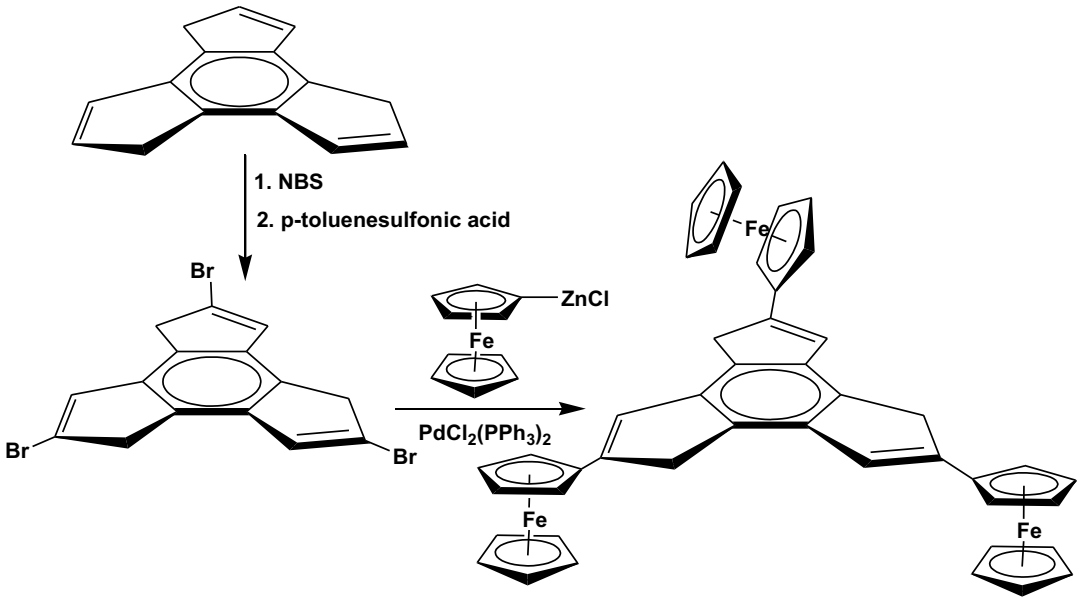

Scheme 4. Synthesis of a Tri-ferrocenyl Complex of Dihydro-1H-trindene

The electrochemical investigation displayed a single reversible redox wave for three ferrocenyl units in $[nBu_4N][PF_6]$ supporting electrolyte while two reversible redox wave in $[nBu_4N][B(C_6H_5)_4]$ supporting electrolyte, suggesting influence on the electronic communication behavior by the variation of counter ion during cyclic voltammetry. The intervalence charge transfer study shows near-IR region absorption which indicates the presence of a class II type mixed valence system [34].

Buntz et al. has reported two isomeric tri-ferrocenyl systems containing a fused dehydroannulene and bridged by 1,3-butadiyne linkage **(**Figure 9).

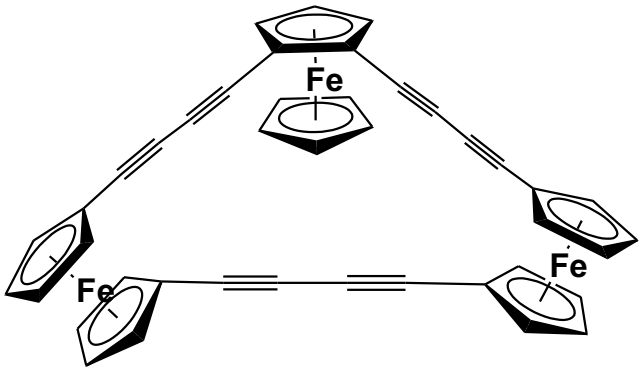

Figure 9. Tri-ferrocenyl System Containing a Fused Dehydroannulene and Bridged by 1,3-Butadiyne Linkage

The compounds have been synthesized from 1,2-diethynylferrocene under Hay conditions in the presence of pyridine and $CuCl_2$/CuCl catalyst. The two isomers have been disting-

uished by an NMR spectroscopy study which shows two chemically equivalent ferrocenyl units in one isomer while three chemically equivalent ferrocenyl units in the other isomer. Electrochemical investigation of one isomer revealed three one-electron oxidation processes and the other isomer shows two one-electron redox processes indicating the formation of mixed-valence species [35].

Another fused cyclic tri-ferrocenyl compound of triindenyl ligand has been synthesized by an exchange reaction of the potassium salt of trindene trianion with [(h^5-C_5H_5)Fe(h^6-fluorenyl)] to give two isomeric compounds, syn-syn-anti and syn- syn-syn (Figure 10).

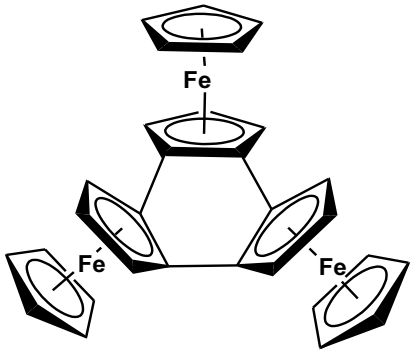

Figure 10. Fused Cyclic Tri-ferrocenyl Compound

The single-crystal X- ray diffraction study shows the cyclopentadienyl ligand orientation of two syn ferrocenes in staggered conformation while anti-ferrocene in eclipsed conformation. Although the entire system is highly conjugated, the central phenyl ring is not a planer. The deviation from planarity is due to the repulsive interaction between the two syn ferrocene units. The cyclic voltammetric study shows two well-defined reversible redox signals and an irreversible signal while the UV-vis/NIR spectral study shows sufficient electronic interaction among the ferrocenyl centers [36].

Another intervalence charge transfer and the presence of mixed-valence species have been reported by Long using a cyclic ferrocenyl alkyne compound (Scheme 5).

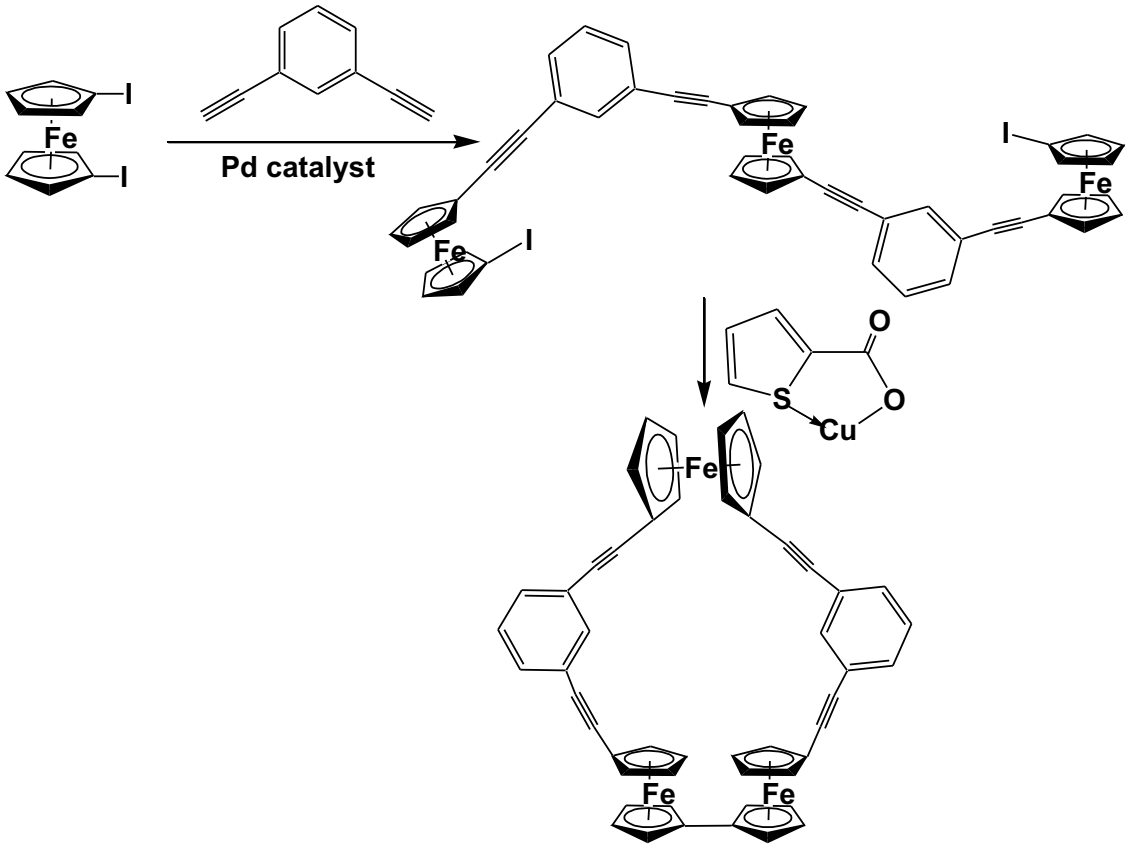

Scheme 5. Synthesis of Cyclic Tri-ferrocenyl System

Sonogashira cross- coupling of 1,1'-Diiodoferrocene and 1,3-diethynylbenzene in the presence of $Pd(PtBu_3)_2$ catalyst gave a tri-ferrocenyl molecule which was cyclized using a copper-mediated Ullmann-like coupling reaction to give a cyclic ferrocenyl structure with alkyne bridging.

The structural study confirmed the presence of tri-ferrocenyl macrocyclic molecules with a cavity, which can act as a place for host-guest interaction. The electrochemical interaction between the ferrocenyl units has been investigated by spectroelectrochemistry. The formation of mixed-valence species has been confirmed by the formation of the absorption band at the near-infrared region [37].

4. Multi-ferrocene Based Compounds

Multinuclear and oligomeric ferrocene complexes have been extensively studied in the last decade for potential applications in multielectron redox catalysis, electron storage devices and as redox switchable molecules. Some of these multi-ferrocenyl systems can selectively vary their electronic properties by oxidation or reduction

processes making them important for miniaturized molecular switches and sensor devices. Mathur et al. designed a low-temperature photolytic reaction of diferrocenyl diynes with metal carbonyl complexes to give three types of polyyne bridged tetra-ferrocenyl metallacyclic compounds (Figure 11).

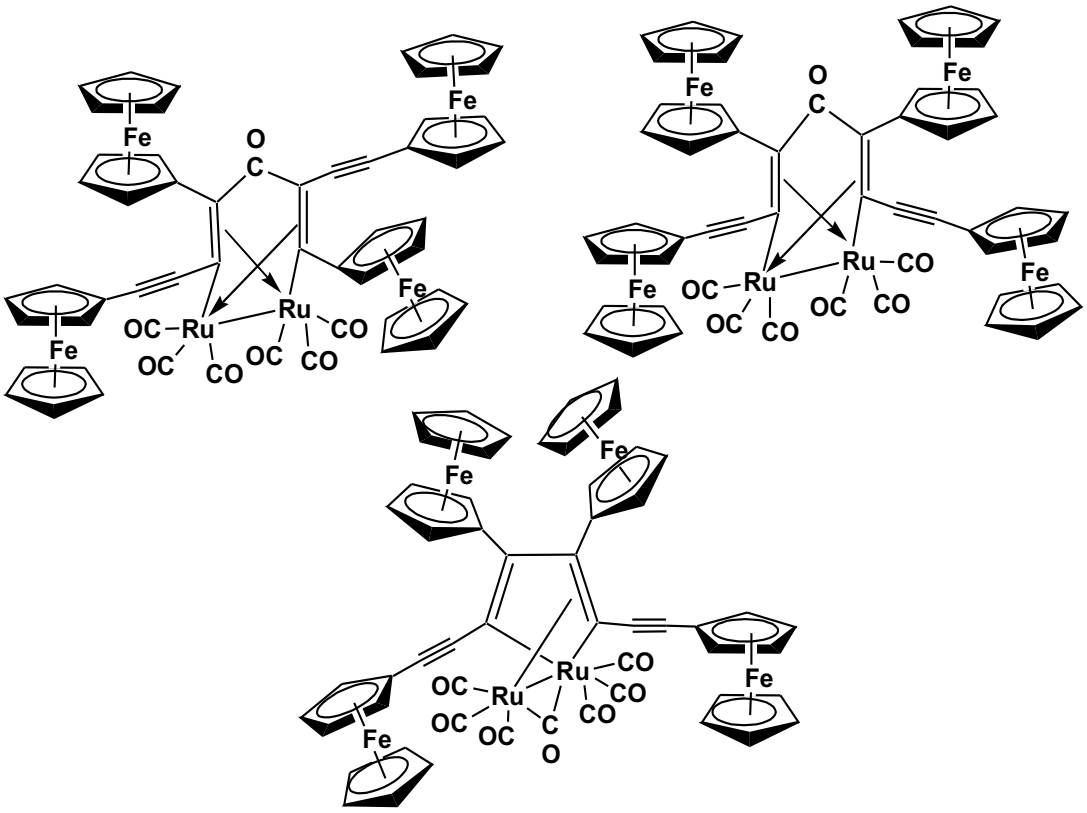

Figure 11. Tetraferrocenyl Metallacyclic Compounds

Reactions of metal clusters with polyenes have attracted significant interest for the synthesis of extended carbon chains with wide coordination modes. In this reaction, a similar technique has been used to make multi-ferrocenyl linkages which are an attractive candidate for the study of electronic communication and mixed-valence species. The structure of the three tetra-ferrocenyl metalacyclic compounds has been evaluated by single-crystal X-ray crystallography which shows three different cyclic bridges with and without the carbonyl incorporation. The ferrocenyl entities are randomly oriented to release the steric strain across the molecule due to the presence of the bulky -C≡C-CFc group [38].

In another reaction involving ferrocenyl acetylene and tungsten hexacarbonyl, metal-assisted alkyne oligomerization type of rearrangement has been observed to give a unique tetraferrocenyl-cycloocta-tetraene ligated tungsten complex (Figure 12).

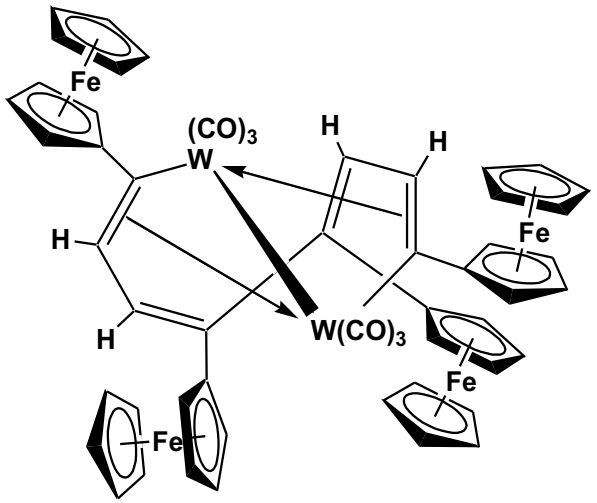

Figure 12. Tetraferrocenyl-cycloocta-tetraene Ligated Tungsten Complex

The structure consists of cyclic tetraferrocenyl dimetallacyclo-decatetraene unit pi-bonded to two tungsten atoms, forming a twisted W_2C_8 ring [39].

Ferrocene linked to porphyrin macrocycle has been an interesting donor-acceptor type molecule with a strong absorbance in the visible spectrum and has been found to show significant electron transfer and redox properties. Porphyrin-ferrocene linkage has shown remarkable optoelectronic properties and is considered to be a potential candidate for their use as molecular electronic devices, in electrocatalysis and sensing of guest molecules. Nemykin et al. has investigated the redox properties of some tetra-ferrocenyl porphyrin type molecule and observed intervalence charge transfer bands in the near-IR region. The charge transfer analysis confirmed the presence of class II type intervalence charge transfer characteristics involving ferrous/ferric centers [40,41]. Synthesis of the metal (M) complexes of tetra-ferrocenyl porphyrin with Zn, Ni, Co and Cu, and their structural study, shows a strong influence of the central metal atom on the degree of non-planarity of the porphyrin ring system which also confirms the presence of numerous metal-to-ligand charge-transfer bands coupled via a configurational interaction, with expected intra-ligand p–p* transitions [42]. Galloni and Nemykin further synthesized tetra-ferrocenyl porphyrin based self-assembled monolayers and investigated their photocurrent generation efficiency [43]. The data of the monofunctionilized monolayers revealed their potential as candidates for the construction of molecular electronic devices. Some of the tetra-ferrocenyl porphyrin derivatives have been used as electrode modifying layer in combination with Prussian blue due to its unique electronic properties and synergic effect between porphyrin ring and peripheral ferrocenyl group. The conjugate has been tested for the sensing of dopamine showing a satisfactory analytical response comparable to other chemically modified electrodes. A magnesium complexed tetraferrocenyl tetraazoporphyrin has been investigated for its use as an energy acceptor from CdS quantum dots as donors. The study showed that CdSe quantum dots can be promising energy transfer donors for NIR-absorbing tetraferrocenyl tetraazaporphyrins to form antenna systems with enhanced light-harvesting efficiency (Figure 1.24).116,117 (Figure 13) [44].

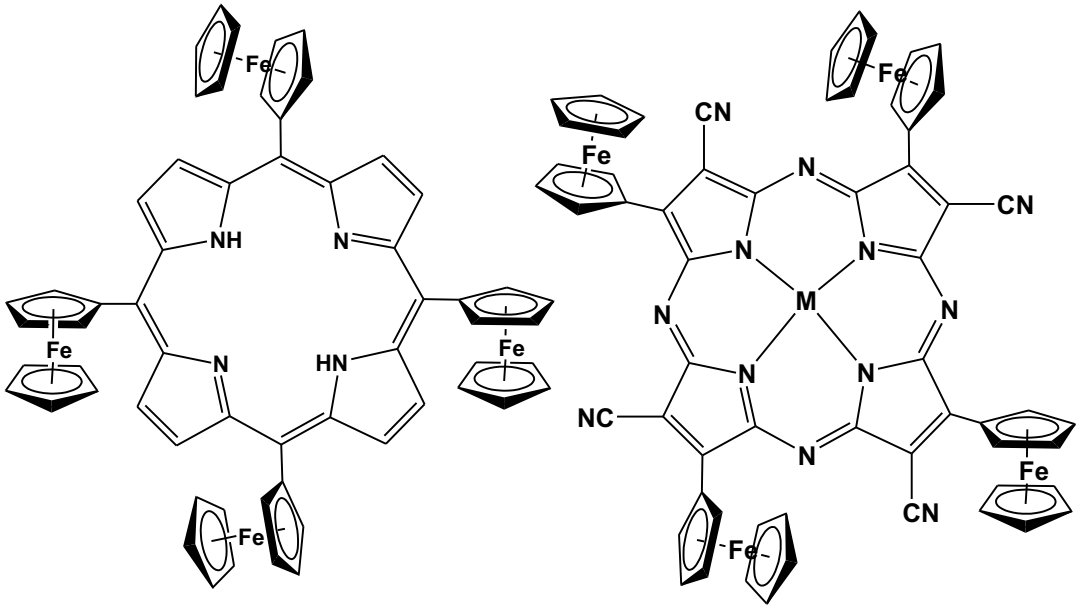

Figure 13. Tetra-ferrocenyl Porphyrin and Tetraazoporphyrins
(M= denotes for metal ions written above text)

A diaminobutane poly(propylene imine) dendrimer functionalized with biferrocenyl units has been synthesized which shows electrochemical anion sensing properties [45]. The compound, synthesized by the reaction of dichlorocarbonyl bisdiferrocenyl derivative with diaminobutane-based poly(propylene imine) dendrimer, shows two reversible redox waves in the cyclic voltammetry study and shows a large cathodic shift due to the interaction of dihydrogen phosphate and hydrogensulfate anion (Scheme 6).

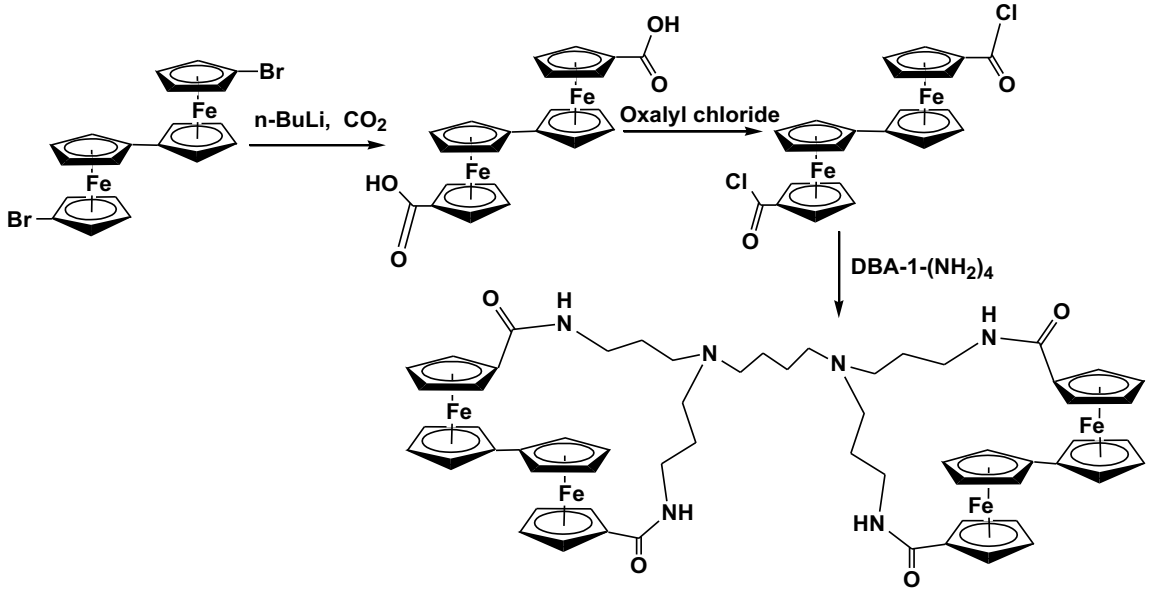

Scheme 6. Biferrocenyl Diaminobutane Poly(propyleneimine) Dendrimer

A range of tetra-ferrocenyl heterocyclic derivatives has been synthesized for their study in understanding electronic communication across the heterocyclic moiety. The iron-iron distances in these tetra-ferrocenyl heterocyclic systems have been kept constant while the heteroatom was changed to S, O, NPh, or NMe groups. The cyclic voltammetry study shows two reversible redox processes in all the system indicating effective electronic communication between the ferrocenyl units and shows the formation of mixed valence species, confirmed by the appearance of inter-valence charge transfer band at the near-infrared region (Figure 14) [46-48].

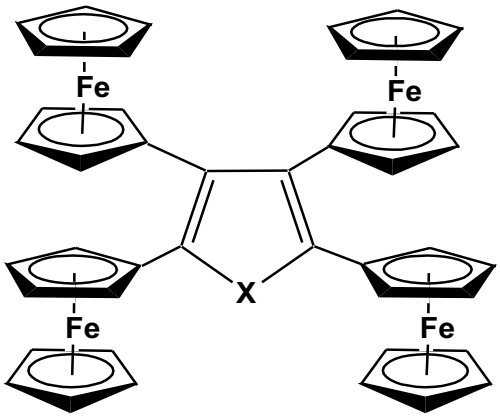

X=S, O, NMe, NPh

Figure 14. Tetra-ferrocenyl Heterocyclic Derivatives

Higher analogs of multi-nuclear ferrocenyl systems are not only difficult to synthesize but also pose challenges to stabilizing the molecular system. To find new synthetic methods to obtain higher ferrocenyl compounds with a conjugated network, Peris et al. have designed a series of palladium-catalyzed reactions directed towards the synthesis of a penta-ferrocenyl complex with a conjugated link in between the ferrocenyl moieties (Figure 15).

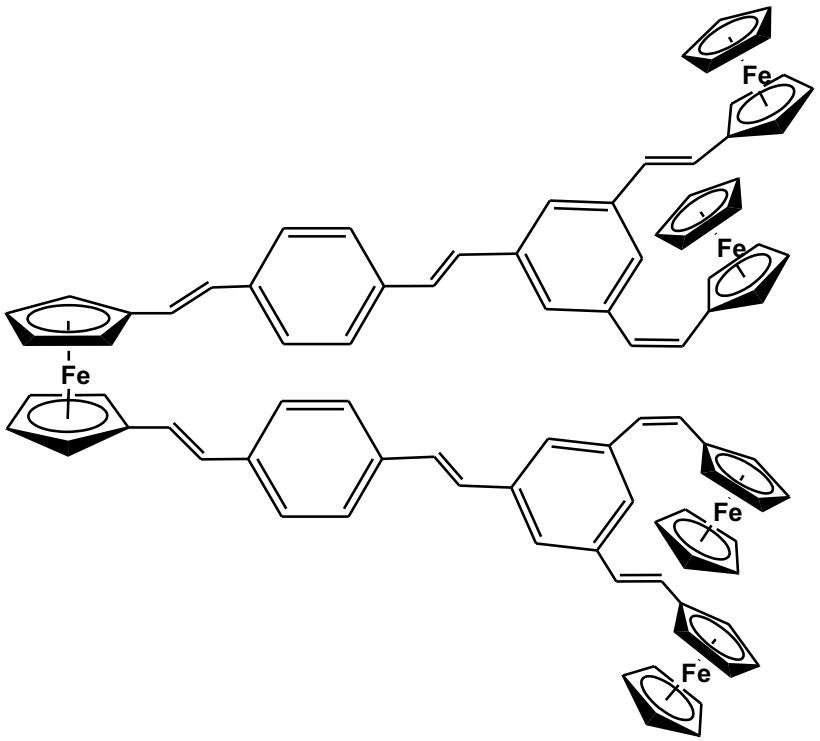

Figure 15. Penta-ferrocenyl Compound Bridged with Conjugated Chain

The synthetic procedure involves an olefination reaction by the Wittig method and a Pd-mediated C-C coupling reaction using a palladium pincer complex. The electrochemical analysis of the compound revealed two separate redox responses for the peripheral ferrocenyl units and the central ferrocenyl unit displaying distinct electronic coupling behavior between the two extreme redox species [49].

In a remarkable use of a multi-ferrocenyl system in miniaturized molecular devices, Rapenne and Launay reported the concept of an electrically fueled single molecular rotary motor based on the transport of electrons between two electrodes by the electroactive groups attached to a central rotatable core. The motor is based on a ruthenium complex with a piano stool geometry bearing two different ligands that act as a rotor and a stator. The stator is a tripodal hydrotris(indazolyl)borate ligand functionalized by ester groups while the rotor is a cyclopentadienyl (Cp) ligand connected to five ferrocenyl groups by linear and rigid arms (Figure 16) [50].

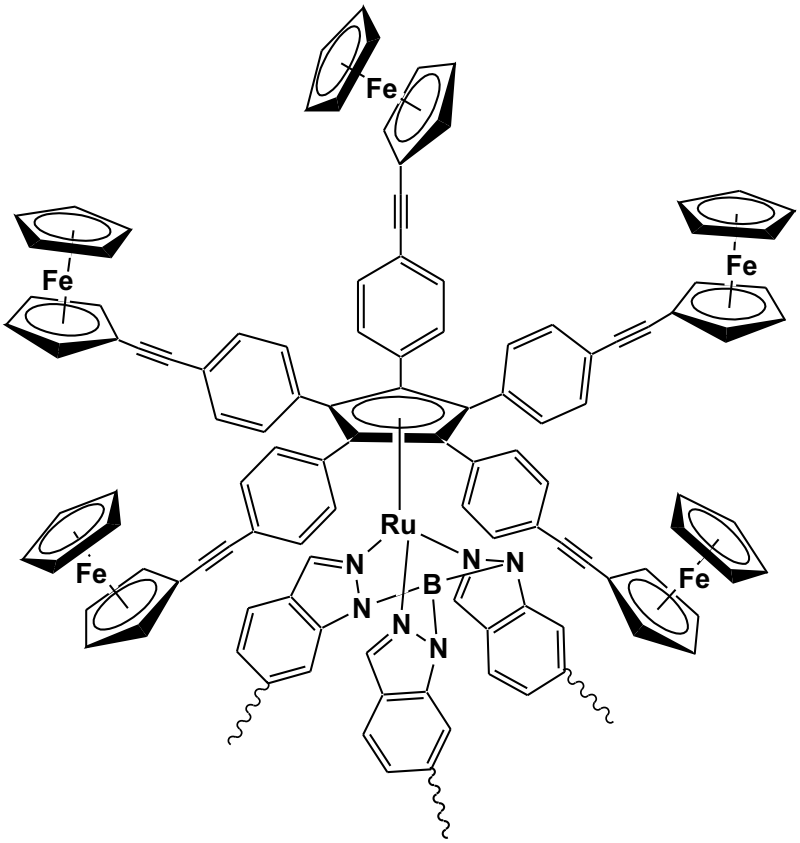

Figure 16. Tripodal Hydrotris(indazolyl)borate Based Penta-ferrocenyl System

The cyclic voltammetry in dichloromethane with nBu_4NPF_6 supporting electrolyte displayed one reversible peak for ferrocenyl units while promising effects appeared on electron exchange which triggers a change in the molecular geometry. Penta- and hexa-ferrocenyl benzenes have been prepared by Negishi type ferrocenylation reaction of hexabromo- or hexaiodobenzene with diferrocenylzinc. The molecules are of great interest due to their electronically tunable dendritic substructure with potential in electronic, magnetic, optical, and catalytic applications and because of the presence of crowded arene type structures that may function as molecular gear.

The single-crystal structural analysis of the hexa-ferrocenyl benzene revealed that the central benzene ring is not planer and adopts a chair conformation. The cyclic voltammetric study showed three well-separated reversible 1e, 2e, and 3e redox couples suggesting effective electronic communication (Figure 17) [51].

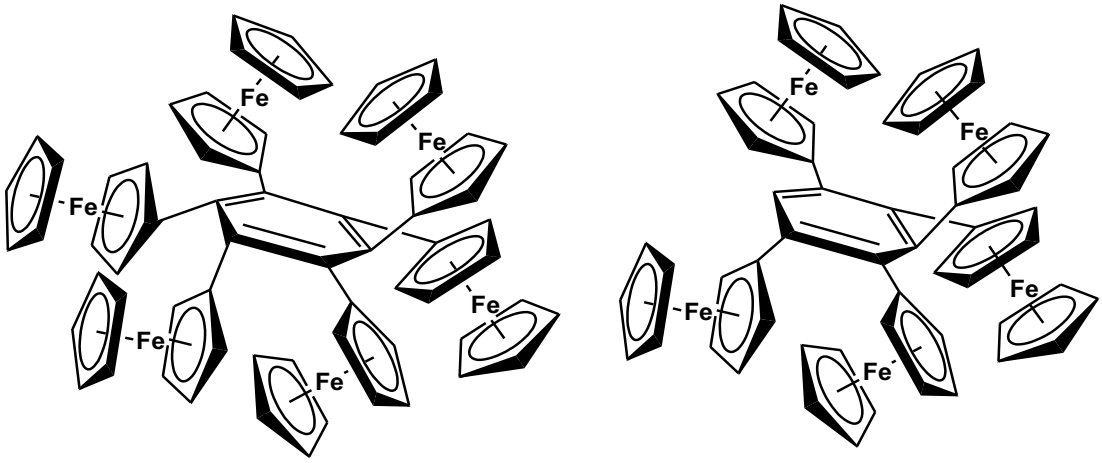

Figure 17. Hexa- and Penta- ferrocenyl Benzene

Electron transfer mechanisms in multi-redox systems like polymers, dendrimers, and macrocyclic moieties are of prime importance due to their relevance with biologically inspired electron transfer and redox processes. Also, these systems have been of interest for their potential as mixed-valence species, redox recognition, and catalysis. Ferrocenyl entities have always been a good choice to act as redox species due to their reversible process and stability of the mixed valence systems. Recently, the research group of Astruc has reported the synthesis of a series of rigid hexa- and dodeca- ferrocenyl arene centered poly(ethynylphenylene) dendrimers with C3 symmetry using Sonogashira type coupling reaction and studied their electron-transfer properties. The polyferrocenyl entities showed distinct communication and stabilization of the mixed valence species (Figure 18) [52,53].

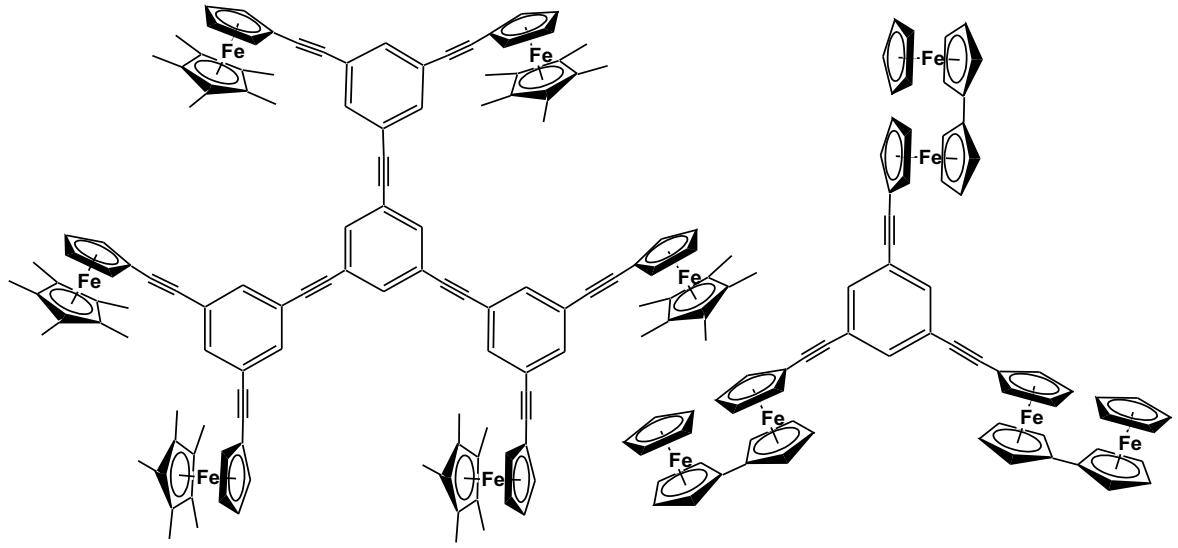

Figure 18. Hexa- and Dodeca- ferrocenyl Arene Dendrimers

5. Conclusion

Multinuclear and oligomeric ferrocene complexes have been extensively studied in the last decade for potential applications in multielectron redox catalysis, electron storage devices and as redox switchable molecules. Some of these multi-ferrocenyl systems can selectively vary their electronic properties by oxidation or reduction processes, making them important for miniaturized molecular switches and sensor devices. Therefore, this review summarizes the recent development of the multi-ferrocenyl system and its synthetic strategies.

Acknowledgments

I very much want to thank Midnapore city college for providing me infrastructure to work and also I am thankful to my family for providing me mental support.

References

1. a) Weiss J. *Coord. Chem. Rev.*, 2010, 254, 2247. (b) Nano and Molecular Electronics Handbook, ed. S.E. Lyshevski, CRC Press, New York, 2007. (c) Bayley H. *Nature*, 2010, 467, 164. (d) Giacalone F, Martin N. *Adv. Mater.*, 2010, 22, 4220. (e) Jurow M, Schuckman AE, Batteas JD, Drain CM. *Coord. Chem. Rev.*, 2010, 254, 2297. (f) Chung A, Deen J, Lee JS, Meyyappan M. *Nanotechnology*, 2010, 21, 412001. (g) Balzani V, Credi V, Venturi M. *Nanotoday*, 2007, 2, 18.
2. (a) Fukino T, Fujita N, Aida T. *Org. Lett.*, 2010, 12, 3074. (b) Manners I. *Science*, 2001, 294, 1664. (c) De Cola L, Belser P in Electron Transfer in Chemistry, ed. V. Balzani, Wiley-VCH, Weinheim, 2001, 5, 97. (d) Paddow-Row MN in Electron Transfer in Chemistry, ed. V. Balzani, Wiley-VCH, Weinheim, 2001, 2, 179. (e) Joachim C, Gimzewski JK, Aviram A. *Nature*, 2000, 408, 541. (f) Astruc D. *Acc. Chem. Res.*, 1997, 30, 383.
3. (a) Astruc D, Ornelas C, Ruiz Aranzaes J. *J. Inorg. Organomet. Polym. Mater.*, 2008, 18, 4. (b) Cowan DO, LeVanda C, Park J, Kaufman F. *Acc. Chem. Res.*, 1973, 6, 1. (c) Wagner M. *Angew. Chem., Int. Ed.*, 2006, 45, 5916. (d) Miller JS, Epstein AJ. *Angew. Chem., Int. Ed. Engl.*, 1994, 33, 385. (e) Barlow S. *Inorg. Chem.*, 2001, 40, 7047. (f) Giuffrida G, Campagna S. *Coord. Chem. Rev.*, 1994, 517, 135-136. (f) Donoli A, Bisello A, Cardena R,

Ceccon A, Bassetti M, Annibale AD, Pasquini C, Raneri A, Santi S. *Inorg. Chim. Acta*, 2011, 374, 442. (g) Steffens S, Prosenc MH, Heck J, Asselberghs I, Clays K. *Eur. J. Inorg. Chem.*, 2008, 1999.
4. Heckmann A, Lambert C. *Angew. Chem., Int. Ed.*, 2012, 51, 326.
5. Vincent KB, Zeng Q, Parthey M, Yufit DS, Howard JAK, Hartl F, Kaupp M, Low PJ. *Organometallics*, 2013, 32, 6022.
6. Bruce MI, Burgun A, Fox MA, Jevric M, Low PJ, Nicholson BK, Parker CR, Skelton BW, White AH, Zaitseva NN. *Organometallics*, 2013, 32, 3286.
7. Vincent KB, Gluyas JBG, Zeng Q, Yufit DS, Howard JAK, Hartl F, Low PJ. *Dalton Trans*., 2017, 46, 5522.
8. Vincent KB, Gluyas JBG, Gückel S, Zeng Q, Hartl F, Kaupp M, Low PJ. *J. Organomet. Chem*., 2016, 821, 40.
9. Xu GL, Xi B, Updegraff JB, Protasiewicz JD, Ren T. *Organometallics*, 2006, 25, 5213.
10. Forrest WP, Choudhuri MMR, Kilyanek SM, Natoli SN, Prentice BM, Fanwick PE, Crutchley RJ, Ren T. *Inorg. Chem*., 2015, 54, 7645.
11. Forrest WP, Cao Z, Hassell KM, Prentice BM, Fanwick PE, Ren T. *Inorg. Chem*., 2012, 51, 3261.
12. Natoli SN, Azbell TJ, Fanwick PE, Zeller M, Ren T. *Organometallics*, 2016, 35, 3594.
13. Cao Z, Ren T. *Organometallics*, 2011, 30, 245.
14. Fan Y, Li H-M, Zou G-D, Zhang X, Pan Y-L, Cao K-K, Zhang M-L, Ma P-L, Lu H-T. *Organometallics*, 2017, 36, 4278.
15. Gao Y, Li H-D, Ke C-F, Xie L-L, Wei B, Yuan Y-F. *Appl. Organomet. Chem*., 2011, 25, 407.
16. Oton F, Gonzalez MDC, Espinosa A, Tarraga A. *Organometallics*, 2012, 31, 2085.
17. Mathur P, Singh AK, Singh VK, Singh P, Rahul R, Mobin SM, Thone C. *Organometallics*, 2005, 24, 4793.
18. Mathur P, Singh AK, Chatterjee S, Singh VK, Mobin SM. *J. Organomet. Chem.*, 2010, 695, 950.
19. Speck JM, Korb M, Rüffer T, Hildebrandt A, Lang H. *Organometallics*, 2014, 33, 4813.
20. Hu Y-Q, Han L-M, Zhu N, Hong H-L, Xie R-J. *J. Coord. Chem*., 2013, 66, 3481.
21. Fan Y, Li H-M, Zou G-D, Zhang X, Li M, Wu J-H, Zhang X, Lu H-T. *J. Organomet. Chem*., 2018, 859, 99.
22. Mishra S, Dewangan S, Giri S, Mobin SM, Chatterjee S. *Eur. J. Inorg. Chem.*, 2016, 5485.
23. Solntsev PV, Dudkin SV, Sabin JR, Nemykin VN. *Organometallics*, 2011, 30, 3037.
24. Eds. A. Togni, T. Hayashi, VCH, Weinheim, 1995, 5, 236.
25. Herberhold M, Leitner P, Dornhofer C, Ott-Lastic J. *J. Organomet. Chem.*, 1989, 377, 281.
26. Delgado-Pena F, Talham DR, Cowan DO. *J. Organomet. Chem*., 1983, 253, 43.
27. Herrero M, Sevilla R, Casado CM, Losada J, Garcia-Armada P, Rodriguez-Dieguez A, Briones D, Alonso B. *Organometallics*, 2013, 32, 5826.
28. Wrackmeyer B, Klimkina EV, Ackermann T, Milius W. *Inorg. Chim. Acta*, 2009, 362, 3941.
29. Lorenzo Á, Aller E, Molina P. *Tetrahedron*, 2009, 65, 1397.
30. Vincent KB, Gluyas JBG, Zeng Q, Yufit DS, Howard JAK, Hartl F, Low PJ. *Dalton Trans*., 2017, 46, 5522.
31. Pfaff U, Hildebrandt A, Schaarschmidt D, Hahn T, Liebing S,

Kortus J, Lang H. *Organometallics*, 2012, 31, 6761.
32. Appel A, Nöth H. *Z. Anorg. Allg. Chem.*, 2010, 636, 2329.
33. Thilagar P, Chen J, Lalancette RA, Jäkle F. *Organometallics*, 2011, 30, 6734.
34. Donoli A, Bisello A, Cardena R, Prinzivalli C, Santi S. *Organometallics*, 2013, 32, 1029.
35. Bunz UH, Roidl G, Altmann M, Enkelmann V, Shimizu KD. *J. Am. Chem. Soc*., 1999, 121, 10719.
36. Santi S, Orian L, Donoli A, Bisello A, Scapinello M, Benetollo F, Ganis P, Ceccon A. *Angew. Chem., Int. Ed.*, 2008, 47, 5331.
37. Wilson LE, Hassenrück C, Winter RF, White AJP, Albrecht T, Long NJ. *Angew. Chem., Int. Ed*., 2017, 56, 6838.
38. Mathur P, Das A, Chatterjee S, Mobin SM. *J. Organomet. Chem*., 2008, 693, 1919.
39. Mathur P, Chatterjee S, Das A, Mobin SM. *J. Organomet. Chem*., 2007, 692, 819.
40. Toledo KC, Pires BM, Bonacin JA, Iglesias BA. *J. Porphyrins Phthalocyanines*, 2016, 20, 2.
41. Sirbu D, Turta C, Gibson EA, Benniston AC. *Dalton Trans.*, 2015, 44, 14646.
42. Vecchi A, Erickson NR, Sabin JR, Floris B, Conte V, Venanzi M, Galloni P, Nemykin VN. *Chem. Eur. J*., 2014, 20, 1.
43. Lvova L, Galloni P, Floris B, Lundström I, Paolesse R, Natale CD. *Sensors*, 2013, 13, 5841.
44. Gautam P, Dhokale B, Shukla V, Singh CP, Bindra KS, Misra R. *J. Photochem. Photobiol.*, 2012, 239, 24.
45. Villena C, Losada J, García-Armada P, Casado CM, Alonso B. *Organometallics*, 2012, 31, 3284.
46. Hildebrandt A, Rüffer T, Erasmus E, Swarts JC, Lang H. *Organometallics*, 2010, 29, 4900.
47. Hildebrandt A, Schaarschmidt D, Lang H. *Organometallics*, 2011, 30, 556.
48. Hildebrandt A, Lang H. *Dalton Trans.*, 2011, 40, 11831.
49. Mata JA, Peris E. *Inorg. Chim. Acta*, 2003, 343, 175.
50. (a) Carella A, Rapenne G, Launay JP. *New J. Chem.*, 2005, 29, 288. (b) Carella A, Coudret C, Guirado G, Rapenne G, Vives G, Launay JP. *Dalton Trans.*, 2007, 177. (c) Vives G, Gonzalez A, Jaud J, Launay JP, Rapenne G. *Chem. Eur. J.*, 2007, 13, 5622. (d) Vives G, Jacquot de Rouville HP, Carella A, Launay JP, Rapenne G. *Coord. Chem. Rev.*, 2008, 252, 1451. (e) Vives G, de Rouville HP, Carella A, Launay JP, Rapenne G. *Chem. Soc. Rev.*, 2009, 38, 1551.
51. Yu Y, Bond AD, Leonard PW, Lorenz UJ, Timofeeva TV, Vollhardt KPC, Glenn DW, Yakovenko AA. *Chem. Commun.*, 2006, 2572.
52. Diallo AK, Ruiz J, Astruc D. *Chem. Eur. J.*, 2013, 19, 8913.
53. Wang Y, Rapakousiou A, Chastanet G, Salmon L, Ruiz J, Astruc D. *Organometallics*, 2013, 32, 6136.

The Chemist
Journal of the American Institute of Chemists

Chemical Characterization, Preparation of Biosurfactant and Biochemical Evaluation of Seed Oil of *Luffa aegyptiaca*

Marili F. Zubair[1], Sulyman O. Ibrahim[1], Olubunmi Atolani[2], Abdulmumeen A. Hamid[2] Olamilekan J. Ibukun[3] Halimat A. Abdulrahim[4]

[1]Department of Industrial Chemistry, Faculty of Physical Sciences, University of Ilorin Ilorin, Nigeria
[2]Department of Chemistry, Faculty of Physical Sciences, University of Ilorin Ilorin, Nigeria
[3]Indian Institute of Science Education and ResearchKolkata, West Bengal, India
4Department of Medical Biochemistry, University of IlorinIlorin, Nigeria
(E-mail: marilizub@unilorin.edu.ng)

Abstract: This study aimed to provide insight to minimize domestic and industrial competition for vegetable oil while limiting the discharge of undegradable synthetic surfactants (pollutants) to the environment by exploring the potential of underutilized sponge seeds. Extraction and characterization of the seed oil were performed using standard procedures by American Oil Chemist Society (AOCS). Fourier transform infrared spectroscopy (FT-IR) was used to characterize the prepared biosurfactant. Four antioxidant assays, namely 2,2′-Azinobis-(3-Ethylbenzthiazolin-6-Sulfonic Acid (ABTS), 1,1-Diphenyl-2-picrylhydrazyl (DPPH), Ferric Reduction Potential (FRAP) and Nitric oxide (NO), were used to determine the antioxidant potential of the seed oil and biosurfactant using gallic acid and sodium lauryl sulfonate (SLS) as standards. The biosurfactant shows appreciable efficiency in a salt tolerance level of 190 ppm above the range of 120 – 180 ppm recommended for hard water. The standard synthetic surfactant SLS shows a salt tolerance of 220 ppm. The clear absence of a hydroxyl group (O-H) in the seed oil and carbonyl group (C=O) in diethanolamine (surfactant), which were more prominent in the biosurfactant at 1618 cm^{-1}, indicate the formation of a biosurfactant. Antioxidant analysis shows that oil has moderate antioxidant potential when compared to gallic acid, while the biosurfactant shows better antioxidant potential against ABTS radicals, DPPH radicals, and FRAP than SLS. SLS indicated improved nitric oxide (NO) antioxidant compared with the biosurfactant. This suggests that the prepared degradable biosurfactant has the potential to replace its synthetic counterparts, thereby mitigating environmental pollution. Biosurfactants with antioxidant properties can serve as additives to protect against oxidative degradation in allied products.

Key Words: biosurfactants, antioxidants, physicochemical, GC-MS characterization, organic chemistry/natural products

1. Introduction

Biosurfactants are amphiphilic surface-active agents with enhanced stability, moderate toxicity and highly degradable properties compared to their synthetic alternatives [1]. In recent times, there has been increased interest in the production of biosurfactants from renewable sources as a result of their advantages over synthetic surfactants with respect to renewability, availability and environmental friendliness. The lower application of biosurfactants is primarily attributable to the cost of production, among other things. However, the negative impact of continuous accumulation of chemical surfactants on the environment makes the renewed search for better eco-friendly surfactants an inevitable option [2-4].

Masakorala et al. [5] reported that the absorption of synthetic surfactants significantly reduces the ability of plants to convert photochemical energy from the sun. Similarly, the growth of lettuce was reportedly affected as a result of synthetic surfactant, as stated by Johnson et al. [6]. Potential applications of biosurfactants include enhanced oil recovery [7], bioremediation processes owing to their potential to emulsify contaminants [8], and stabilization of food as a result of their antioxidant potential [9].

Growing interest in naturally preserved foods has further necessitated research into surfactants of fat and oil origin that are capable of abolishing the use of synthetic surfactants [10]. These other reasons are why this research on the properties and antioxidant potential of biosurfactants produced from seed oil of sponge seeds was carried out.

Sponge seed "*Luffa aegyptiaca"* is a subtropical vegetable and widely cultivated plant in tropical and subtropical countries. In many countries, the plant grows as a weed, particularly in Nigeria, where it is often thrown away as waste as the fibre part is much desired as a natural sponge. Stephens [11] reported that the plant contains both medicinal and nutritional agents and has been used for cleaning, filtering, and bathing. Balakrishnan and Huria [12] reported the pharmacological activities of *L. cylindrica,* another common species of the plant*,* which include antiplasmodial and antibacterial activities. In another study, the antihyperglycemic and antihyperlipidemic activities of ethanolic and aqueous extracts of the fruit of *L. aegyptiaca* were attributed to the presence of various phytochemicals, such as alkaloids, steroids, triterpinoids, flavonoids, and glycosides [13].

This work focused on the preparation, physicochemical properties, characterization, and antioxidant properties of diethanolamide from underutilized sponge seeds.

2. Materials and Methods

Sample Preparation

A fully matured sample of sponge seed was collected from Ogbondoroko, Afon area of Kwara State, Nigeria. The plant material was identified at the Herbarium of Plant Biology, University of Ilorin, Ilorin, Nigeria, where a voucher specimen was deposited. The seeds were deshelled, pulverized, dried, and kept in a cool dark place until needed for analysis.

Methods

Extraction and Physicochemical Analysis of the Seed Oil

Oil extraction was carried out using n-hexane (1000 mL) according to the method of Zubair et al. [14]. A 500 g sample material of pulverized dried seeds was extracted using a Soxhlet extractor at 55°C for 7 hours. The oil was obtained using a rotary evaporator at 40°C. Physicochemical properties such as acid value, iodine value, saponification value, peroxide value, and free fatty acids were determined using AOCS methods as described by Zubair et al. [14].

Preparation of the Fatty Acid Methyl Ester (FAMEs)

Fatty acid methyl ester was prepared according to the method of Zubair et al. [14]. 50 g oil was refluxed for one hour with 0.2 M methanolic HCl. At the end of the reflux, the FAMEs were obtained using n-hexane and concentrated using a rotary evaporator.

Preparation of the Biosurfactant

This was carried out following the method of Adewuyi et al. [15]. The reaction was carried out in a round bottom Pyrex glass. The reaction flask was equipped with a mechanical stirrer, thermometer and condenser. Esterified sponge seed oil and diethanolamine were reacted at a molar ratio of 1:6 in the presence of sodium methoxide as a catalyst (2% by weight of diethanolamine and oil). The reaction was carried out at a temperature of 115°C, while the formation of diethanolamine was monitored with TLC. At the end of the reaction, the mixture was allowed to cool and later dissolved in diethyl ether to recover the biosurfactant, and separation was performed using a separating funnel. The ether phase was washed with water and passed over sodium sulfate. The resulting ether fraction was later concentrated using a rotary evaporator. The scheme of the reaction is shown in Scheme 1.

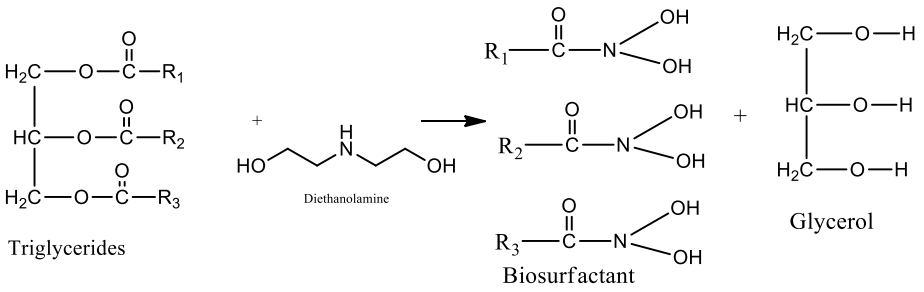

Scheme 1: Preparation of the Biosurfactant

GC-MS Characterization of the Seed Oils

The esterified oil from the seeds was analysed using a gas chromatograph (6890N, Agilent Technologies Network) coupled to an Agilent technology inert mass selective detector (MSD) (5975B, Agilent Technologies Inc., Palo Alto, CA). Constituents were identified primarily based on the comparison of retention time with those of the authentic standards and further confirmed by comparing mass fragmentation patterns with those of the NIST library [14].

Fourier Transform Infrared (FT-IR) Spectroscopic Analysis

The infrared spectra were recorded on a Shimadzu 8400s according to the methods of Jain et al. [16] using a KBr pellet. The seed oil, diethanolamine and biosurfactant were each subjected to infrared spectroscopic analyses separately to identify associated functional groups.

Antioxidant Activities of the Biosurfactant

Four antioxidant assays were used to determine the antioxidant potential of the seed oil, biosurfactants and the controls (gallic acid and sodium lauryl sulfonate).

***In vitro* DPPH Radical Scavenging Activity**

This test was measured as described by Nishaa et al. [17] with little modification. The stock solution of the oil was prepared in dichloromethane to achieve a concentration of 100 µg/ml. Dilutions were made to obtain concentrations of 50, 25, 12.5, 6.25, 3.125, 1.562, 0.781, 0.390, 0.195 and 0.098 µg/ml. Two milliliters of each of the diluted solutions was added to 2 ml of a DPPH solution (10 µg/mL). It was further incubated for 30 min of reaction in a dark compound. Absorbance of the solutions was taking at 517 nm. The DPPH radical scavenging activity was calculated using the following formula (equation 1):

$$\text{DPPH scavenging activity (\%)} = (A_0 - A_1)/A_0 \times 100 \quad (1)$$

where A_0 is the absorbance of the control and A_1 is the absorbance of the sample.

***In vitro* ABTS Radical Scavenging Activity**

The 2,2′-Azinobis-(3-Ethylbenzthiazolin-6-Sulfonic Acid (ABTS) antioxidant potential of seed oil, biosurfactant and sodium lauryl sulfonate (SLS) surfactant used as a control was established by reacting 2 mL of various concentrations 50, 25, 12.5, 6.25, 3.125, 1.562, 0.781, and 0.391 µg/ml of the samples with 2 mL ABTS cation solution following a standard assay procedure by mixing freshly prepared $ABTS^+$ standard solution (7 mM). with potassium persulfate (2.45 mM). The resultant mixture was kept in the dark for 12 hours at room temperature, after which it was further diluted with methanol to achieve an optical density of 0.7 ± 0.01 when measured on a UV spectrophotometer at 734 nm. The ABTS solution will be allowed to react for 60 sec with various concentrations of the oil, biosurfactant and control surfactant, and the optical density will be read at the same wavenumber. Garlic acid was used as a standard control, and the experiment was carried out in triplicate [18].

The inhibition percentage of ABTS radicals was calculated using the following formula (equation 2):

$$\text{ABTS scavenging activity (\%)} = (A_0 - A_1) / A_0 \times 100 \quad (2)$$

where A_0 is the absorbance of the control and A1 is the absorbance of the sample.

In vitro Nitric Oxide Scavenging Activity

The Nitric oxide (NO) scavenging activity was determined according to the methods of Dash et al. [19]. Samples of different concentrations of 50, 25, 12.5, 6.25, 3.125, 1.562, 0.781, and 0.391 µg/ml were prepared. Griess reagent was prepared by mixing the same amounts of 1% sulphanilamide in 2.5% phosphoric acid and 0.1% naphthyl ethylene diamine dihydrochloride in 2.5% phosphoric acid immediately before use. A volume of 0.5 mL of 10 mM sodium nitroprusside in phosphate buffered saline was mixed with 1 mL of the different concentrations of the samples and incubated at 25°C for 180 mins. The samples were then mixed with an equal volume of freshly prepared Griess reagent. Gallic and SLS were used as control samples. The absorbance was measured at 546 nm using a UV-visible spectrophotometer.

Inhibition was calculated (equation 3) as:

$$\text{NO scavenging activity (\%)} = (A_0 - A_1) / A_0 \times 100 \quad (3)$$

where A_0 is the absorbance of the control and A_1 is the absorbance of the sample.

In vitro Ferric Reducing Antioxidant Power (FRAP) Assay

Gangwar et al. [20] reported method was adopted for the FRAP assay. The reagent was activated by mixing 300 mM sodium acetate buffer (pH 3.6), 10.0 mM (tripyridyl triazine) solution and 20.0 mM $FeCl_3.6H_2O$ solution in a ratio of 10:1:1 in volume. Two milliliters of each sample at different concentrations (50, 25, 12.5, 6.25, 3.125, 1.562, 0.781, and 0.391 µg/ml) was then added to 2 ml of FRAP reagent, and the reaction mixtures were incubated at 37°C for 30 min. Absorbance was measured at 593 nm spectrophotometrically. Fresh working solutions of $FeSO_4$ were used for the calibration curve. The antioxidant potential was calculated from the linear calibration curve and expressed as mmol equivalents of $FeSO_4$ per gram of sample.

3. Results and Discussion

Biosurfactants are amphiphilic substances with a wide range of applications. Their renewable nature made them perfectly fit to replace synthetic counterparts that are often attributed to as source of environmental pollution [6]. There is a wide range of underutilized seeds in tropical countries, such as Nigeria, that produce year in, year

out without being put to appropriate use. These seeds are wasted beside the fact that the seeds themselves constitute environmental nuisance. Therefore, of the exploration of these underutilized tropical seeds as sources of raw materials in preparing biosurfactants can help in getting rid or minimizing environmental pollution.

The physical and chemical properties of the oil are presented in Table 1. Seed oil shows viability for use as an industrial source of raw material owing to its high oil yield of 25.96 ± 0.47%. The high acid value of 84.15±0.58 mg KOH/g indicates that the seed oil is not edible, as it is more than the recommended value for edible oil (4 mg KOH/g) by the WHO/FAO [14] and should be explored as raw materials for vegetable oil-dependent companies. Sponge seed oil shows a free fatty acid content of 1.09±0.01 mg KOH/g, a clear indicator that the oil will have a long shelf-life and stability to autooxidation [21]. The low free fatty acid content may be due to the low peroxide value of 3.95±0.14 meq kg^{-1}, which indicates the presence of natural phytochemicals present in the oil preventing the oxidation and hydrolysis of the oil and hence the low free fatty acids. The high iodine value of 165.07±0.85 $I_2100\ g^{-1}$ of oil exhibited by the seed oil indicates a high degree of unsaturation by the oil. The oil was liquid at ambient temperature, and the high degree of unsaturation was further confirmed by gas chromatography-mass spectrometry (GC-MS), as indicated in Table 2, with a total degree of unsaturation calculated to be 70.23%.

Table 1. Physical and Chemical Properties of Sponge Seed Oil

Physicochemical Analysis	*Luffa aegyptiaca* Seed Oil
% Yield	25.96 ± 0.47
Specific gravity	0.886±0.02
Saponification value (mg KOH/g)	82.51±0.12
Acid value (mg KOH/g)	84.15±0.58
% Free fatty acid	1.09±0.01
Peroxide value (meq Kg^{-1})	3.95±0.14
Iodine value ($I_2100\ g^{-1}$ of oil)	165.07±0.85
Physical state at ambient temperature (25°C)	Liquid

Values are mean of triplicate determinations ± standard error of mean (SEM).

Table 2. Fatty Acids Composition of Sponge Seed Oil

S/N	Fatty Acid	Saturation	% Composition
1	Pentadecanoic acid	15:0	4.87
2	Palmitic acid	16:0	14.73
3	Palmitoleic acid	16:1	23.0
4	Stearic acid	18:0	10.17
5	Oleic acid	18:1	47.23
	Total Saturation		**29.35**
	Total Monounsaturate		**70.23**
	Total Polyunsaturate		**-**
	Total Unsaturation		**70.23**

The fatty acid composition of the oil obtained from GC-MS is shown in Table 2. The most abundant fatty acids are oleic acid, a monounsaturated fatty acid that accounts for 47.23% of the total oil, followed by palmitoleic acid, another monounsaturated fatty acid that accounts for 23.0%, and stearic and palmitic acid, which both accounts for 10.17 and 14.73 degrees, respectively. The oil is largely made of unsaturated fatty acids.

The FT-IR spectra of sponge seed oil, biosurfactant and diethanolamine (superimposed) are shown in Figure 1 below.

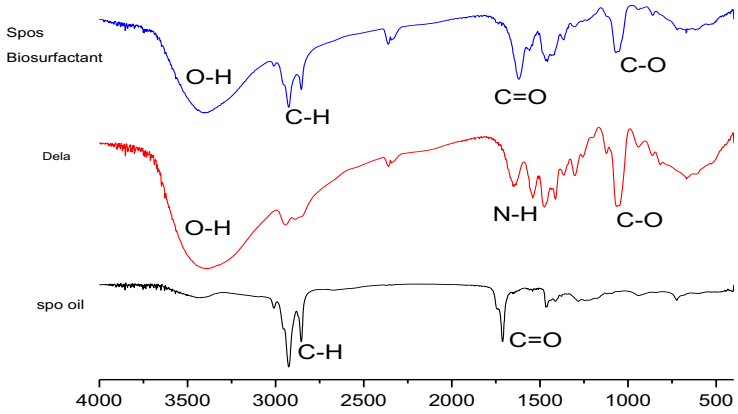

Figure 1. FT-IR Characterization of Sponge Seed Oil, Diethanolamine and Sponge Seed Oil Biosurfactant

Spos Biosurfactant – Sponge seed oil biosurfactant
Dela – Diethanolamine
Spo oil – Sponge seed oil

Table 3 shows deductions from the FT-IR spectra.

Table 3. Interpretation of FT-IR Spectra of Sponge Seed Oil, Diethanolamine and Sponge Seed Biosurfactant

	Absorption bands (cm^{-1})		
Functional Groups	Sponge Seed Oil	Diethanolamine	Sponge Biosurfactant
C-O	1262	1064	1068
C-N		1301	1232 – 1303
C=O	1712		1618
N-H		1635	
C-H	2854 - 2926	2945	2926
O-H		3394	3404

The results obtained and the emulsion stability test in Table 4 confirmed the preparation of the biosurfactant. The clear absence of a hydroxyl group (O-H) in the seed oil, whose presence was confirmed in the diethanolamine and the biosurfactant at 3394 cm^{-1} and 3404 cm^{-1}, respectively, implied a possible difference in functional groups between the seed oil and the two other substances. Biosurfactant was also confirmed to have been produced by the absence of a carbonyl group (C=O) in diethanolamine, which was more prominent in the biosurfactant at 1618.33 cm^{-1}. The prepared biosurfactant was further confirmed by comparing its emulsion stability to sodium lauryl sulfonate (SLS), as shown in Table 4. The biosurfactant shows a lower emulsion stability of 87.50 ± 2.53 seconds to 394 ± 1.41 seconds for SLS; however, the foaming stability shown by the biosurfactant for SLS was appreciable at 202.5 ± 3.44 cm to 250 ± 11.31 cm. The biosurfactant shows a greater ability to be effective in hard water, as it shows a salt tolerance level of 220 ppm well above the range of 120 – 180 ppm for hard water, as stipulated by the US Water Corporation. SLS shows a salt tolerance of 190 ppm.

Table 4: Emulsion Stability Study of the Biosurfactants

Emulsion	SPOS	SLS
Emulsion stability (s)	87.50 ± 2.53	394 ± 1.41
Foaming stability (cm)	202.5 ± 3.44	250 ± 11.31
Salt tolerance (ppm)	220	190

One of the key functions of biosurfactants is corrosion inhibition, which is helped by their ability to resist oxidation, thereby offering protection to surface covers. The

potential of the oil and biosurfactant produce to be used as an additive in corrosion inhibition was determined using four different in vitro antioxidant assays, and the results are reported below.

Table 5a shows the results of the ABTS Radical Antioxidant Potential *Luffa aegyptiaca* seed oil. Gallic acid was used as possible control. Figure 2a shows the graphical plots of the concentration in µg/mL and % inhibition from which the IC_{50} values were calculated.

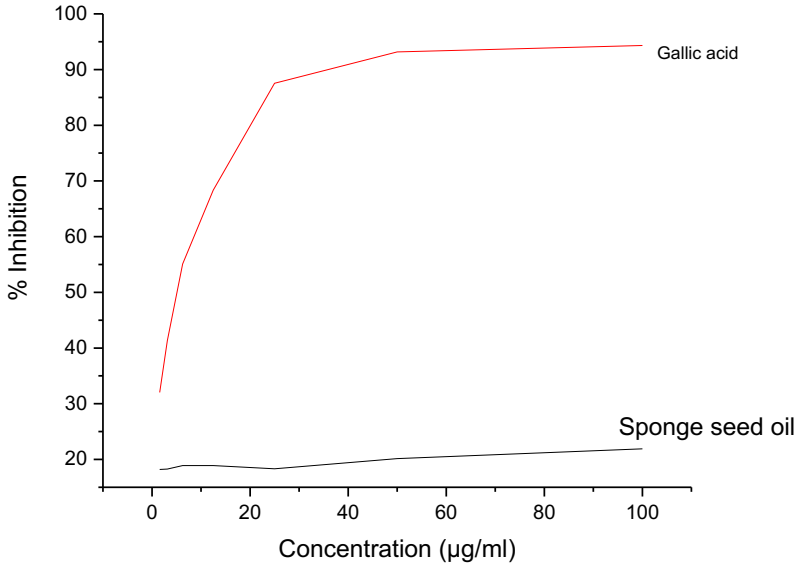

Figure 2a. ABTS Radical Scavenging Assay of Sponge Seed Oil and Gallic Acid

Table 5a. ABTS Radical Antioxidant Potential Sponge Seed Oil

	ABTS Radical Antioxidant Potential	
Concentration (µg/ml)	Sponge Seed Oil (%)	Gallic Acid (%)
100	21.91 ± 0.022	94.33 ± 0.002
50	20.15 ± 0.022	93.17 ± 0.002
25	18.33 ± 0.005	87.55 ± 0.007
12.5	18.89 ± 0.012	68.35 ± 0.006
6.25	18.89 ± 0.004	55.10 ± 0.018
3.125	18.26 ± 0.001	41.34 ± 0.065
1.563	18.21 ± 0.012	32.02 ± 0.006
IC_{50}	46.06	2.98

Values are mean of triplicate determinations ± standard error of mean (SEM).

The results showed a concentration-dependent antioxidant potential, and the highest inhibition potential was recorded at 100 µg/mL for both the oil and gallic acid, where the oil showed a maximum inhibition potential of 21.91 ± 0.022 compared to 94.33 ± 0.002 for gallic acid against ABTS radicals. The seed oil shows a far higher IC_{50} value of 46.06 µg/mL compared to 2.98 µg/mL, indicating that gallic acid has superior ABTS radical scavenging antioxidant potential than *Luffa aegyptiaca*.

Similarly, Table 5b shows the result of the DPPH Radical Antioxidant Assay *L. aegyptiaca* seed oil, with a dose-dependent inhibition range of 15.55 ± 0.002 - 7.63 ± 0.004 for *L. aegyptiaca* seed oil and 89.50 ± 0.006 - 29.70 ± 0.018% for gallic acid.

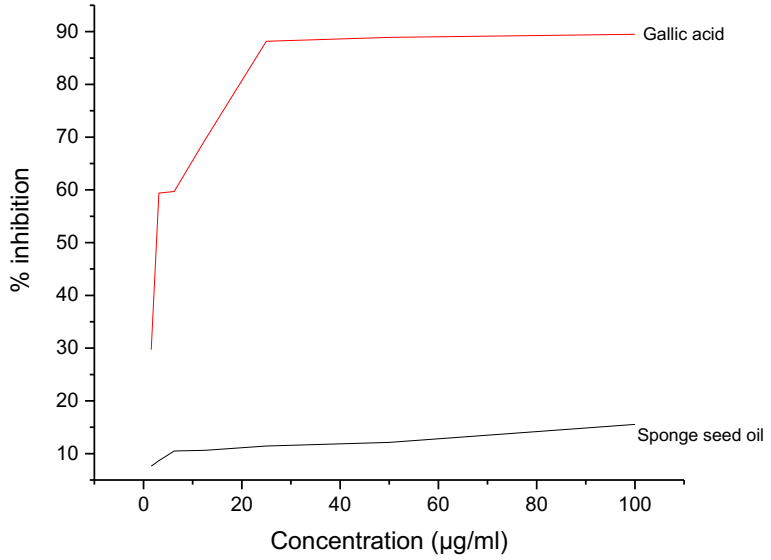

Figure 2b. DPPH Radical Scavenging Assay of Sponge Seed Oil and Gallic Acid

The IC_{50} value obtained for the DPPH assay from Figure 2b further indicates that gallic acid has better antioxidant potential than seed oil, 28.60 and 1.62 for *L. aegyptiaca* seed oil and gallic acid, respectively. *Persea americana* seed oil also shows limited DPPH antioxidant capability compared to gallic acid, as reported by Adaramola et al. [22].

Table 5b. DPPH Radical Antioxidant Potential Sponge Seed Oil

DPPH Radical Antioxidant Assay		
Concentration (µg/ml)	Sponge Seed Oil (%)	Gallic Acid (%)
100	15.55 ± 0.002	89.50 ± 0.006
50	12.14 ± 0.019	88.92 ± 0.004
25	11.44 ± 0.007	88.18 ± 0.003
12.5	10.63 ± 0.010	69.42 ± 0.012
6.25	10.50± 0.007	59.70 ± 0.009
3.125	8.66 ± 0.007	59.41 ± 0.012
1.563	7.63 ± 0.004	29.70 ± 0.018
IC_{50}	28.60	1.62

Values are mean of triplicate determinations ± standard error of mean (SEM).

Table 5c shows the results of the ferric reduction antioxidant potential (FRAP) of *Luffa aegyptiaca* seed oil across a concentration range of 100 to 1.563 µg/ml. The seed oil shows the highest inhibition of 6.42 ± 0.004 compared to 35.63 ± 0.022% for gallic acid. The better antioxidant activity of gallic acid over the seed oil was further confirmed from the IC_{50} value calculated from Figure 2c, which shows IC_{50} values of 28.00 and 1.59 µg/ml for seed oil and gallic acid, respectively.

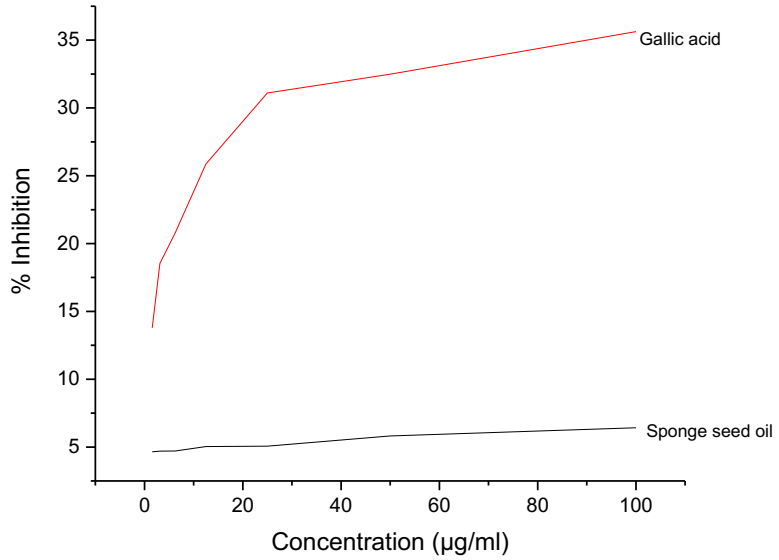

Figure 2c. Ferric Reducing Antioxidant Potential (FRAP) Assay of Sponge Seed Oil and Gallic Acid

The lower the antioxidant value, the higher the antioxidant potential.

Table 5d shows the nitric oxide scavenging antioxidant assay of *Luffa aegyptiaca* seed oil and gallic acid. The seed oil shows improved antioxidant activity comparable to gallic acid, as determined by the improved % inhibition and IC_{50} value in Figure 2d.

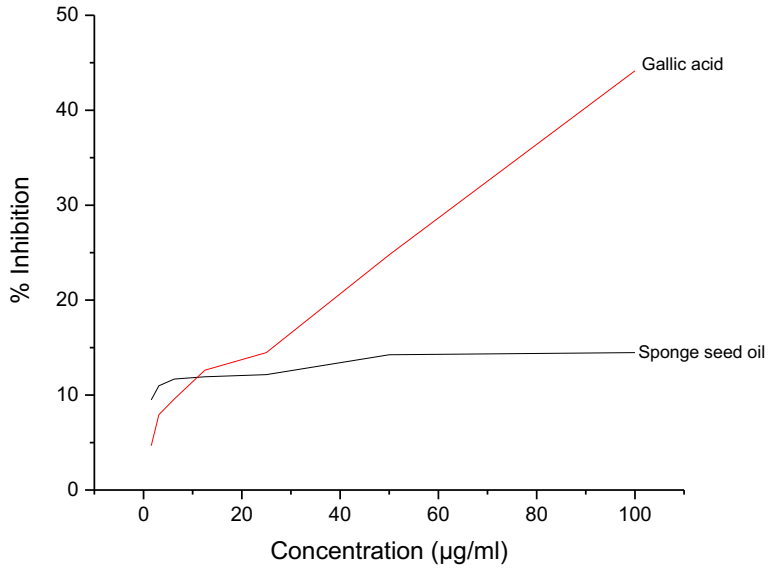

Figure 2d. Nitric Oxide Scavenging Antioxidant Assay of Sponge Seed Oil and Gallic Acid

The low IC_{50} value of 3.75 µg/ml by the seed oil is comparable to that of gallic acid (1.16 µg/ml), indicating the huge potential of the seed oil to inhibit nitric oxide-induced oxidation of corrosion inhibition materials.

Table 5c. Ferric Reduction Antioxidant Potential (FRAP) Sponge Seed Oil

	Ferric Reduction Antioxidant Potential (FRAP)	
Concentration (µg/ml)	Sponge Seed Oil (%)	Gallic Acid (%)
100	6.42 ± 0.004	35.63 ± 0.022
50	5.82 ± 0.005	32.49 ± 0.002
25	5.07 ± 0.005	31.10 ± 0.014
12.5	5.04 ± 0.004	25.86 ± 0.040
6.25	4.71 ± 0.002	20.79 ± 0.007
3.125	4.70 ± 0.005	18.53 ± 0.017
1.563	4.65 ± 0.001	13.79 ± 0.027
IC_{50}	28.00	1.59

Values are mean of triplicate determinations ± standard error of mean (SEM).

Table 5d. Nitric Oxide Scavenging Antioxidant Assay Sponge Seed Oil

	Nitric Oxide Scavenging Antioxidant Assay	
Concentration (µg/ml)	Sponge Seed Oil (%)	Gallic Acid (%)
100	14.47 ± 0.001	24.77 ± 0.007
50	14.25 ± 0.001	14.48 ± 0.006
25	12.15 ± 0.002	12.62 ± 0.004
12.5	11.92 ± 0.006	9.58 ± 0.003
6.25	11.68 ± 0.001	7.94 ± 0.005
3.125	10.98 ± 0.007	44.16 ± 0.004
1.563	9.50 ± 0.009	4.67 ± 0.003
IC_{50}	3.75	1.16

Values are mean of triplicate determinations ± standard error of mean (SEM).

The presence of antioxidants in corrosion inhibition materials can help prevent oxidation of the materials, thereby improving the life span of corrosion inhibitors. The results are presented in Tables 6a – 6d for the initial antioxidant assay to which the oil was subjected. The antioxidant potential of renewable biosurfactant made from *Luffa*

aegyptiaca seed oil was compared to sodium lauryl sulfonate (SLS), a synthetic surfactant.

Table 6a gives the results of the ABTS Radical Antioxidant Potential *L. aegyptiaca* seed oil biosurfactant and positive control SLS. As shown in Table 6a and Figure 3a, the biosurfactant shows a much better ABTS scavenging ability than SLS. The inhibition potential was dose dependent, and the highest inhibition of 15.58 ± 0.011 % was obtained for the seed oil biosurfactant compared to 11.14 ± 0.002 % for SLS. The IC50 value of the biosurfactant was lower (11.53 µg/ml) than the value (21.64 µg/ml) obtained for SLS, indicating the superior ABTS scavenging potential of the prepared biosurfactant and its potential to be incurporated into corrosion inhibition materials.

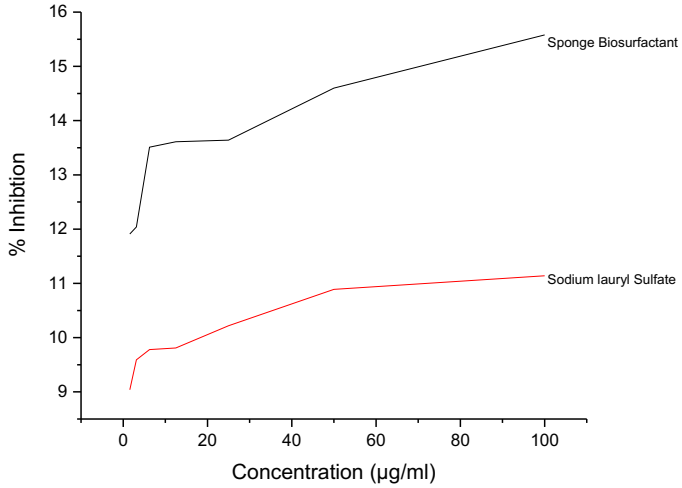

Figure 3a. ABTS Radical Scavenging Assay of Sponge Biosurfactant and Sodium Lauryl Sulfate

Table 6a. ABTS Radical Antioxidant Potential Sponge Seed Biosurfactant

	ABTS Scavenging Antioxidant Potential	
Concentration (µg/ml)	Sponge Seed Biosurfactant (%)	Sodium Lauryl Sulfonate (%)
100	15.58 ± 0.011	11.14 ± 0.002
50	14.6 ± 0.14	10.89 ± 0.001
25	13.64 ± 0.005	10.22 ± 0.001
12.5	13.61 ± 0.001	9.81 ± 0.005
6.25	13.51 ± 0.015	9.78 ± 0.009
3.125	12.04 ± 0.022	9.59 ± 0.004
1.563	11.91 ± 0.05	9.04 ± 0.008
IC_{50}	11.53	21.64

Values are mean of triplicate determinations ± standard error of mean (SEM).

The biosurfactant shows a consistent superior antioxidant potential over SLS, a synthetic antioxidant across Tables 6b – 6c and Figures 3b – 3c, with lower IC50 values for the biosurfactant to that of SLS, 1.97 to 2.08 µg/ml for DPPH radical antioxidant assay, 34.21 to 91.63 µg/ml for FRAP assay, respectively.

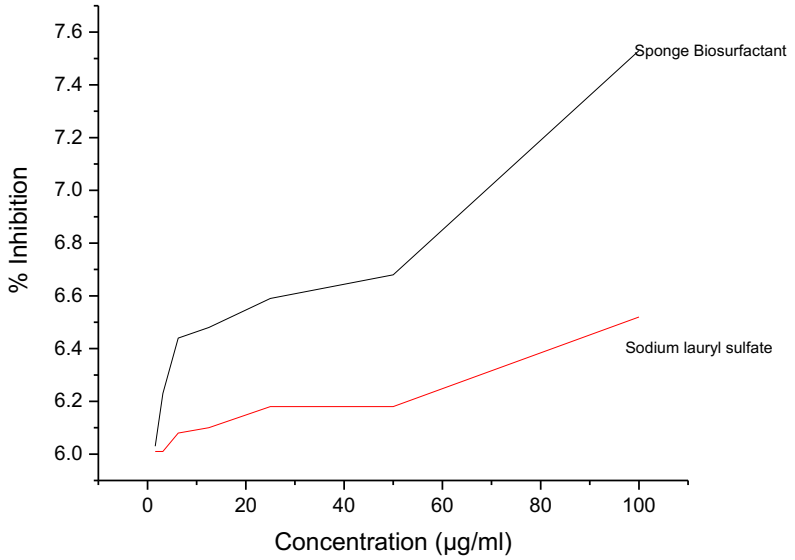

Figure 3b. DPPH Radical Scavenging Assay of Sponge Biosurfactant and Sodium Lauryl Sulfate

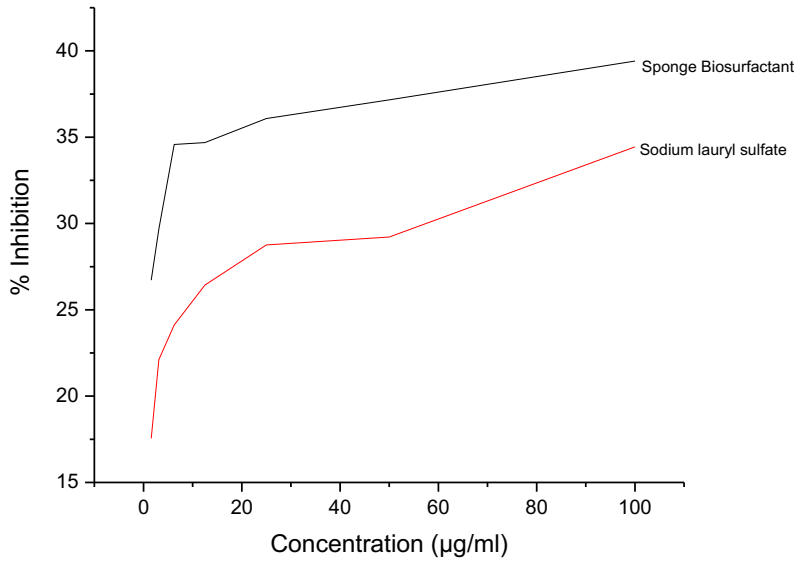

Figure 3c. Ferric Reducing Antioxidant Potential (FRAP) Assay of Sponge Biosurfactant and Sodium Lauryl Sulfate

However, SLS shows better nitric oxide antioxidant assay than the prepared biosurfactant with IC_{50} value of 1.74 to 5.44 µg/ml in Table 6d and Figure 3d. The antioxidant activities shown by sponge seed oil biosurfactants are comparable to reported values by Rinaldi et al. [23] for neem oil biosurfactants.

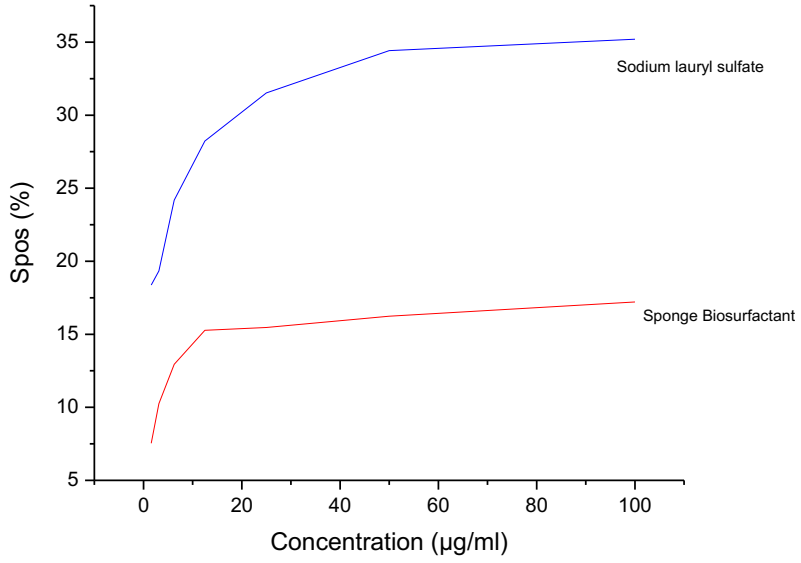

Figure 3d. Nitric Oxide Scavenging Antioxidant Assay of Sponge Biosurfactant and Sodium Lauryl Sulfate

Table 6b. DPPH Radical Antioxidant Potential Sponge Seed Biosurfactant

	DPPH Scavenging Antioxidant Assay	
Concentration (µg/ml)	Sponge Seed Biosurfactant (%)	Sodium Lauryl Sulfonate (%)
100	39.41 ± 0.006	34.44 ± 0.002
50	37.16 ± 0.042	29.22 ± 0.002
25	36.08 ± 0.040	28.76 ± 0.003
12.5	34.69 ± 0.083	26.43 ± 0.005
6.25	34.58 ± 0.012	24.12 ± 0.001
3.125	29.69 ± 0.027	22.12 ± 0.006
1.563	26.72 ± 0.007	17.51 ± 0.003
IC_{50}	1.97	2.08

Values are mean of triplicate determinations ± standard error of mean (SEM).

Table 6c. Ferric Reduction Antioxidant Potential (FRAP) Sponge Seed Biosurfactant

	Ferric Reduction Antioxidant Potential (FRAP)	
Concentration (µg/ml)	Sponge Seed Biosurfactant (%)	Sodium Lauryl Sulfonate (%)
100	7.53 ± 0.002	6.52 ±0.003
50	6.68 ± 0.001	6.18 ± 0.002
25	6.59 ± 0.001	06.18 ± 0.001
12.5	6.48 ± 0.001	6.1 ± 0.002
6.25	6.44 ± 0.12	6.08 ± 0.002
3.125	6.23 ± 0.004	6.01 ± 0.001
1.563	6.03 ± 0.001	6.01 ± 0.003
IC_{50}	34.21	91.63

Values are mean of triplicate determinations ± standard error of mean (SEM).

Table 6d. Nitric Oxide Scavenging Antioxidant Assay Sponge Seed biosurfactant

	Nitric Oxide Scavenging Antioxidant Assay	
Concentration (µg/ml)	Sponge Seed Biosurfactant (%)	Sodium Lauryl Sulfonate (%)
100	17.21 ± 0.10	35.20 ± 0.002
50	16.24 ± 0.008	34.42 ± 0.002
25	15.47 ± 0.004	31.52 ± 0.003
12.5	15.27 ± 0.003	28.23 ± 0.001
6.25	12.95 ± 0.002	24.18 ± 0.001
3.125	10.25 ± 0.005	19.34 ± 0.007
1.563	7.54 ± 0.004	18.37 ± 0.003
IC_{50}	5.44	1.74

Values are mean of triplicate determinations ± standard error of mean (SEM).

4. Conclusion

The physical and chemical properties of the sponge seed make it viable for use as an industrial source of fat and oil due to its high yield of 25.96 ± 0.47%. The low free fatty acid content may be accounted for by the low peroxide value of 3.95±0.14 meq kg^{-1}, which indicates the presence of natural phytochemicals present in the oil preventing the oxidation and hydrolysis of the oil and hence the low free fatty acids. The low free fatty acids also show that the oil is of high quality and has a long shelf-life. The high iodine value of 165.07±0.85 I_2100 g^{-1} of oil exhibited by the seed oil accounts for why the oil is liquid at room temperature. The oil is largely made of unsaturated fatty acids with a total degree of unsaturation of 70.23%, as obtained from GC-MS analysis.

The biosurfactant shows appreciable efficiency in a salt tolerance level of 190 ppm above the range of 120 – 180 ppm for hard water, as stipulated by the US Water Corporation. Control synthetic surfactant SLS shows a salt tolerance of 220 ppm.

The clear absence of a hydroxyl group (O-H) in the seed oil and carbonyl group (C=O) in diethanolamine, which were prominent in the biosurfactant at 1618.33 cm^{-1}, indicate the formation of a biosurfactant. The prepared biosurfactant shows a lower emulsion stability of 87.50 ± 2.53 seconds to 394 ± 1.41 seconds but better foaming stability, comparable to SLS used as a control.

Antioxidant analysis shows that oil has moderate antioxidant potential when compared to gallic acid, but the biosurfactant shows better antioxidant potential against ABTS radicals, DPPH radicals, and FRAP than SLS. SLS shows better nitric

oxide (NO) antioxidant activity than the biosurfactant. This implies that the biosurfactant replaces its synthetic counterparts and helps against environmental pollution. It also shows that oil and biosurfactants can be used as starting ingredients for making protective coatings such as alkyd resin, while biosurfactants can be used as additives to protect against oxidation attacks by reactive chemical species.

References

1. Araújo HW, Andrade RF, Montero-Rodríguez D, Rubio-Ribeaux D, Da Silva CAA, Campos-Takaki GM. Sustainable biosurfactant produced by Serratia marcescens UCP 1549 and its suitability for agricultural and marine bioremediation applications. *Microb. Cell Fact.*, 2019, 18(1), 1-13.
2. Lima RA, Andrade RF, Rodríguez DM, Araújo HW, Santos VP, Campos-Takaki GM. Production and characterization of biosurfactant isolated from Candida glabrata using renewable substrates. *Afr. J. Microbiol. Res.*, 2017, 11(6), 237-244.
3. Marchant R, Banat IM. Biosurfactants: A sustainable replacement for chemical surfactants? *Biotechnol. Lett.*, 2012, 34(9), 1597-1605.
4. Montero-Rodríguez D, Andrade RF, Ribeiro DLR, Rubio-Ribeaux D, Lima RA, Araújo H, Campos-Takaki GM. Bioremediation of petroleum derivative using biosurfactant produced by Serratia marcescens UCP/WFCC 1549 in low-cost medium. *Int. J. Curr. Microbiol. Appl. Sci.*, 2015, 4(7), 550-562.
5. Masakorala K, Turner A, Brown MT. Toxicity of synthetic surfactants to the marine macroalga, Ulva lactuca. *Water, Air, Soil Pollut.*, 2011, 218(1), 283-291.
6. Johnson P, Pinfield VJ, Starov V, Trybala A. Effect of synthetic surfactants on the environment and the potential for substitution by biosurfactants. *Adv. Colloid Interface Sci.*, 2020, 102340.
7. Geetha S, Banat IM, Joshi SJ. Biosurfactants: Production and potential applications in microbial enhanced oil recovery (MEOR). *Biocatal. Agric. Biotechnol.*, 2018, 14, 23-32.
8. Atlas RM, Hazen TC. Oil biodegradation and bioremediation: A tale of the two worst spills in U.S. history. *Environ. Sci. Technol.*, 2011, 45(16), 6709-6715.
9. Nitschke M, Costa S. Biosurfactants in food industry. *Trends Food Sci. Technol.*, 2007, 18(5), 252-259.
10. Jahan R, Bodratti AM, Tsianou M, Alexandridis P. Biosurfactants, natural alternatives to synthetic surfactants: physicochemical properties and applications. *Adv. Colloid Interface Sci.*, 2020, 275, 102061.
11. Stephens J. Gourd Luffa – Luffa cylindrica, Luffa aegyptiaca and Luffa acutangula. *J. Hortic. Sci. Univ. Fla.*, 2003, 3, 19-21.
12. Balakrishnan N, Huria T. Protective effect of Luffa cylindrica L. fruit in paracetamol induced hepatotoxicity in rats. *Int. J. Pharm. Biol. Arch.*, 2011, 2(6), 1761-1764.
13. Partap S, Kumar A, Sharma NK, Jha K. Luffa cylindrica: An important medicinal plant. *J. Nat. Prod. Plant*

Resour., 2012, 2(1), 127-134.
14. Zubair MF, Atolani O, Ibrahim SO, Oguntoye OS, Abdulrahim HA, Oyegoke RA, Olatunji GA. Chemical and biological evaluations of potent antiseptic cosmetic products obtained from Momordica charantia seed oil. *Sustainable Chem. Pharm.*, 2018, 9, 35-41.
15. Adewuyi A, Oderinde RA, Rao B, Prasad R. Synthesis of alkanolamide: A nonionic surfactant from the oil of Gliricidia sepium. *J. Surfactants Deterg.*, 2012, 15(1), 89-96.
16. Jain RM, Mody K, Mishra A, Jha B. Physicochemical characterization of biosurfactant and its potential to remove oil from soil and cotton cloth. *Carbohydr. Polym.*, 2012, 89(4), 1110-1116.
17. Nishaa S, Vishnupriya M, Sasikumar J, Hephzibah PC, Gopalakrishnan V. Antioxidant activity of ethanolic extract of Maranta arundinacea L. tuberous rhizomes. *Asian J. Pharm. Clin. Res.*, 2012, 5(4), 85-88.
18. Atolani O, Areh E, Oguntoye O, Zubair M, Fabiyi O, Oyegoke R, Tarigha D, Adamu N, Adeyemi O, Kambizi L, Olatunji G. Chemical composition, antioxidant, anti-lipooxygenase, antimicrobial, anti-parasite and cytotoxic activities of Polyalthia longifolia seed oil. *Med. Chem. Res*., 2019, 28(4), 515-527.
19. Dash P, Panda P, Ghosh G. Free radical scavenging activities and nutritional value of Lagenaria siceraria: A nutriment creeper. *Iran. J. Sci. Technol., Trans. A: Sci.*, 2018, 42(4), 1743-1752.
20. Gangwar M, Gautam MK, Sharma AK, Tripathi YB, Goel R, Nath G. Antioxidant capacity and radical scavenging effect of polyphenol rich Mallotus philippenensis fruit extract on human erythrocytes: An in vitro study. *Sci. World J.*, 2014.
21. Alemayhu A, Admassu S, Tesfaye B. Shelf-life prediction of edible cotton, peanut and soybean seed oils using an empirical model based on standard quality tests. *Cogent Food Agric.*, 2019, 5(1), 1622482.
22. Adaramola B, Onigbinde A, Shokunbi O. Physiochemical properties and antioxidant potential of Persea americana seed oil. *Chem. Int.*, 2016, 2(3), 168-175.
23. Rinaldi F, Hanieh PN, Longhi C, Carradori S, Secci D, Zengin G, Ammendolia MG, Mattia E, Del Favero E, Marianecci C, Carafa M. Neem oil nanoemulsions: Characterisation and antioxidant activity. *J. Enzyme Inhib. Med. Chem.*, 2017, 32(1), 1265-1273.

The Chemist
Journal of the American Institute of Chemists

Low-cost, Environmentally Friendly Galvanic Cells

Mohammad Ali Amayreh

Department of Chemistry, Al-Balqa Applied University
19110, Al-Salt, Jordan
(E-mail: mohammad.amayreh@bau.edu.jo)

Abstract: This study aimed to develop a new model of galvanic cells, which are small-scale, low-cost and environmentally friendly. Copper wires and galvanized nails were used as metal electrodes with known concentrations of $CuSO_4.5H_2O$ and $ZnSO_4.7H_2O$. The results showed that the average generated potential of the small-scale galvanic cell was 1.083 volt when the solution concentration was 1 M for each solution. The generated potential difference from the galvanic cell decreased from 1.083 to 0.786 volt when the concentration of $CuSO_4.5H_2O$ and $ZnSO_4.7H_2O$ decreased from 1 M to 0.001 M for each solution. While the decrease in potential difference was small, there is a clear difference in the cost of a single experiment: \$0.13 US for the modified new cell while it is \$14.72 US for the traditional Zn-Cu galvanic cell. The new galvanic cell is more cost-effect and environmentally friendly with zero pollutants.

Key Words: small-scale, Zn-Cu galvanic cell

1. Introduction

Environmental issues are considered one of the most important problems that human-kind faces in the modern era. Its types rang the bell of the waist around what must be done to effectively reduce the risks facing the earth. International, regional, and local conferences have been held to reduce environmental problems. Awareness has increased on environmental issues and countries have begun to try to reduce pollutants and produce environmentally friendly and biodegradable materials.

Interest began to increase until the individual, in his school, his home, and his community, became morally obligated to be behaviorally friendly to the environment. Environmental issues have been raised in the

curricula of schools since the first grade, in order to instill awareness among students of this issue that has become life threatening.

Scientists have begun, in each field, to develop methods and materials aimed at reducing the production of environmental pollutants and even reaching what is known as preventing pollution, if possible. In the field of chemistry, what is known as narrow-field chemistry has emerged at the end of the last decade under the auspices of the United Nations Culture and Science Organization (UNESCO). Educational workshops in many countries have developed a new mechanism for the implementation of laboratory experiments in schools mainly aimed at reducing the amount of pollutants as much as possible.

This indicates that a revolution in chemistry education has begun. Experimental work is an integral part of science education and this is what you can get when you ask a teacher or science teacher. The experimental work should include active participating students. Subsequently, chemistry is primarily an experimental topic ... and education in chemistry must contain an unavoidable experimental component [1].

Nevertheless, the truth in science education is completely different, and this can be identified by asking any honest and sincere science teacher, and the frightening truth will always be discovered. In most science rooms in schools there are no practical activities. In rich societies you may find practical alternatives; but in poor societies you will find everything written on the board only. Likewise, the experimental work in these societies is old, retroactive, eroding and extended until students graduate from school with simple practical experience and a modest understanding of science [1].

Hence, this problem has been identified for several years through UNESCO as well as IUPAC-CTC (International Union of Chemistry and Theoretical Chemistry and Applied Chemistry - Center for Chemistry Education). A number of founders have taken it upon themselves to start the International Narrow Band Chemistry Program, which started in 1996 and aimed to tackle problems by developing a small-scale, low-cost method. This is due to the widespread belief that experimental work is an essential and necessary part of teaching chemistry [1].

There are several definitions for the small-scale chemistry concept, including: "Small-scale chemistry is simply the process of performing and conducting chemical experiments within a greatly narrowed range" [2]. It is also a way to teach traditional laboratory chemical experiments in an exciting and attractive way to integrate with modern analysis techniques and implement them, even in the classroom, as well as to improve and strengthen educational curricula and raise scientific standards, which is a method for teaching chemistry by doing chemistry [3].

It is also a low-cost, safe and time-saving innovation based on keeping educational chemistry models. It is also not a curriculum, but it is a very flexible method for teaching chemistry at all levels by using inexpensive materials and common plastic materials, such as lollipops, plastic cups, disposable pipettes, petri dishes and syringes. And, so that there is no misconception, the narrow-band chemistry describes body or behavior, more than describing size [4].

This concept has been applied in many countries of the world, especially the United

States of America, to include schools and the first stage of study in universities. There are many educational and environmental goals that can be achieved by applying this concept at all educational levels.

Our interest in our environment, the development of the educational process in Jordanian schools, and participation in the research and development of experiments carried out within the activities established in curricula, lead us to choose the topic of galvanic cells (which is one of the main topics in the chemistry curriculum scheduled for 9-12 grade students) and this subject, whose experiences are rarely implemented due to students' lack of sufficient time and materials to go to the laboratory to do the experiment. So, it was necessary to review and develop these experiments so that we get to know the ways of implementing them in a new, environmentally friendly and low-cost scientific method.

The galvanic cell's modification to be more environmentally friendly, inexpensive and simple has been reported previously [5-7].

The most important objectives of this research are: 1) Developing a significantly lower cost small-scale Zn-Cu galvanic cell instead of the traditional one that is cost prohibitive and cannot be carried out in a classroom (Figure 1).

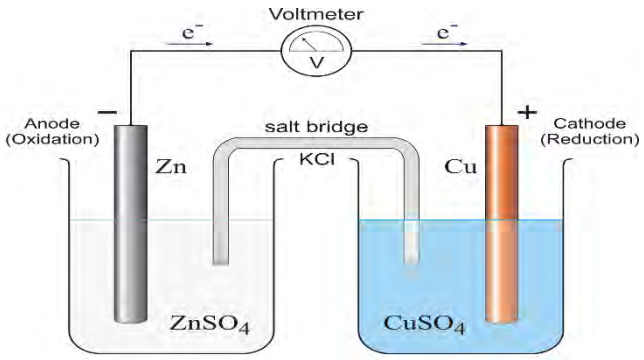

Figure 1. Standard Zinc-Copper Galvanic Cell (Zn|$ZnSO_4$(1.00M)||$CuSO_4$(1.00M)|Cu)

2) Study the effect of volume reduction on the amount of potential difference generated compared to the global standard value. 3) Study the effect of low concentration in this developed cell compared to the standard potential value of Zn-Cu galvanic cells. 4) Identify the oxidation and reduction reactions that occur on the electrodes. 5) Calculating the costs of implementing the experiment compared with the cost of the standard Zn-Cu galvanic cell. 6) Calculating that amount of solutions that were not consumed and not disposed of in the environment.

2. Experimental

Preparation of electrolytes and electrodes

A 1 M of $ZnSO_4.7H_2O$ and 1 M of $CuSO_4.5H_2O$ were prepared. Copper sulfate and zinc sulfate solutions with the concentrations of 0.1, 0.01, 0.001 M were prepared by serial dilution for the standard zinc sulfate and copper sulfate with distilled water.

Preparation of galvanic cells

To build the small galvanic cell (Figure 2), Zn| $ZnSO_4$(1.00M)||$CuSO_4$(1.00M)|Cu, 5 mL of 1 M zinc sulfate was put in a small vial and another 5 mL of 1 M copper sulfate was put in another small vial; then, the two vials were connected by saturated filter paper which was soaked in sodium chloride solution for 5 minutes. Finally, the galvanized nail was inserted in zinc sulfate solution where a copper wire was inserted in copper sulfate solution. These electrodes were then connected with the multimeter to measure the generated potential difference. The readings were recorded and carried out in triplicate.

Figure 2. Small-scale Galvanic Cell (Zn|$ZnSO_4$(1.00M)||$CuSO_4$(1.00M)|Cu) (5 mL vials)

To build a rolled small-scale galvanic cell, Zn|$ZnSO_4$(1.0M)||$CuSO_4$(1.0M)|Cu (Figure 3), 1 mL of 1 M zinc sulfate was put in a small dish and another 1 mL of 1 M copper sulfate was put in another dish, then a filter paper was soaked in this solution for 5 minutes .The galvanized nail was rolled by the filter paper which was soaked in zinc sulfate solution; afterward, this part of the cell was rolled by semi-permeable paper and rolled again by the filter paper which was soaked in copper sulfate. Finally, all these parts were rolled with 10 rolls of copper wire and connected with the multimeter from the copper wire and galvanized nail to measure the generated potential difference. The readings were then recorded, and the experiment was carried out in triplicate.

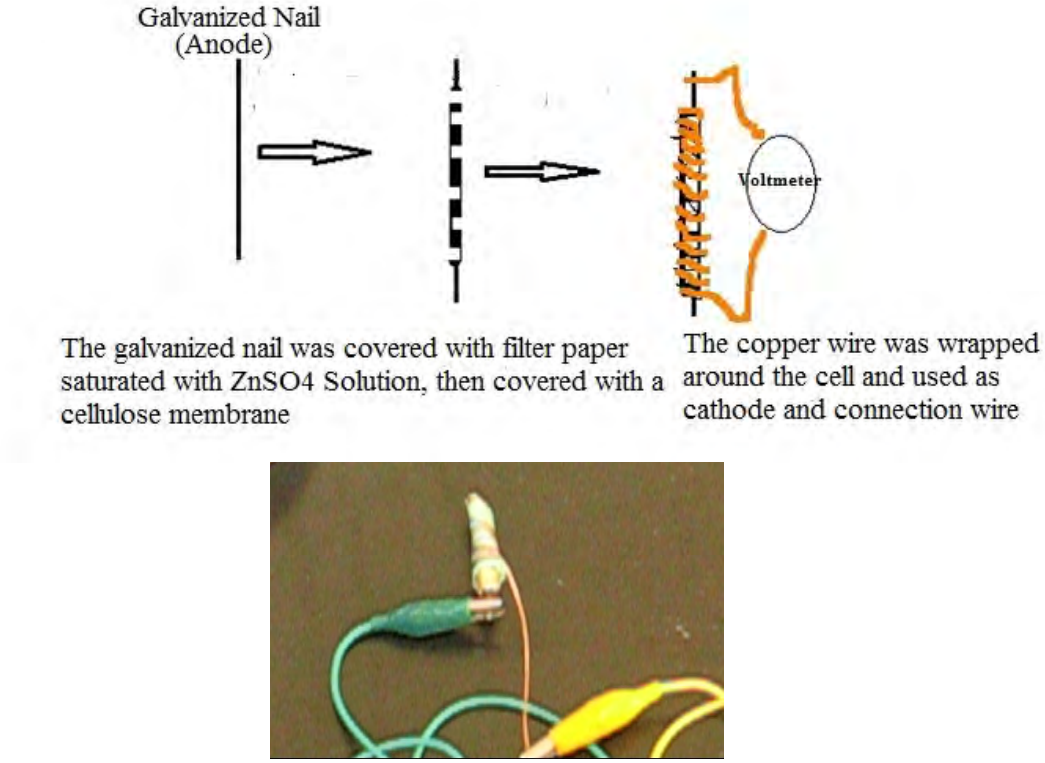

Figure 3. The Rolled Small-scale Galvanic Cell (Zn|$ZnSO_4$(1.00M)||$CuSO_4$(1.00M)|Cu)

To prepare the other galvanic cell the same procedure for the small-scale galvanic cell was carried out with the concentrations of the solutions changed in accordance to the experiment. The galvanic cells were prepared, and the generated potential differences were examined. Each experiment was carried out in triplicate.

To investigate the effect of concentration on the generated potential difference in the rolled small-scale galvanic cell, the following galvanic cells were prepared and the generated potential differences were recorded. Each experiment was carried out in triplicate:

- Zn|$ZnSO_4$(0.1M)||$CuSO_4$(0.1M)|Cu
- Zn|$ZnSO_4$(0.01M)||$CuSO_4$(0.01M)|Cu
- Zn|$ZnSO_4$(0.001M)||$CuSO_4$(0.001M)|Cu
- Zn|$ZnSO_4$(1M)||$CuSO_4$(0.01M)|Cu
- Zn|$ZnSO_4$(0.01M)||$CuSO_4$(1M)|Cu

3. Result and Discussion

Parameters affecting the generated cell potential were investigated using the separated cells. At first, the effect of reducing the solution's volume on the generated potential was investigated (Figure 4). Regarding the small-scale galvanic cell (Figure 2) where 5 mL of each solution was used, the average of the generated potential of 1.045, 1.043, and 1.035 volt was 1.041±0.0043, which is 94.6% of the potential of the Zn-Cu galvanic cell (1.10 volt) at the standard conditions. Also, the effect of size and volume of the rolled small-scale galvanic cell was recorded. The obtained potentials for the rolled small-scale galvanic cell

$$(Zn|ZnSO_4(1.00M)||CuSO_4(1.00M)|Cu$$

were 1.015, 1.036, and 1.033 volt with average of 1.028±0.0093, which is 93.0% of generated potential of Zn-Cu at the standard conditions.

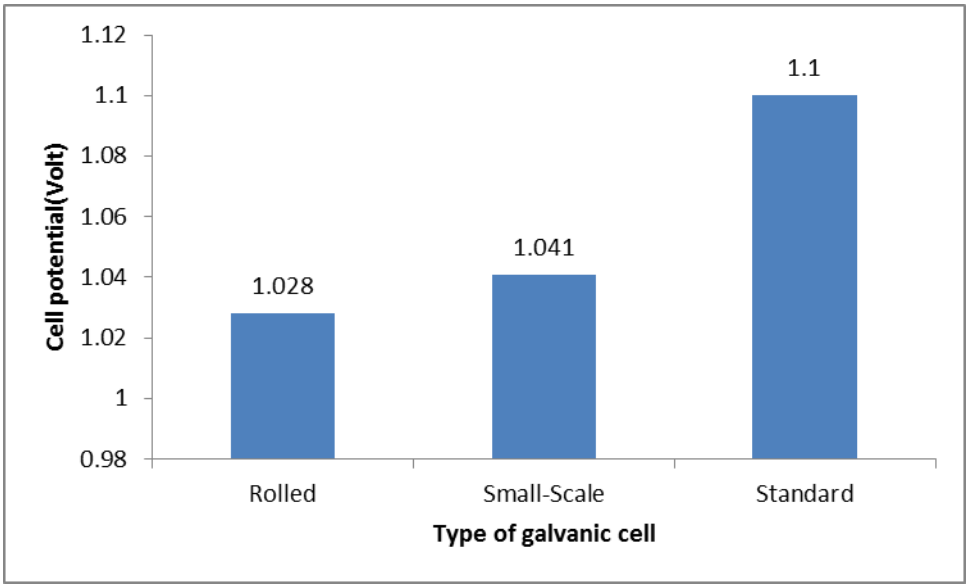

Figure 4. The Generated Potential of Galvanic Cell, Small-scale Galvanic Cell, and Rolled Galvanic Cell

The effect of zinc sulfate and copper sulfate concentration on the generated potential was examined. Figure 5 shows that as the concentration of zinc sulfate and copper sulfate decreases the obtained potential decreases.

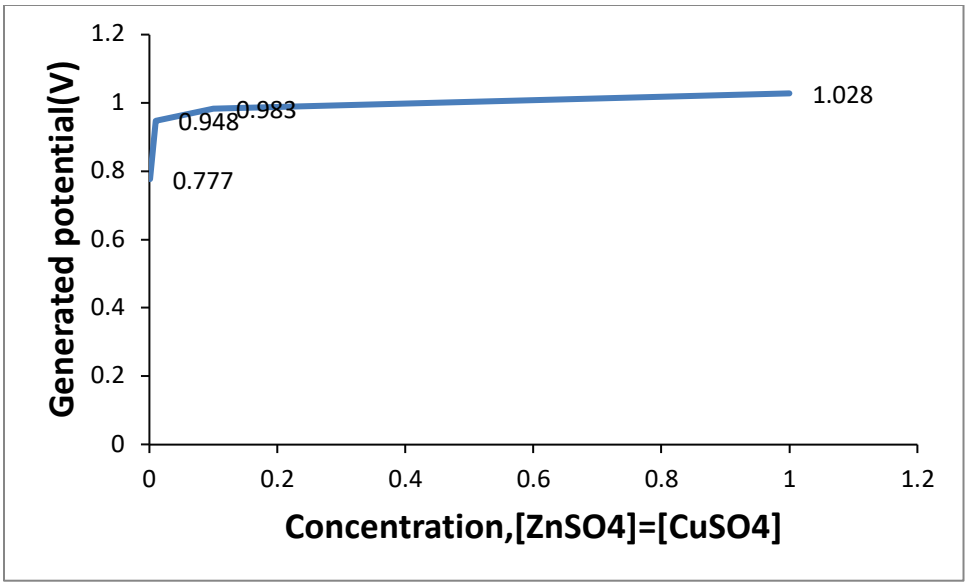

Figure 5. The Relationship between [$ZnSO_4$] and [$CuSO_4$] Concentrations and Generated Potential

Table 1 shows the results of changing the concentration of zinc sulfate and copper sulfate on obtained potentials.

Table 1. The Obtained Potentials of the Rolled Small-scale Zn-Cu Galvanic Cell at Different Concentrations

Zinc sulfate concentration (M)	Copper sulfate concentration (M)	Average of generated potential (V)	RSD (%, n=3)	% of Potential compared with Zn-Cu standard cell potential
1.0	1.0	1.028	1.10	93.45
0.1	0.1	0.983	1.79	89.36
0.01	0.01	0.948	0.68	86.18
0.001	0.001	0.777	0.84	70.64

As Table 2 shows, the generated potential difference of the Zn-Cu galvanic cell decreases as the concentration of both solutions ($[Zn^{2+}]$ =$[Cu^{2+}]$) is diluted from 1 M to 0.001 M, even though the generated potential for the more diluted solutions ($[Zn^{2+}]$ =$[Cu^{2+}]$ =0.001M) is 70.64% of the standard potential of the Zn-Cu galvanic cell.

Table 2. The Generated Potentials for the Modified Small-scale Galvanic Cell (Rolled Form) as a Function of Changing the Concentrations of Copper Sulfate and Zinc Sulfate Solutions

[ZnSO4] (mol/L)	[CuSO4] (mol/L)	Generated cell potential (E_{cell})
1.0	1.0	1.027
0.1	0.1	0.983
0.01	0.01	0.948
0.001	0.001	0.777
1.0	0.01	0.944
0.01	1.0	0.905

The cost of the standard Zn-Cu galvanic cell materials compared with the cost of the rolled small-scale model was carried out as shown in Tables 3 and 4 according to Jordanian local market prices for chemicals and materials.

Table 3. The Cost of Materials of One Standard Zn-Cu Galvanic Cell According to Local Prices in Jordan

Material	Per experiment	Cost($)
$CuSO_4.5H_2O$(gram)	50	1.14
$ZnSO_4.7H_2O$(gram)	57.5	3.29
Copper electrode	1	1.43
Zinc electrode	1	1.43
Salt-bridge	1	1.43
Beaker(250ml)	2	5.71
NaCl (gram)	5	0.29
Total		$4.72

Table 4. The Cost of One Rolled Small-scale Galvanic Cell Using Model

Material	Per experiment	Cost($)
$CuSO_4.5H_2O$(gram)	0.5	0.01
$ZnSO_4.7H_2O$(gram)	1.15	0.066
Copper wire(10cm)	1	0.014
Galvanized nail	1	0.04
Semi-permeable membrane	1	-
Total		$0.13

According to the data mentioned in Tables 3 and 4, the cost of one rolled small-scale Zn-Cu galvanic cell is 0.88% of the cost of one of the standard Zn-Cu galvanic cells. This is considered an excellent indicator for the applicability of this cell in the labs and classrooms individually or within groups. Also, there is no disposal solutions where 1 mL of each solution was used via soaking the filter papers during cell preparation.

4. Conclusion

A simple and cheap small-scale Zn-Cu galvanic cell with zero waste was successfully constructed and used as a teaching material in electrochemistry topics in teaching laboratories and classrooms. Based on this design the students will be able to construct a small-scale battery able to operate low resistance circuits and design more small-scale electrochemical cell.

Acknowledgments

The author would like to thank the Department of Chemistry at Al-Balqa University for providing laboratory facilities and support.

References

1. Bradley J D. "UNESCO/IUPAC-CTC Global Program in Microchemistry". *Pure Appl. Chem.*, 2001, 73, 1215-1219.
2. Tesfamariam G, Lykknes A, Kvittingen L. "Small-scale chemistry for a hands-on approach to chemistry practical work in secondary schools: Experiences from Ethiopia". *Afr. J. Chem. Educ.*, 2014, 4, 1-47.
3. Education Programs Teacher Training, Small-scale Chemistry, Florida Division, Midwest research Institute-Florida Division [last accessed: ??] www.mriresearch.org.
4. Small-scale Chemistry: An Innovation Approach to Teaching Traditional Chemistry-2001 Workshop [last accessed: ??] www.csmate.colostate.edu.
5. Eggen P-O, Grønneberg T, Kvittingen L. "Small-scale and low-cost galvanic cells". *J. Chem. Educ.*, 2006, 83, 1201-1203.
6. Khattiyavong P, Jarujamrus P, Supasorn S, Kulsing C. "The development of small scale and low-cost galvanic cells as a teaching tool for electrochemistry". *J. Res. Unit Sci. Technol. Environ. Learn.*, 2014, 5, 146-154.
7. Supasorn S. "Grade 12 students' conceptual understanding and mental models of galvanic cells before and after learning by using small-scale experiments in conjunction with a model kit". *Chem. Educ. Res. Pract.*, 2015, 16, 393-407.

The Chemist
Journal of the American Institute of Chemists

Synthesis of α-Methylene Cinnamic Acid Using Sodium Hydroxide as a Catalyst Under Microwave Irradiation

Jayashri Jasud,[a] Sharmila Walunj,[a] Pramod Kulkarni[a*]

Department of Chemistry and Postgraduate Department and Research Center in Organic Chemistry, Hutatma Rajguru Mahavidyalaya, Rajgurunagar, Pune-410505, India (Corresponding E-mail: pramodskulkarni3@gmail.com; Mobile No.: 9850658087)

Abstract: A simple, convenient synthesis of α-methyl cinnamic acid derivatives had been achieved by the Knoevenagel-Doebner condensation between succinic anhydride and substituted benzaldehyde using sodium hydroxide as a base under microwave irradiation. The present protocol has merits like easy workup, high yield, and avoiding the use of toxic solvents.

Key Words: α-methyl cinnamic acids, Knoevenagel condensation, sodium hydroxide, microwave irradiation, succinic anhydride, aromatic aldehyde

1. Introduction

Cinnamic acids are a type of compound constructed through the phenylpropanoid backbone (C6-C3) isolated from plants and microorganisms, showing fascinating biological activities [1]. They have been produced in the biochemical path that yields lignin, the polymeric material that furnishes mechanical assistance to the plant cell wall [2]. Cinnamic acids are generated in the biosynthetic pathway leading to phenylpropanoids, coumarins, lignans, isoflavonoids, flavonoids, stilbenes, aurones, anthocyanins, spermidines, and tannins [3]. Cinnamic acid, a natural aromatic carboxylic acid, is an important chemical found in plants such as Cinnamomum cassia (Chinese Cinnamon) and Panax ginseng, fruits, whole grains, vegetables, and honey. The presence of an acrylic acid group substituted on the phenyl ring gives cinnamic either a cis or a trans configuration, with the latter being the most common of the two [4]. Some naturally occurring bioactive cinnamic acid derivatives are shown in Figure 1. The cinnamic acid derivatives have been shown to have various biological activities [11].

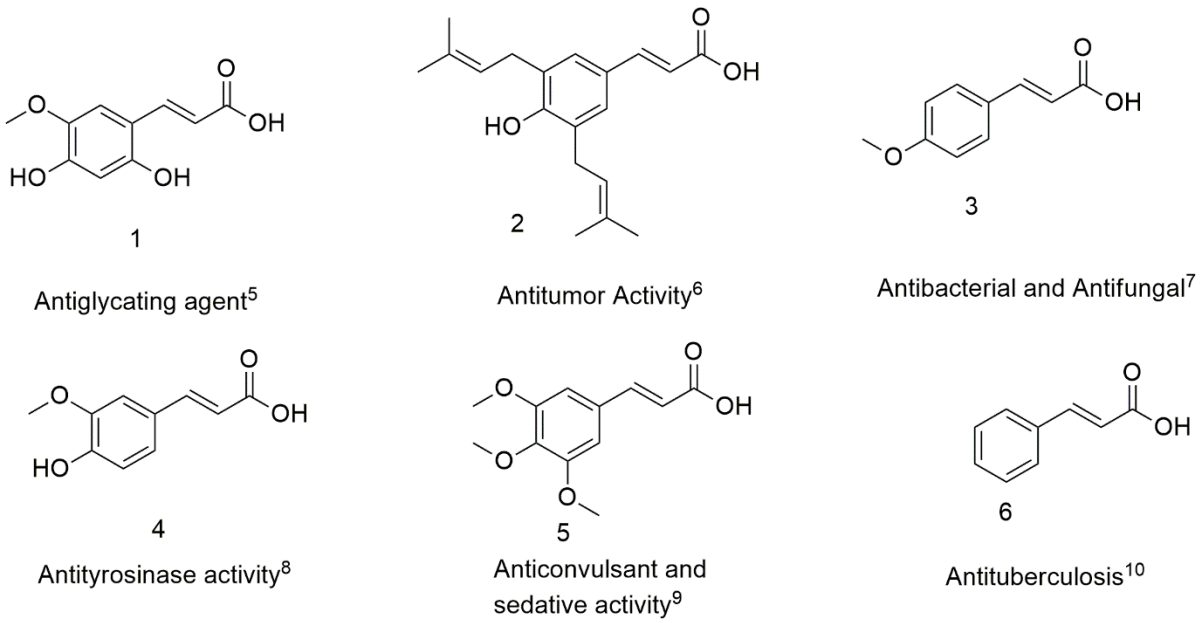

Figure 1. Naturally Occurring Cinnamic Acid Derivatives

Cinnamic acids (α, β-unsaturated carboxylic acids) are reactive molecules due to the carboxylic acid and the polarized alkenyl moiety. Cinnamic acid derivatives are key starting materials for the synthesis of natural products, heterocyclic molecules, and biologically important molecules [12]. α-Methyl cinnamic acid moieties are the crucial structural units present in various biologically active molecules [13]. α-Methyl cinnamic acid derivatives are a valuable synthon for the synthesis of serine protease inhibitors. Due to the pharmaceutical importance of α-methyl cinnamic acids, many synthetic organic chemists are attracted to the synthesis of them. Very few methods have been reported in the literature for the synthesis of α-methyl cinnamic acid derivatives [14-22]. Some of these reported methods have shortcomings such as long reaction times, hazardous reaction conditions, use of toxic solvents. Hence, there is a need to develop a new synthetic methodology for such attractive molecules.

Microwave irradiation has gained much attraction in organic synthesis because it can be applied to activate numerous organic reactions efficiently. This technology furnishes a speedy way to obtain the desired products in high yield with a few minutes. Microwave irradiation was used in various organic transformations [23-30]. Here, we have studied the synthesis of α-methyl cinnamic acid starting from succinic anhydride and various substituted benzaldehyde. Sodium hydroxide was used as a base reagent under microwave irradiation.

2. Results and Discussion

The condensation of benzaldehyde and succinic anhydride with a base was selected as a model reaction (Figure 2). Initially, the various metal hydroxide and carbonates,

such as sodium carbonate, potassium carbonate, calcium carbonate, magnesium carbonate, sodium hydroxide, potassium hydroxide, lithium hydroxide, sodium hydrogen carbonate, strontium carbonate, and barium carbonate, act as a catalyst for the condensation reaction at room temperature and microwave conditions.

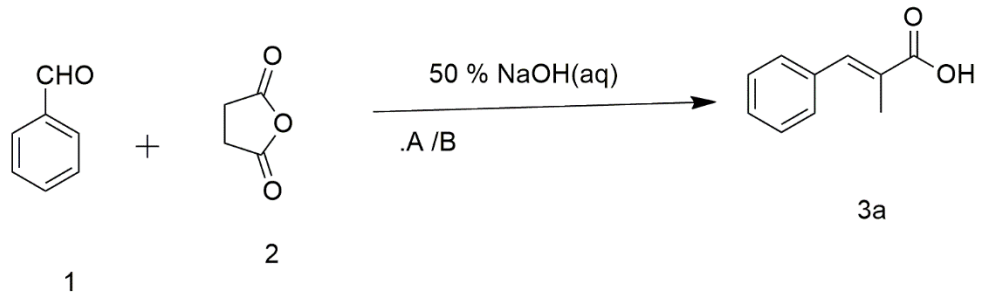

A = Microwave Irradiation
B = Room Temperature

Figure 2. Model Reaction for Screening of Catalyst

Results are summarized in Table 1. The model reaction is performed in a 50-mL beaker using 5 mmol of benzaldehyde, 5 mmol of succinic anhydride and catalyst in microwave ovens. From Table 1, it was observed that NaOH was found to be an efficient catalyst for the synthesis of α-methyl cinnamic acid with 95% yield.

Table 1. Screening of Basic Reagent[a]

Entry	Catalyst	Product	Time in sec (Microwave)	Time in hrs (Room Temp.)	% Yield[b] (Microwave)	% Yield[b] (Room Temperature)
1	Na_2CO_3	**3a**	160	34	55	43
2	K_2CO_3	**3a**	120	28	68	46
3	$CaCO_3$	**3a**	200	26	62	44
4	$MgCO_3$	**3a**	140	33	75	60
5	NaOH	**3a**	50	6	95	80
6	KOH	**3a**	120	10	85	62
7	LiOH	**3a**	180	12	78	60
8	$NaHCO_3$	**3a**	230	27	65	53
9	$SrCO_3$	**3a**	240	48	80	58
10	$BaCO_3$	**3a**	250	45	68	49

[a] Reaction condition – Benzaldehyde (5 mmol), succinic anhydride (5 mmol) and Base (2.5 mmol) of catalyst under solvent free condition at microwave at 600 W and room temperature. [b]: isolated yield.

Similarly, succinic anhydride (5 mmol) and benzaldehyde (5 mmol) were selected as the model substrate to optimize the amount of NaOH. The catalyst loading has been optimized by increasing the amount of NaOH from 10 mol % to 50 mol % for a 5 mmol scale reaction. When the reaction was carried out in the absence of a catalyst, the product formed in minor quantities and the time required to form the product was long (Table 2, entry 1). The yield has increased with the increase in catalyst amount (Table 2, entry 2-5). From the table, it was observed that a 50 mol % catalyst is sufficient to obtain the best yield in a short reaction time.

Table 2. Optimizing Amount of Sodium Hydroxide[a]

Entry	Catalyst %	Time in sec	% Yield
1	0 (without catalyst)	360	25
2	10	240	40
3	20	160	65
4	30	80	78
5	50	50	95

[a] Reaction condition – Benzaldehyde (5 mmol), succinic anhydride (5 mmol) and NaOH (mol %) of catalyst under solvent free condition at microwave at 600 W.

To study the effect of power watt on the reaction, the model reaction of 1 mmol of benzaldehyde, 1 mmol of benzaldehyde, and 50 mol % of sodium hydroxide was used. The reaction was irradiated at 100W, 200W, 300W, 400W, 600W, 800W and 1200W. The results of the study are tabulated in Table 3 and the reaction well proceeded at 600W. Hence, all the reactions were performed at 600W in the microwave oven.

Table 3. Effect Power on Synthesis of α-Methyl Cinnamic Acid (3a)[a]

Entry	Power Watt	Time in Seconds	% Yield[b]
1	100	180	82
2	200	140	85
3	300	110	86
4	400	80	89
5	600	50	95
6	800	30	decomposed
7	1200	10	decomposed

[a]: Reaction conditions are: 5 mmol benzaldehyde, 5 mmol of succinic anhydride and 50 mol % of sodium hydroxide in a 50-mL beaker in microwave oven. [b]: isolated yield after purification.

With these optimized reaction conditions in hand, we have studied the convenience of the method and it has been well evaluated using a variety of substituted aryl aldehydes for the synthesis of a series of compounds with this simple approach (Figure 3).

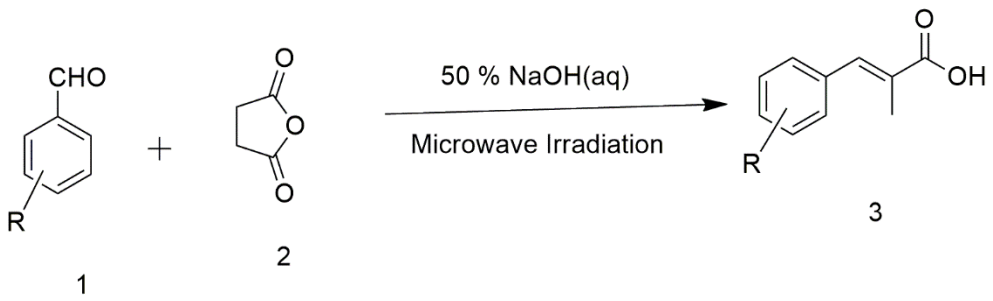

Figure 3. Synthesis of Substituted α-Methylene Cinnamic Acid Catalysed by NaOH

The results are summarized in Table 4. The nature and position of the functional groups on the phenyl ring affected the reaction time and yields of the product. The results indicated that aromatic ring bearing electron-donating groups such as -OCH_3, -CH_3, -NMe_2 and withdrawing groups like nitro were afforded high yields of product. The hydroxy substituted aldehydes did not yield the respective cinnamic acid due to reaction of sodium hydroxide with phenolic -OH group, rather with succinic anhydride and decrease in electrophilicity of aldehyde carbonyl carbon by phenoxide ion.

Table 4. Synthesis of α-Methylene Cinnamic Acid Catalysed by NaOH[a]

Entry	Aldehyde	Product (**3**)	Time in sec	% Yield[b]	M.P. ºC [Ref]
1	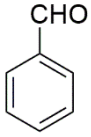	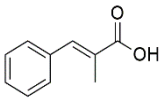 **3a**	50	95	79-80 [15]
2	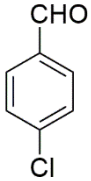	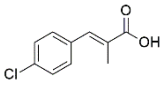 **3b**	30	85	167-168[13]
3	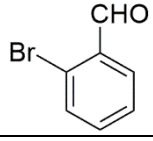	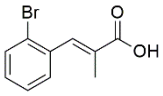 **3c**	45	86	218
4	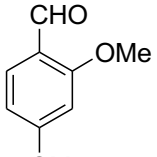	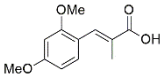 **3d**	80	75	162-163

5	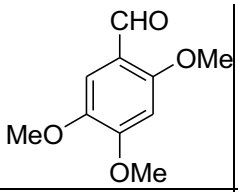	**3e**	180	NR[c]	
6	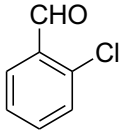	**3f**	105	88	109-111[31]
7	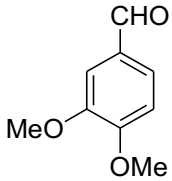	**3g**	55	90	142-143[31]
8	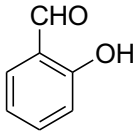	**3h**	200	NR[c]	--
9	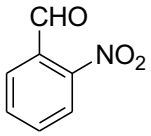	**3i**	150	55	198-199[31]
10	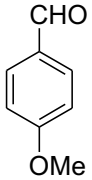	**3j**	75	80	157-158[31]
11	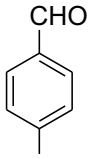	**3k**	55	85	166-168[31]
12	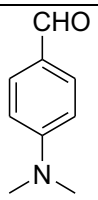	**3l**	90	75	205-206[31]
13	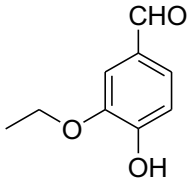	**3m**	110	NR[c]	

14	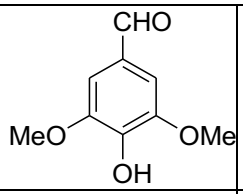	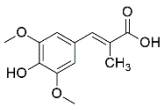 **3n**	125	NR[c]	
15	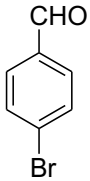	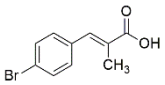 **3o**	40	89	175-176[31]
16	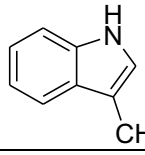	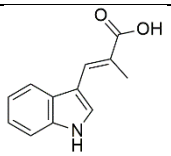 **3p**	130	NR[c]	--
17	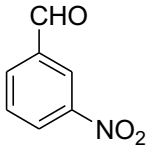	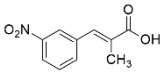 **3q**	45	91	201-202 [31]
18	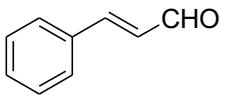	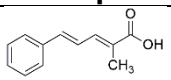 **3r**	130	60	165-166[32]
19	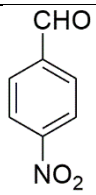	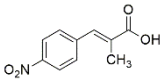 **3s**	140	55	206-207 [31]
20	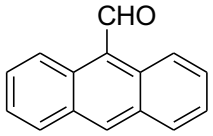	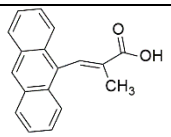 **3t**	130	65	221-223

[a] Reaction condition: 5 mmol benzaldehyde, 5 mmol succinic anhydride and 2.5 mmol of NaOH in 50-mL beaker and irradiated in microwave oven. [b] isolated yield. [c] no reaction.

3. Conclusion

Here, we have reported the efficient synthesis of α-methyl cinnamic acid via a condensation reaction between an aromatic aldehyde and succinic anhydride using aqueous sodium hydroxide solution under microwave irradiation. This novel approach has been used in the preparation of various α-methyl cinnamic acids at good to high yields (up to 95%). The main advantage of the present protocol is the high yield, operational simplicity, easy workup, easily available, and inexpensive catalyst. The present protocol did not proceed with the free -OH group and indole due to the acidic character of the phenolic OH and indole.

4. Experimental

General

Melting points were measured using the open capillary method and are uncorrected. IR spectra were recorded on Alpha T BRUKER model. ^{1}H NMR and ^{13}C NMR spectra were recorded at ambient temperature on a BRUKER AVANCE DRX-400 MHz spectrophotometer using $CDCl_3$ or DMSO-d6 as the solvent and TMS as an internal standard. The purity of newly synthesized compounds and the development of reaction were monitored by thin layer chromatography (TLC) on Merck pre-coated silica gel 60 F254 aluminium sheets, visualized by UV light.

General procedure for preparation of cinnamic acids:

A mixture of aromatic aldehyde (5 mmol), succinic anhydride (5 mmol) and sodium hydroxide (2.5 mmol) was placed in a 50-mL borosil beaker. The reaction mixture was mixed properly with a glass rod. The mixture was irradiated in a microwave oven at 600 W for an appropriate time (monitored by TLC, Table 4). On cooling, the reaction mass was acidified with dil. HCl; the product was precipitated out from the reaction mixture. The product was isolated by filtration followed by washing with water. The isolated product was pure enough and further purified by crystallization from ethanol. All products were known, and their structure has confirmed by spectral data matching with authentic samples.

4. References

1. Zolfaghari B, Yazdiniapour Z, Sadeghi M, Akbari M, Troiano R, Lanzotti V. *Phytochem. Anal.*, 2021, 32(1), 84-90.
2. Inokuchi R, Takaichi H, Kawano T. *Environ. Control Biol.*, 2016, 54(1), 57-64.
3. Vogt T. Phenylpropanoid biosynthesis. *Mol. Plant*, 2010, 3, 2-20.
4. Ruwizhi N, Aderibigbe BA. *Int. J. Mol. Sci.*, 2020, 21, 5712.
5. Muhammad N, Saeed M, Adhikari A, Khan KM, Khan H. *J. Enzyme Inhib. Med. Chem.*, 2013, 28, 997-1001.
6. Del P, Baltas M, Bedos-Belval F. *Curr. Med. Chem.*, 2011, 18, 1672-1703.
7. Nakazono Y, Watanabe Y, Hashinaga F, Tadera K. *J. Biol. Sci.*, 2006, 6, 135-139.
8. Lee H.-S. *J. Agric. Food Chem.*, 2002, 50, 1400-1403.
9. Zhao Z, Song H, Xie J, Liu T, Zhao X, Chen X, He X, Wu S, Zhang Y, Zheng X. *Eur. J. Med. Chem.*, 2019, 173, 213-227.
10. De P, B-Belvala F, V-Bacquéa C, Balts M. *Curr. Org. Chem.*, 2012, 16, 747-768.
11. Asif M, Imran M. *Prog. Chem. Biochem. Res.*, 2019, 2, 12-210.

12. Chen L, Zhang L, Yan G, Huang D. *Asian J. Org. Chem.*, 2020, 9, 842-862.
13. Basavaiah D, Krishnamacharyulu M, Hyma RS, Sarma PKS, Kumaragurubaran N. *J. Org. Chem.*, 1999, 64, 1197-1200.
14. Still WC, Gennari C. *Tetrahedron Lett.*, 1983, 24, 4405-4408.
15. Teulade M-P, Savignac P, About-jaudet E, Collignon N. *Synth. Commun.*, 1989, 19, 71-81.
16. Rossi R, Carpit A, Cossi P. *Tetrahedron*, 1992, 48, 8801-8824.
17. Myrboh B, Ila H, Junjappa H. *J. Org. Chem.*, 1983, 48, 5327-5332.
18. Zargarian D, Alper H. *Organometallics*, 1993, 12, 712-724.
19. Beesu M, Periasamy M. *J. Organomet. Chem.*, 2012, 705, 30-33.
20. Song C-X, Chen P, Tang Y. *RSC Adv.*, 2017, 7, 11233-11243.
21. Carpino LA. *J. Am. Chem. Soc.*, 1958, 80, 601-604.
22. Wehrmeister HL. *J. Org. Chem*, 1962, 27, 4418-4420.
23. Ahmadi M, Moradi L, Sadeghzadeh M. *J. Mol. Struct.*, 2021, 1235, 130183.
24. Dev D, Kalita T, Mondal T, Mandal B. *Adv. Synth. Catal.*, 2021, 363, 1427-1435.
25. Singh J, Nickel GA, Cai Y, Jones DD, Nelson TJ, Small JE, Castle SL. *Org. Lett.*, 2021, 23, 3970-3974.
26. Wolf L, Mayer JCP, Quoos N, Sauer AC, Schwab RS, Rodrigues OED, Dornelles L. *Tetrahedron*, 2021, 91, 132222.
27. Abirami M, Selvi ST, Nadaraj V. *Lett. Org. Chem.*, 2021, 18, 156-159.
28. Kulkarni P. *J. Indian Chem. Soc.*, 2021, 98, 100013.
29. Shahari MSB, Junaid A, Tiekink ERT, Dolzhenko AV. *Synthesis*, 2021, 53, 2457-2468.
30. Kadagathur M, Sigalapalli DK, Patra S, Tangellamudi ND. *Synth. Commun.*, 2021, 51, 2213-2224.
31. Gensler WJ, Berman E. *J. Am. Chem. Soc.*, 1958, 80, 494-4954.
32. Myrboh B, Asokan CV, Ila H, Junjappa H. *Synthesis*, 1984, 50-51.

The AIC Code of Ethics

Approved by the AIC Board of Directors, April 29, 1983

The profession of chemistry is increasingly important to the progress and the welfare of the community. The Chemist is frequently responsible for decisions affecting the lives and fortunes of others. To protect the public and maintain the honor of the profession, the American Institute of Chemists has established the following rules of conduct. It is the Duty of the Chemist:

1. To uphold the law; not to engage in illegal work nor cooperate with anyone so engaged;

2. To avoid associating or being identified with any enterprise of questionable character;

3. To be diligent in exposing and opposing such errors and frauds as the Chemist's special knowledge brings to light;

4. To sustain the institute and burdens of the community as a responsible citizen;

5. To work and act in a strict spirit of fairness to employers, clients, contractors, employees, and in a spirit of personal helpfulness and fraternity toward other members of the chemical profession;

6. To use only honorable means of competition for professional employment; to advertise only in a dignified and factual manner; to refrain from unfairly injuring, directly or indirectly, the professional reputation, prospects, or business of a fellow Chemist, or attempting to supplant a fellow chemist already selected for employment; to perform services for a client only at rates that fairly reflect costs of equipment, supplies, and overhead expenses as well as fair personal compensation;

7. To accept employment from more than one employer or client only when there is no conflict of interest; to accept commission or compensation in any form from more than one interested party only with the full knowledge and consent of all parties concerned;

8. To perform all professional work in a manner that merits full confidence and trust; to be conservative in estimates, reports, and testimony, especially if these are related to the promotion of a business enterprise or the protection of the public interest, and to state explicitly any known bias embodied therein; to advise client or employer of the probability of success before undertaking a project;

9. To review the professional work of other chemists, when requested, fairly and in confidence, whether they are:
    a. subordinates or employees
    b. authors of proposals for grants or contracts
    c. authors of technical papers, patents, or other publications
    d. involved in litigation;

10. To advance the profession by exchanging general information and experience with fellow Chemists and by contributing to the work of technical societies and to the technical press when such contribution does

not conflict with the interests of a client or employer; to announce inventions and scientific advances first in this way rather than through the public press; to ensure that credit for technical work is given to its actual authors;

11. To work for any client or employer under a clear agreement, preferable in writing, as to the ownership of data, plans, improvements, inventions, designs, or other intellectual property developed or discovered while so employed, understanding that in the absence of a written agreement:
    a. results based on information from the client or employer, not obtainable elsewhere, are the property of the client or employer
    b. results based on knowledge or information belonging to the Chemist, or publicly available, are the property of the Chemist, the client or employer being entitled to their use only in the case or project for which the Chemist was retained
    c. all work and results outside of the field for which the Chemist was retained or employed, and not using time or facilities belonging to a client or employer, are the property of the Chemist;

12. Special data or information provided by a client or employer, or created by the Chemist and belonging to the client or employer, must be treated as confidential, used only in general as a part of the Chemist's professional experience, and published only after release by the client or employer;

13. To report any infractions of these principles of professional conduct to the authorities responsible for enforcement of applicable laws or regulations, or to the Ethics Committee of The American Institute of Chemists, as appropriate.

The Chemist
Journal of the American Institute of Chemists

Manuscript Style Guide

The Chemist is the official online refereed journal of The American Institute of Chemists (AIC). We accept submissions from all fields of chemistry defined broadly (e.g., scientific, educational, socio-political). *The Chemist* will not consider any paper or part of a paper that has been published or is under consideration for publication anywhere else. The editorial office of *The Chemist* is located at: The American Institute of Chemists, Inc. 315 Chestnut Street Philadelphia, PA 19106-2702, Email: aicoffice@theaic.org.

Categories of Submissions

RESEARCH PAPERS

Research Papers (up to ~5000 words) that are original will only be accepted. Research Papers are peer-reviewed and include an abstract, an introduction, up to 5 figures or tables, sections with brief subheadings and a maximum of approximately 30 references.

REPORTS

Reports (up to ~3000 words) present new research results of broad interest to the chemistry community. Reports are peer- reviewed and include an abstract, an introductory paragraph, up to 3 figures or tables, and a maximum of approximately 15 references.

BRIEF REPORTS

Brief Reports (up to ~1500 words) are short papers that are peer-reviewed and present novel techniques or results of interest to the chemistry community.

REVIEW ARTICLES

Review Articles (up to ~6000 words) describe new or existing areas of interest to the chemistry community. Review Articles are peer-reviewed and include an abstract, an introduction that outlines the main point, brief subheadings for each section and up to 80 references.

LETTERS

Letters (up to ~500 words) discuss material published in The Chemist in the last 8 months or issues of general interest to the chemistry community.

BOOK REVIEWS

Book Reviews (up to ~ 500 words) will be accepted.

Manuscript Preparation

RESEARCH PAPERS, REPORTS, BRIEF REPORTS & REVIEW ARTICLES

- **The first page** should contain the title, authors and their respective institutions/affiliations and the corresponding author. The general area of chemistry the article represents should also be indicated, i.e. General Chemistry, Organic Chemistry, Physical Chemistry, Chemical Education, etc.

- **Titles** should be 55 characters or less for Research Papers, Reports, and Brief Reports. Review articles should have a title of up to 80 characters.

- **Abstracts** explain to the reader why the research was conducted and why it is important to the field. The abstract should be 100-150 words and convey the main point of the paper along with an outline of the results and conclusions.

- **Text** should start with a brief introduction highlighting the paper's significance and should be understood to readers of all chemistry disciplines. All symbols, abbreviations, and acronyms should be defined the first time they are used. All tables and figures should be cited in numerical order.

- **Units** must be used appropriately. Internationally accepted units of measurement should be used in conjunction with their numerical values. Abbreviate the units as shown: cal, kcal, µg, mg, g (or gm), %, ^{o}C, nm, µm (not m), mm, cm, cm^{3}, m, in. (or write out inch), h (or hr), min, s (or sec), ml [write out liter(s)], kg. Wherever commonly used units are used their conversion factors must be shown at their first occurrence. Greek symbols are permitted as long as they show clearly in the soft copy.

- **References and notes** should be numbered in the order in which they are cited, starting with the text and then through the table and figure legends. Each reference should have a unique number and any references to unpublished data should be given a number in the text and referred to in the references. References should follow the standards presented in the AIC Reference Style Guidelines below.

REFERENCE STYLE GUIDELINES

References should be cited as numbers within square brackets [] at the appropriate place in the text. The reference numbers should be cited in the correct order throughout the text (including those in tables and figure captions, numbered according to where the table or figure is designated to appear). The references themselves are listed in numerical order at the end of the final printed text along with any Notes. Journal abbreviations should be consistent with those presented in Chemical Abstracts Service Source Index (CASSI) (http://www.cas.org) guide available at most academic libraries.

- **Names** and initials of all authors should always be given in the reference and must not be replaced by the phrase *et al*. This does not preclude one from referring to them by the first author, et al in the text.

- **Tables** should be in numerical order as they appear in the text and they should not duplicate the text. Tables should be completely understandable without reading the text. Every table should have a title. Table titles should be placed above the respective tables.

  Table 1. Bond Lengths (Å) of 2-aminophenol

- **Figure legends** should be in numerical order as they appear in the text. Legends should be limited to 250 words.

  Figure 1. PVC Melt Flow Characterized by Analytical Structural Method

- **Letters and Book Reviews** should be clearly indicated as such when being submitted. They are not peer-reviewed and are published as submitted. Legends should be placed after/under the respective figures.

- **Journals -** The general format for citations should be in the order: **author(s), journal, year, volume, page**. Page number ranges are preferred over single values, but either format is acceptable. Where page numbers are not yet known, articles may be cited by DOI (Digital Object Identifier). For example:

  Booth DE, Isenhour TL. *The Chemist*, 2000, 77(6), 7-14.

- **Books -** For example:

  Turner GK in *Chemiluminescence: Applications*, ed. Knox Van Dyke, CRC Press, Boca Raton, 1985, vol 1, ch. 3, pp 43-78.

- **Patents** should be indicated in the following form:

  McCapra F, Tutt D, Topping RM, UK Patent Number 1 461 877, 1973.

- **Reports and bulletins, etc. -** For example:

  Smith AB, Jones CD, *Environmental Impact Report for the US*, final report to the National Science Foundation on Grant AAA-999999, Any University, Philadelphia, PA, 2006.

- **Material presented at meetings -** For example:

  Smith AB. Presented at the Pittsburgh Conference, Atlantic City, NJ, March 1983, paper 101.

- **Theses -** For example:

  Jones AB, Ph.D. Thesis, Columbia University, 2004.

- For material presented at a meeting, congress or before a Society, etc., but not published, the following form should be used:

  Jones AB, presented in part at the 20th American Institute of Chemists National Meeting, Philadelphia, PA, June, 2004.

- For material accepted for publication, but not yet published, the following form should be used:

  Smith AB. *Anal. Chem*., in press

- For material submitted for publication but not yet accepted the following form should be used:

  Jones AB, *Anal. Chem*. submitted for publication.

- For personal communications the following should be used:

  Smith AB, personal communication.

- If material is to be published but has not yet been submitted the following form should be used:

  Smith AB, unpublished work.

Reference to unpublished work should not be made without the permission of those by whom the work was performed.

Manuscript Selection

The submission and review process is completely electronic. Submitted papers are assigned by the Editors, when appropriate, to at least two external reviewers anonymously. Reviewers will have approximately 10 days to submit their comments. In selected situations the review process can be expedited. Selected papers will be edited for clarity, accuracy, or to shorten, if necessary. The Editor-in-Chief will have final say over the acceptance of submissions. Most papers are published in the next issue after acceptance. Proofs will be sent to the corresponding author for review and approval. Authors will be charged for excessive alterations at the discretion of the Editor-in-Chief.

Conditions of Acceptance

When a paper is accepted by *The Chemist* for publication, it is understood that:

- Any reasonable request for materials to verify the conclusions or experiments will be honored.

- Authors retain copyright but agree to allow *The Chemist* to exclusive license to publish the submission in print or online.
- Authors agree to disclose all affiliations, funding sources, and financial or management relationships that could be perceived as potential conflicts of interest or biases.
- The submission will remain a privileged document and will not be released to the public or press before publication.
- The authors certify that all information described in their submission is original research reported for the first time within the submission and that the data and conclusions reported are correct and ethically obtained.
- The Chemist, the referees, and the AIC bear no responsibility for accuracy or validity of the submission.

Authorship

By submitting a manuscript, the corresponding author accepts the responsibility that all authors have agreed to be listed and have seen and approved of all aspects of the manuscript including its submission to *The Chemist*.

Submissions

Authors are required to submit their manuscripts, book reviews and letters electronically. They can be submitted via email at aicoffice@theaic.org with "Submission for consideration in *The Chemist*" in the subject line. All submissions should be in Microsoft® Word format.

Copyright Assignment & Warranty Form for The Chemist

It is the policy of *The Chemist* to require all contributors to transfer the copyright for their contributions (hereafter referred to as the manuscript) to The American Institute of Chemists, Inc. (hereafter referred to as The AIC) the official publisher of *The Chemist*. By signing this agreement you assign to The AIC to consider publishing your manuscript the exclusive, royalty-free, irrevocable copyright in any medium internationally for the full term of the copyright. This agreement shall permit The AIC to publish, distribute, create derivative works, and otherwise use any materials accepted for publication in *The Chemist* internationally. A copy of the Copyright and Warranty Form for *The Chemist* will be sent to the author(s) whose manuscript is accepted for publication. The AIC will not publish any accepted manuscript in *The* Chemist without its author(s) fully complying with this requirement.

For further information or if you can any questions please contact the Publisher of *The Chemist* at (215) 873-8224 or via email at publications@theaic.org.

Website: http://www.theaic.org/ Email: aicoffice@theaic.org Phone: 215-873-8224

Announcements

INVITATION TO AUTHORS

Authors are invited to submit manuscripts for ***The Chemist,*** the official online refereed journal of The American Institute of Chemists (AIC). We accept submissions from all fields of chemistry defined broadly (e.g., scientific, educational, socio-political). *The Chemist* will not consider any paper or part of a paper that has been published or is under consideration for publication anywhere else.

Research Papers (up to ~5000 words) that are original will only be accepted. Research Papers are peer-reviewed and include an abstract, an introduction, up to 5 figures or tables, sections with brief subheadings and a maximum of approximately 30 references.

Reports (up to ~3000 words) present new research results of broad interest to the chemistry community. Reports are peer- reviewed and include an abstract, an introductory paragraph, up to 3 figures or tables, and a maximum of approximately 15 references.

Brief Reports (up to ~1500 words) are short papers that are peer-reviewed and present novel techniques or results of interest to the chemistry community.

Where to Send Manuscripts?

Please submit your manuscripts by email (aicoffice@theaic.org) to the attention of:

The Editor-in-Chief, The Chemist
The American Institute of Chemists, Inc.
315 Chestnut Street,
Philadelphia, PA 19106-2702
Email: aicoffice@theaic.org

Review Articles (up to ~6000 words) describe new or existing areas of interest to the chemistry community. Review Articles are peer-reviewed and include an abstract, an introduction that outlines the main point, brief subheadings for each section and up to 80 references.

Letters (up to ~500 words) discuss material published in *The Chemist* in the last 8 months or issues of general interest to the chemistry community.

Book Reviews (up to ~ 500 words) will be accepted.

American Institute of Chemists

www.TheAIC.org

From its earliest days in 1923 to the present, the American Institute of Chemists has fostered the advancement of the chemical profession in the United States.

The Institute has a corresponding dedication "to promote and protect the public welfare; to establish and maintain standards of practice for these professions; and to promote the professional experience through certification as to encourage competent and efficient service."

The AIC engages in a broad range of programs for professional enhancement through the prestigious Fellow membership category, awards program, certification programs, meetings, publications and public relations activities.

Advertising: Send insertion orders and advertising materials to AIC. Visit The AIC Web site for additional information at www.TheAIC.org.

The American Institute of Chemists, Inc.
315 Chestnut Street, Philadelphia, PA 19106-2702.
Phone: (215) 873-8224 | Fax: (215) 629-5224 | E-mail: aicoffice@TheAIC.org